DYNAMIC RESPONSE OF THIN, RIGID-PLASTIC SHELLS SUBJECTED TO TRANSVERSE LOADS

Robert Monroe Walters

DYNAMIC RESPONSE OF THIN, RIGID-PLASTIC SHELLS SUBJECTED TO TRANSVERSE LOADS

by

ROBERT MONROE WALTERS
Lieutenant Commander, United States Navy

B.S., United States Naval Academy
(1960)

S.M., Massachusetts Institute of Technology
(1969)

Nav.E., Massachusetts Institute of Technology
(1969)

M.C.E., The Catholic University of America
(1971)

SUBMITTED IN PARTIAL FULFILLMENT OF THE REQUIREMENTS FOR THE DEGREE OF DOCTOR OF PHILOSOPHY

at the

MASSACHUSETTS INSTITUTE OF TECHNOLOGY
June, 1971

DYNAMIC RESPONSE OF THIN, RIGID-PLASTIC SHELLS SUBJECTED TO TRANSVERSE LOADS

by

Robert Monroe Walters

Submitted to the Department of Naval Architecture and Marine Engineering on May 7, 1971, in partial fulfillment of the requirement of the degree of Doctor of Philosophy.

ABSTRACT

The exact response of thin shells loaded dynamically is extremely complicated and often cannot be expressed in closed analytical form. Approximate energy dissipation solution techniques are developed herein for rigid-perfectly plastic thin shells of arbitrary shape subjected to short duration dynamic loads. The effect of finite deflections is considered. Approximate results are compared with some exact analytic results for simple problems and with some experimental results for more complicated problems.

Thesis Supervisor: Norman Jones
Title: Associate Professor of Naval Architecture

TABLE OF CONTENTS

LIST OF FIGURES

LIST OF TABLES

LIST OF SYMBOLS

$a_{\alpha\beta}$	Surface metric tensor
a_1 to a_9	Coefficients defined in Ch. 6
$\bar{a}$, (a_α)	Surface base vector (components)
$\bar{b}$, (b_i)	Orthogonal cartesian base vector (components)
c	Cylinder parameter (Ch. 8)
e	Inertial coefficient (Ch. 8)
f	Frequency (Ch. 8)
g_{ij}	Spatial metric thesor
g	Pressure coefficient (Ch. 8)
h	Shell thickness
i, j, k, ℓ, m, n	Indices (range 1, 2, 3)
ℓ_e	Sheet explosive length parameter (Ch. 8)
$\bar{n}$, (n^i)	Unit normal vector (components)
p	Pressure
$\bar{r}$, (r^i)	Position vector (components)
s	Arc length of a curve

t	Time
$\{x^i\}$	Set of orthogonal cartesian coordinates
x	Longitudal coordinate of cylinder (Ch. 8)
x_0	Parameter (Ch. 8)
u_α, $u_{\alpha 0}$ u, v, w	Physical displacements defined in text
$\dot{w}_0$	Characteristic modal transverse velocity
A and B	Surface metric scale factors
C	Curve
D_i, (D_E)	Internal (external) energy dissipation rate
E_{ij}	Strain tensor
F	Dissipation factor (Ch. 8)
J	Factor defined in Ch. 8
J_1 to J_8	Coefficients defined in Ch. 8
L	Length parameter (Ch. 8)
M	Bending or twisting moment generalized stress
M_0	Yield moment $(\frac{\sigma_0 h^2}{4})$
N	Membrane force generalized stress

N_0	Yield force ($\sigma_0 h$)
P	Various points defined in text
P_c	Static collapse pressure
Q	Transverse shear force
R	Radius of curvature
S	Midsurface area
U	Displacement (Ch. 7)
V	Velocity (Ch. 4)
$\dot{W}$	Work rate
Z	Local coordinate nomial to M/S
$\alpha, \beta, \gamma, \delta$	Indices (range 1, 2)
β_1 to β_4	Coefficients defined in Ch. 8
γ_0	Membrane shear strain
Γ^i_{jk}	Christoffel Symbol
ε_{ij}	Physical strain tensor
$\varepsilon_{\alpha 0}$	Membrane normal strain
κ	Change in curvature
$\{\eta^\alpha\}$	Orthogonal, principal surface coordinates

λ Hinge width (Ch. 7)

λ Impulse parameter (Ch. 8)

ϕ Meridional coordinate (Ch. 6)

θ Circumferential coordinate (Ch. 6)

ϕ_0, ϕ_ℓ, θ_a, θ_e, θ_0 Shell parameters defined in Ch. 8

ψ Impulse parameter (Ch. 8)

μ_i Vector displacement

μ Mass density per unit midsurface area

ν Martin & Symonds mode factor (Ch. 8)

σ Normal stress

τ Shear stress

τ Time (Ch. 8)

$\dot{\Omega}$ Relative rotation rate (Ch. 7)

CHAPTER 1

INTRODUCTION

In recent years realization has grown in the engineering community that structural designs for certain uses can be improved by allowing some plastic deformation.

Elastic-plastic analysis of structures can be quite complex. It has been found, however, that elastic deformation can reasonably be neglected if plastic deformation plays the predominant role in a problem. Analysis has been simplified by considering materials to be rigid-plastic.

Even with use of the rigid-plastic model of material behavior, there are few plasticity problems for which exact solutions have been found. Great emphasis has been placed on finite difference and finite element methods of solution.

This thesis investigates the dynamic plastic behavior of thin, rigid-perfectly plastic shells and indicates approximate solution methods which can be used alone or as an early design aid in conjunction with more complete numerical methods.

CHAPTER 2

SOLUTION TECHNIQUES FOR RIGID-PLASTIC STRUCTURES

The stress level at which plastic flow (yielding) begins in a material subjected to simple tension is called the yield stress or the yield strength, σ_0. A perfectly plastic material can suffer indefinitely large strain once the yield stress is reached. A strain hardening material requires increased stress if plastic flow is to continue. The yield stress of a strain rate sensitive material depends upon the rate at which the material is loaded. The material considered in this thesis is rigid-perfectly plastic.

If a solid is subjected to a multiaxial stress field, the onset of plastic flow depends on the nine (six independent) stress tensor components σ_{ij}. The relationship of the stress tensor components and the yield stress in simple tension can be expressed as a yield function

$$F(\sigma_{ij}) = 0 \tag{2.1}$$

If plotted in six-dimensional stress space, equation (2.1) is a hyper-surface and is called the yield surface.

Drucker has shown that the yield surface is convex everywhere and that its shape governs the stress-strain rate relationship of the material [2-1].

If the σ_{ij} axes are also used as the corresponding $\dot{\varepsilon}_{ij}$ (plastic strain rate) axes, the strain rate vector must be normal to the yield surface at the point corresponding to the state of stress. If the stress point is a corner or vertex point of the convex yield surface, then the associated plastic strain rate vector must be a linear combination of the normal vectors to the surface at the singular point.

The strain rate vector is, therefore, proportional to the gradient of the yield function and

$$\dot{\varepsilon}_{ij} = \lambda \frac{\partial F(\sigma_{ij})}{\partial \sigma_{ij}} \tag{2.2}$$

where λ is a positive parameter.

The principle of normality which led to equation (2.2) is often called the associated flow rule.

Many yield functions or yield criteria have been proposed. Two which are commonly used and which are in good agreement with experimental results are the VonMises yield criterion and the Tresca yield criterion [2-2].

The VonMises yield criterion assumes that yielding under multiaxial stress conditions begins when the distortion energy is the same as that at yielding under simple tension. The VonMises yield function in terms of principal stresses is

$$\tfrac{1}{2}[(\sigma_1 - \sigma_2)^2 + (\sigma_2 - \sigma_3)^2 + (\sigma_3 - \sigma_1)^2] - \sigma_0^2 = 0 \tag{2.3}$$

The Tresca yield criterion assumes that yielding begins when the maximum shear stress is the same as that at yield under simple tension. The Tresca yield function can be expressed as

$$\text{Max}\{|\sigma_1 - \sigma_2|, |\sigma_2 - \sigma_3|, |\sigma_3 - \sigma_1|\} - \sigma_0 = 0 \qquad (2.4)$$

If these yield functions are plotted in Haigh-Westergaard stress space (principal stress coordinate axes), the Tresca yield surface is found to be a regular hexagonal prism inscribed within the VonMises yield surface, a right circular cylinder [2-2].

The state of stress at a point in a plate or shell very closely approximates a biaxial state of stress ($\sigma_3 = 0$). Figure 2.1 shows the form of the VonMises and Tresca yield curves in two-dimensional stress space.

A perfectly plastic material can suffer unlimited deformation once the state of stress reaches any point on the yield surface. However, a structure made of such a material will not suffer unlimited deformation until enough parts of the structure have reached yield to produce a collapse mechanism.

Determination of the exact static load level which will cause collapse of a structure (i.e., the load at which large plastic deformation just begins) is often very difficult or practically impossible. The static collapse load can be

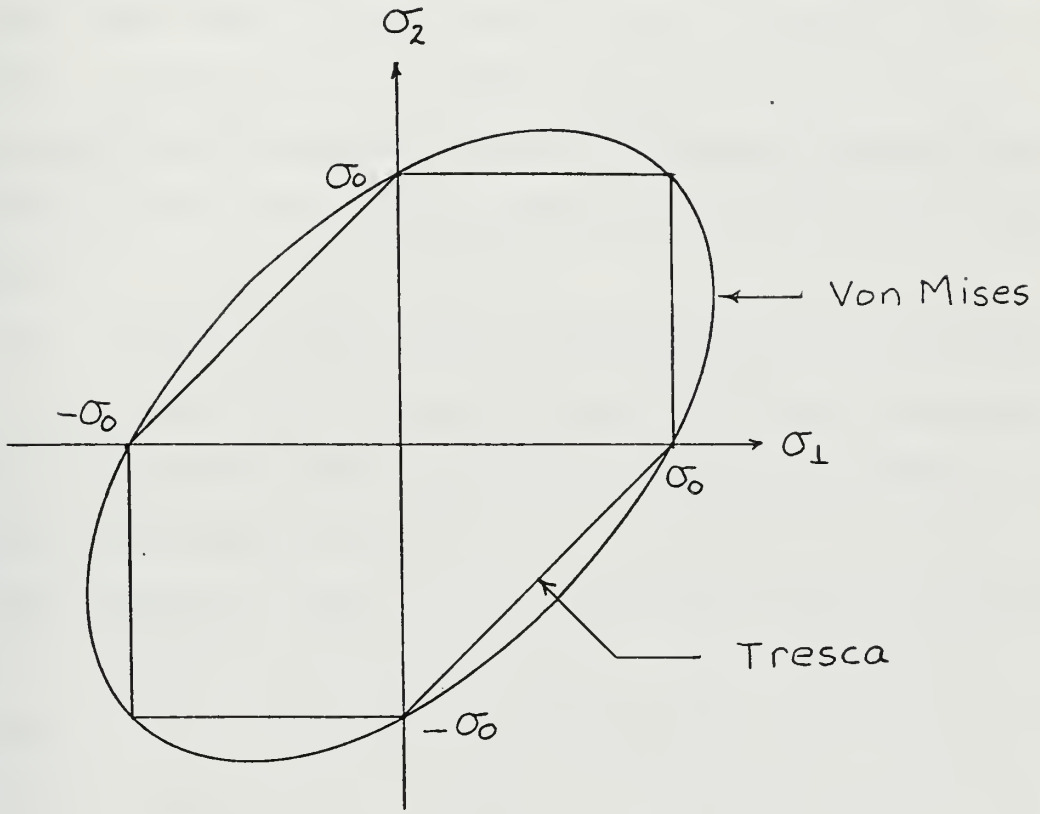
σ_2
σ_o
Von Mises
$-\sigma_o$
σ_1
σ_o
Tresca
$-\sigma_o$

Fig. 2.1

bounded, however, by use of the Upper Bound and the Lower Bound Theorems of Limit Analysis [2-3, 2-4, 2-5, 2-6].

The upper bound theorem states that a structure will collapse under the applied load if there is any kinematically admissible pattern of plastic deformation (i.e., one which satisfies boundary conditions and yields admissible strain rates) for which the rate at which the external load does work equals or exceeds the internal energy dissipation rate.

The lower bound theorem states that a structure will not collapse (or will just be at the state of collapse) if an equilibrium set of stresses can be found which balance the applied load and which are everywhere on or within the yield surface.

Both theorems assume that at the beginning of collapse there is no appreciable change in geometry of the structure. Results are the same for rigid-plastic material as for elastic-plastic material [2-7].

The methods of limit analysis have been used successfully to find or bound the collapse loads of beams and framed structures (2-8, etc.], circular plates [2-9, 2-10, etc.], rectangular plates [2-11], shells of revolution [2-12, 2-13, 2-14, etc.], and non-symmetric shells [2-15].

In the case of plates and shells, generalized stresses and generalized strains (defined in Chapter 3) are used in place of the usual stresses and strains defined at a point. The yield function and the associated flow rule are then expressed in terms of the generalized stresses and generalized strain rates.

If the load applied to a structure is in excess of the static collapse load, acceleration will result. Actual collapse of the structure may be averted if the duration of loading is very short.

Exact solution of such dynamic problems is more difficult than exact solution of static collapse problems. The time history of the loading process may affect the results, and the shape of the deformation may vary during the deformation process.

Few exact solutions have been found for dynamic plasticity problems of plates and shells. Some solutions are exact only for simplified yield criteria.

Exact dynamic solutions have been obtained, for example, for circular plates [2-16], cylindrical shells [2-17, 2-18], and spherical shells [2-19], under certain conditions of loading.

Stable geometry-change effects caused by finite deflections have also been incorporated for some problems with beams [2-20, 2-21], plates [2-22, 2-23], and shells of revolution [2-24, 2-25].

The complexity of dynamic problems in plasticity has led to the search for relatively simple approximate methods of solution. Techniques have been found which, in principle, provide upper and lower displacement bounds for a structure which is loaded impulsively [2-26, 2-27]. Unfortunately, the upper displacement bound technique requires a lower

bound (equilibrium) point load collapse solution, which is extremely difficult to find for complex structures.

An approximate method for describing the dynamic behavior of rigid-plastic beams and flat plates was recently developed by Jones [2-28]. The method assumes a time-independent deformation mode shape, ignoring the motion of travelling hinges, and accounts for the effects of finite transverse deflections. Comparison with experimental results in [2-28] and in [2-23] showed good corelation.

The major development of this thesis is an extension of Jones' approximate method for beams and plates to the dynamic behavior of thin, rigid-plastic shells.

CHAPTER 3

BASIC EQUATIONS FOR AN ARBITRARY THIN SHELL

Section 1. Assumptions

The development of certain sets of equations basic to the deformation process of an arbitrary shaped shell is outlined in this chapter. The equations developed are those which relate generalized strain rates to the displacement rates of the shell (strain/curvature rate equations) and those which relate the generalized stresses and their derivatives to the external load and the D'Alembert forces (the equilibrium equations or equations of motion).

Several simplifying assumptions have been made in the development. The results are applicable to the wide class of problems for which the transverse deformation (perpendicular to the mid surface of a shell) is the predominant deformation.

The major assumptions are listed below.

1. The shell is thin; i.e., the smallest radius to wall thickness ratio is greater than or equal to about ten.
2. Material is homogeneous and isotropic.
3. Straight lines perpendicular to the undeformed midsurface of the shell remain straight and perpendicular to the deformed midsurface. This is usually known as the Love-Kirchoff assumption.

4. Displacements in the transverse direction and their derivatives are much larger than the displacements and derivatives of displacements tangential to the shell midsurface.
5. Transverse displacements may be moderately large, but the strains which they produce are infinitesimal.
6. The effects of rotary inertia are small compared to those of linear or translational inertia.
7. The normal stress in the transverse direction is small and is assumed to be zero.

Section 2. Differential Geometry

In order to find the strain rate, curvature rate, and equilibrium equations one must be able to describe the geometry of the shell. Therefore, some space will be devoted to the differential geometry of a curved surface (the midsurface of a shell, for example).

The midsurface of a shell is a two-dimensional space. Some information about the surface is intrinsic, that is, it can be expressed in terms of the two-dimensional surface alone. For a complete representation of the surface, however, other information is required which relates the surface to the three-dimensional space. [3-1]

Consider the surface element shown in Figure (3.1). Each point in the surface can be represented by a three-dimensional position vector $\bar{r}$ (with components r^i) with

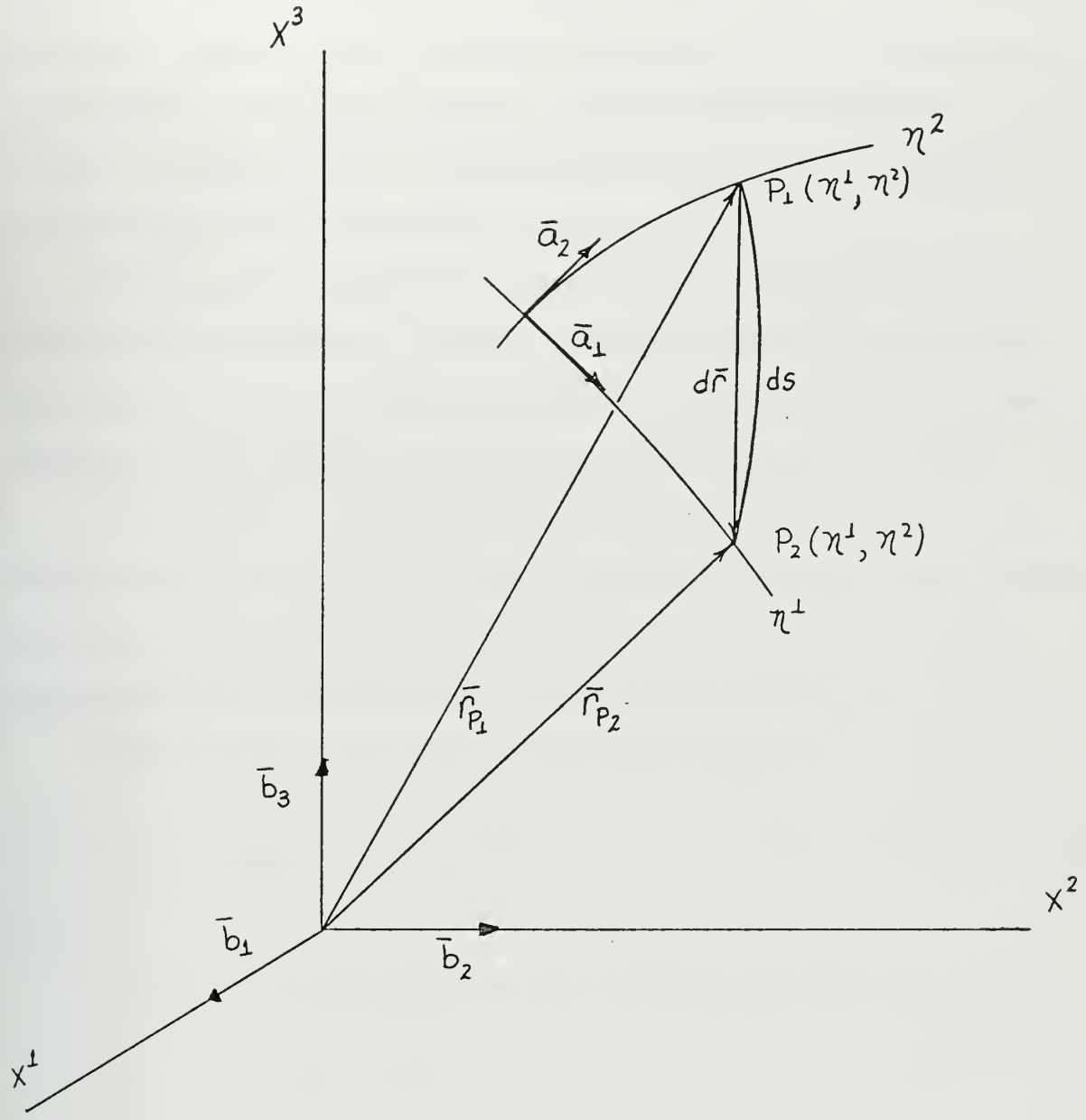
X^3
η^2
$P_1(\eta^1, \eta^2)$
$\bar{a}_2$
$\bar{a}_1$
$d\bar{r}$
ds
$P_2(\eta^1, \eta^2)$
η^1
$\bar{r}_{P_1}$
$\bar{r}_{P_2}$
$\bar{b}_3$
X^2
$\bar{b}_1$
$\bar{b}_2$
X^1

Fig. 3.1

respect to the rectangular cartesian coordinates X^i. Each point can also be represented by its coordinates with respect to a curvilinear coordinate system which lies in the surface. The most simple surface coordinate system, η^α, is the family of mutually orthogonal surface curves which correspond to the curves of maximum and minimum normal curvature. The spatial coordinates can be expressed as $X^i = X^i(\eta^\alpha)$.

It should be noted that Roman indices (i, j, k, etc.) will be used to denote spatial tensor variance and will have the range 1 to 3. Surface variance will be denoted by Greek indices (α,β,γ, etc.) which will have the range 1 to 2.

Consider two adjacent points, P_1 and P_2, lying in the surface defined by η^α. As the two points approach each other closely, the length of the spatial differential vector $\overline{dr}$ approaches the differential curve element length ds.

Thus in the limit as ds approaches zero,

$$(ds)^2 = \overline{dr} \cdot \overline{dr} \tag{3.1}$$

By use of the Chain Rule of differentiation,

$$dr^i = r^i_{,\alpha}\, d\eta^\alpha \tag{3.2}$$

and

$$\overline{dr} \cdot \overline{dr} = r^i{}_{,\alpha}\, r^i{}_{,\beta}\, d\eta^\alpha d\eta^\beta \tag{3.3}$$

Therefore

$$(ds)^2 = r^i{}_{,\alpha}\, r^i{}_{,\beta}\, d\eta^\alpha d\eta^\beta \tag{3.4a}$$

or

$$(ds)^2 = a_{\alpha\beta} d\eta^\alpha d\eta^\beta \tag{3.4b}$$

where

$$a_{\alpha\beta} = r^i{}_{,\alpha}\, r^i{}_{,\beta} = \text{surface metric tensor}$$

Since the η^α are orthogonal, $a_{12} = a_{21} = 0$. Equation (3.4b) is called the first fundamental form of the surface.

The surface coordinate system also has a set of base vectors, $\bar{a}_\alpha$. These base vectors are tangent to the surface in the direction of the corresponding surface coordinate η^α.

The surface base vectors are defined as

$$\bar{a}_\alpha = \frac{\partial \bar{r}}{\partial \eta^\alpha} \tag{3.5}$$

The surface base vectors are needed to relate the surface to three-dimensional space. This is done by forming the unit normal vector to the surface. Since the $\bar{a}_\alpha$ are tangent to the surface, their cross product will be normal to the surface and

$$\bar{n} = \frac{\bar{a}_\alpha \times \bar{a}_\beta}{|\bar{a}_\alpha \times \bar{a}_\beta|} \tag{3.6}$$

with the order of multiplication chosen so that, by convention, the direction of $\bar{n}$ is from the concave side toward the convex side.

The additional relationship needed to represent a surface is that which relates the change in the normal vector, $\bar{n}$, to change of the position vector, $\bar{r}$, as one progresses along the surface. This relationship is called the second fundamental form of the surface and is expressed as

$$\overline{dn} \cdot \overline{dr} = b_{\alpha b}\, d\eta^{\alpha} d\eta^{\beta} \tag{3.7}$$

where

$$b_{\alpha\beta} \equiv \tfrac{1}{2}\left(\frac{\overline{\partial n}}{\partial \eta^{\alpha}} \cdot \frac{\overline{\partial r}}{\partial \eta^{\beta}} + \frac{\overline{\partial n}}{\partial \eta^{\beta}} \cdot \frac{\overline{\partial r}}{\partial \eta^{\alpha}}\right)$$

In order to find the elements $b_{\alpha\beta}$, one must differentiate the unit normal vector $\bar{n}$ with respect to the curvilinear surface coordinates η^{α}.

Recall that $\bar{a}_{\alpha} = \dfrac{\overline{dr}}{\partial \eta^{\alpha}}$

and that $\bar{r}$ is the position vector

$$\bar{r} = \bar{b}_i r^i = \bar{b}_j x^j$$

Since the spatial base vectors, $\bar{b}_j$, for a rectangular cartesian system are constants,

$$\frac{\overline{\partial r}}{\partial \eta^{\alpha}} = \bar{b}_j \frac{\partial x^j}{\partial \eta^{\alpha}} = \bar{b}_j x^j_{\alpha} \tag{3.8}$$

where

x^j_{α} denotes $\dfrac{\partial x^j}{\partial \eta^{\alpha}}$

which is the rate of change of the spatial coordinate X^i with respect to that of the surface coordinate η^α.

The numerator of equation (3.6) using the orientation of Figure (3.1) is

$$\bar{a}_1 \times \bar{a}_2 = (\bar{b}_j \, x_1^j) \times (\bar{b}_k \, x_2^k) \tag{3.9a}$$

which is expressible in tensor notation as

$$\bar{a}_1 \times \bar{a}_2 = \varepsilon_{ijk} \, x_1^j \, x_2^k \, \bar{b}_i \tag{3.9b}$$

where ε_{ijk} is the alternator symbol.

$\varepsilon_{ijk} = 1$ for ijk an even permutation of 123

$\varepsilon_{ijk} = -1$ for ijk an odd permutation of 123

$\varepsilon_{ijk} = 0$ for two or more indices being equal.

The denominator of equation (3.6) is the magnitude of the numerator.

$$|\bar{a}_1 \times \bar{a}_2| = |\bar{a}_1| \; |\bar{a}_2| \sin\theta \tag{3.10}$$

Since the η^α are specified to be mutually orthogonal, $\sin\theta = 1$.

Furthermore, since the magnitude of a vector is the square root of the scalar product of the vector with itself,

$$|\bar{a}_\alpha| = [r^i{}_{,\alpha}\, r^i{}_{,\alpha}]^{\frac{1}{2}} = \sqrt{a_{\alpha\alpha}}$$

(No summation on α)

Equation (3.10) therefore reduces to

$$|\bar{a}_1 \times \bar{a}_2| = [a_{11}\, a_{22}]^{\frac{1}{2}} \tag{3.11}$$

and equation (3.6) takes the form

$$\bar{n} = \frac{\varepsilon_{ijk}\, x_1^j\, x_2^k\, \bar{b}_i}{[a_{11}\, a_{22}]^{\frac{1}{2}}} \tag{3.12}$$

To find the absolute rate of change of the normal vector with respect to the change of position on the curved surface one must subtract the apparent change due to the curvature of the η^α coordinate system. Thus the tensor (or covariant) derivatives of $\bar{n}$ must be used.

$$\bar{n}/\alpha = \bar{b}_i\, n^i/\alpha \tag{3.13}$$

where

$$n^i/\alpha \equiv n^i{}_{,\alpha} + \Gamma^i_{jk}\, n^j\, x^k_\alpha$$

and Γ^i_{jk} is the Christoffel symbol of the second kind for the three-dimensional space X^i.

The X^i being used form a rectangular cartesian coordinate system and

$$\Gamma^i_{jk} = 0.$$

Therefore, the covariant derivative of a space vector with respect to the surface coordinates is identically equal to the partial derivative of the space vector with respect to the surface coordinates.

That is

$$n^i/\alpha = n^i{}_{,\alpha} \tag{3.14}$$

Equation (3.7) can be expanded using (3.8) as

$$\overline{dn} \cdot \overline{dr} = (\bar{n}/\alpha \; d\eta^\alpha) \cdot (\bar{b}_j \; X^j_\beta \; d\eta^\beta) \tag{3.15a}$$

which in turn, by using equation (3.14), may be cast in the form

$$d\bar{n} \cdot d\bar{r} = n^i{}_{,\alpha} \; X^i{}_\beta \; d\eta^\alpha d\eta^\beta \tag{3.15b}$$

Comparing equations (3.15b) and (3.7) shows that $b_{\alpha\beta}$ may be found from

$$b_{\alpha\beta} = n^i{}_{,\alpha} \; X^i_\beta \tag{3.16}$$

The normal curvature of a surface curve is related to the tensors $a_{\alpha b}$ and $b_{\alpha\beta}$ [3-1]. Passing through every point on the surface there are two mutually orthogonal curve segments

whose normal curvatures have extreme values. If the coordinate curves η^{α} are aligned with these lines of principal curvature,

$$b_{12} = b_{21} = 0$$

and the principal curvatures are

$$\frac{1}{R_1} = \frac{b_{11}}{a_{11}} \qquad \text{and} \qquad \frac{1}{R_2} = \frac{b_{22}}{a_{22}} \tag{3.17}$$

Where R_{α} is the radius of curvature of the coordinate curve η^{α}.

In order to fully describe a shell one must bring in a third local coordinate normal to the midsurface. This direction, Z or η^3, is used to express shell thickness.

Therefore we shall now consider a family of surfaces which are parallel to the shell midsurface. That is, surfaces each of which is a constant distance Z away from the midsurface. The sense of Z agrees with that of the unit normal vector $\bar{n}$.

The surface metric tensor of a parallel surface is designated $\hat{a}_{\alpha\beta}$. Since the surface is parallel to the midsurface, it has the same principal directions and

$$\hat{a}_{12} = \hat{a}_{21} = 0.$$

The nonzero values of $\hat{a}_{\alpha\beta}$ are found from the application of equation (3.1) to the parallel surface at distance Z from

the midsurface. The position vector $\hat{r}$ to a point on the parallel surface is

$$\hat{r}^i = r^i + Zn^i \tag{3.18}$$

and

$$d\hat{r}^i = (r^i{}_{,\alpha} + Zn^i{}_{,\alpha})\, d\eta^\alpha \tag{3.19}$$

Proceeding as in equations (3.3) and (3.4) one defines

$$\hat{a}_{\alpha\beta} = (r^i{}_{,\alpha} + Zn^i{}_{,\alpha})\ (r^i{}_{,\beta} + Zn^i{}_{,\beta}) \tag{3.20a}$$

which, when the indicated multiplication has been carried out, becomes

$$\hat{a}_{\alpha\beta} = r^i{}_{,\alpha}\, r^i{}_{,\beta} + Zr^i{}_{,\alpha}\, n^i{}_{,\beta} + Zr^i{}_{,\beta}\, n^i{}_{,\alpha} + Z^2 n^i{}_{,\alpha}\, n^i{}_{,\beta} \tag{3.20b}$$

Since the position vector component r^i is the coordinate X^i, the second and third terms of equation (3.20b) may be expressed through the use of equation (3.16) as

$$Zr^k{}_{,\gamma}\, n^k{}_{,\delta} = Zb_{\delta\gamma} \tag{3.21}$$

The Weingarten formula [3-1] for a unit normal vector directed outward states that

$$n^i{}_{,\alpha} = a^{\delta\gamma}\, b_{\delta\alpha}\, X^i_\gamma \tag{3.22a}$$

which permits expression of the third term of equation (3.20b) as

$$n^i{}_{,\alpha}\, n^i{}_{,\beta} = a^{\delta\gamma}\, b_{\delta\alpha}\, X^i_\gamma\, a^{\lambda\mu}\, b_{\lambda\beta}\, X^i_\mu = a^{\delta\gamma}\, a^{\lambda\mu}\, b_{\delta\alpha}\, b_{\lambda\beta}\, a_{\gamma\mu} \tag{3.22b}$$

since

$$X^i_\gamma\, X^i_\mu = a_{\gamma\mu}$$

For the principal, orthogonal coordinate system η^α,

$$a^{\alpha\beta} = \frac{1}{a_{\alpha\beta}} \qquad \text{for } \alpha = \beta$$

and

$$a^{\alpha\beta} = a_{\alpha\beta} = 0 \qquad \text{for } \alpha \neq \beta.$$

Therefore

$$n^i{}_{,\alpha}\, n^i{}_{,\alpha} = \frac{b^2{}_{\alpha\alpha}}{a_{\alpha\alpha}} \qquad \text{(no sum on } \alpha\text{)} \tag{3.23}$$

Applying equations (3.21) and (3.23) to equation (3.20b) yields the result

$$\hat{a}_{\alpha\alpha} = a_{\alpha\alpha}\left[1 + 2Z\frac{b_{\alpha\alpha}}{a_{\alpha\alpha}} + Z^2\left(\frac{b_{\alpha\alpha}}{a_{\alpha\alpha}}\right)^2\right]$$

(no sum on α) (3.24a)

However

$$\frac{b_{\alpha\alpha}}{a_{\alpha\alpha}} = \frac{1}{R_\alpha} \qquad \text{(no sum)}$$

and, therefore,

$$\hat{a}_{\alpha\alpha} = a_{\alpha\alpha}\left(1 + \frac{Z}{R\alpha}\right)^2 \qquad \text{(no sum on } \alpha\text{)} \qquad (3.24b)$$

With this result a shell of finite thickness can be described in terms of the first and second quadratic forms (and tensors) of the shell middle surface and directed distance normal to the midsurface.

Section 3. Strain Rate and Curvature Rate

The geometric representation of a shell developed in the preceding section may now be combined with the definition of strain. The approximations of Section 1 are then used to develop the generalized strains of a thin shell.

Consider the local normal direction, the Z coordinate. It is also the third coordinate in the right-handed, orthogonal curvilinear system η^1, η^2, $\eta^3 = Z$. The corresponding metric tensor component is $a_{33} = 1$.

As the shell deforms, let the coordinate system also deform such that the coordinates after deformation are numerically equal to the coordinates before deformation. In general, the metric tensor will change to accommodate the deformation. Since the normals to the midsurface remain normal during deformation, a_{13}, a_{31}, a_{23} and a_{32} will remain zero.

Interest has been limited to finite-deflection with infinitesimal strains, and for convenience the undeformed shape is used as reference. The description of motion is therefore Lagrangian.

The Lagrangian strain tensor in terms of the three-dimensional curvilinear coordinate system η^i and in terms of the covariant and contravariant vector displacement components μ_i and μ^i is [3-2]:

$$E_{ij} = \tfrac{1}{2}(\mu_{j/i} + \mu_{i/j} + \mu^{k/i}\,\mu_{k/j}) \tag{3.25}$$

where $(\ )_{/\ell}$ denotes covariant differentiation of $(\ )$ with respect to η^ℓ.

Since the local three-dimensional coordinate system η^i is orthogonal,

$$\hat{a}^{ii} = \frac{1}{\hat{a}_{ii}} \tag{3.26a}$$

and

$$\hat{a}_{ii}\mu^i = \mu_i \tag{3.26b}$$

(no sum on i)

The form of the covariant differentiations referred to in equation 3.25 is

$$\mu_{j/i} = \mu_{j,i} - \Gamma^{\ell}_{ji}\,\mu_{\ell} \tag{3.27a}$$

and

$$\mu^{u/i} = \mu^{j}_{,i} + \Gamma^{j}_{\ell i}\,\mu^{\ell} \tag{3.27b}$$

where $(\ )_{,i}$ indicates $\frac{\partial(\ )}{\partial \eta^{i}}$ and the Christoffel symbol Γ^{ℓ}_{mn} is

$$\Gamma^{\ell}_{mn} = \tfrac{1}{2}\,\hat{a}^{\ell k}\{\hat{a}_{mk,n} + \hat{a}_{nk,m} - \hat{a}_{mn,k}\} \tag{3.28a}$$

But $a^{ij} = a_{ij} = 0$ for $i \neq j$ and Γ^{ℓ}_{mn} is different from zero only if $k = \ell$. Then

$$\Gamma^{\ell}_{mn} = \tfrac{1}{2}\hat{a}^{\ell\ell}\{\hat{a}_{m\ell,n} + \hat{a}_{n\ell,m} - \hat{a}_{mn,\ell}\} \tag{3.28b}$$

(no sum on ℓ)

Furthermore, if ℓ, m, and n are all different, all three terms in the bracket of equation (3.28b) are equal to zero and thus Γ^{ℓ}_{mn} is zero.

Therefore Γ^{ℓ}_{mn} is different from zero if and only if at least two of the indices ℓ, m, and n are equal.

The coordinate curve $\eta^{3} = Z$ is a straight line and $a_{33} = 1$. So $a_{33,j} = 0$. Also since $a_{i3} = 0$ for $i \neq 3$, $a_{i3,j} = 0$.

The three components of Γ^{ℓ}_{mn} can therefore be written as

$$\Gamma^{1}_{mn} = \tfrac{1}{2}\,\hat{a}^{11}(\hat{a}_{m1,n} + \hat{a}_{n1,m} - \hat{a}_{mn,1})$$

$$\Gamma^{2}_{mn} = \tfrac{1}{2}\,\hat{a}^{22}(\hat{a}_{m2,n} + \hat{a}_{n2,m} - \hat{a}_{mn,2})$$

$$\Gamma^{3}_{mn} = -\tfrac{1}{2}\,\hat{a}_{mn,3} \qquad (3.29)$$

Let us look now at one term of the strain tensor E_{ij}.

$$E_{11} = \mu_{1/1} + \tfrac{1}{2}(\mu^{1/1}\,\mu_{1/1} + \mu^{2/1}\,\mu_{2/1} + w^{3/1}\,w_{3/1}) \qquad (3.30)$$

Before expanding this representative term, let us invoke the assumption that transverse deflections w are much larger than the in-surface physical deflections u_1 and u_2. Therefore, the only terms retained which involve products of displacements (or products which indicate derivatives of displacements) are those for which w is involved in each factor. Because the Z coordinate is a straight line, $w^3 = w_3 = w$. With this fact and the approximation noted above, rewrite equation (3.30) as

$$E_{11} = \mu_{1/1} + \tfrac{1}{2}\,w_{/1}\,w_{/1} \qquad (3.31a)$$

which becomes

$$E_{11} = \mu_{1,1} - \Gamma^{k}_{11}\,\mu_{k} + \tfrac{1}{2}(w_{,1})^{2} \qquad (3.31b)$$

after performing the covariant differentiation and eliminating the mixed product displacement (because of the assumption that transverse displacements are much larger than in-surface displacements).

Expanding this by using equation (3.29) yields

$$E_{11} = \mu_{1,1} - \frac{\hat{a}^{11}\,\hat{a}_{11,1}\,\mu_1}{2} + \frac{\hat{a}^{22}\,\hat{a}_{11,2}\,\mu_2}{2} + \frac{\hat{a}_{11,3}}{2} w + \frac{(w_{,1})^2}{2} \tag{3.31c}$$

The relationship between the strain tensor E_{ij} and the physical strain tensor ε_{ij} is derived from the expression [3-2]

$$\frac{2E_{ij}}{[\hat{a}_{ii}\,\hat{a}_{jj}]^{\frac{1}{2}}} = (1+\varepsilon_{ii})(1+\varepsilon_{jj}) \sin \gamma_{ij} - 1 \tag{3.32a}$$

(no sum)

where θ_{ij} is the amount by which the right angle between coordinate curves η^i and η^j changed during deformation.

For infinitesimal strains, $\varepsilon_{kk} << 1$ (no sum) and the physical strain tensor can be expressed as

$$\varepsilon_{ij} = \frac{E_{ij}}{[\hat{a}_{ii}\,\hat{a}_{jj}]^{\frac{1}{2}}} \qquad \text{(no sum)} \tag{3.32b}$$

where $\varepsilon_{ij} + \varepsilon_{ji} = \gamma_{ij}$ for $i \neq j$.

The vector displacements μ are related to the physical displacements by [3-1]

$$u_i = \sqrt{\hat{a}^{ii}}\ \mu_i = \frac{\mu_i}{\sqrt{\hat{a}_{ii}}} \tag{3.33a}$$

and

$$u_i = \sqrt{\hat{a}_{ii}}\ \mu^i = \frac{\mu^i}{\sqrt{a^{ii}}} \tag{3.33b}$$

(no sum on i)

and, as noted earlier,

$$w = w^3 = w_3 \tag{3.33c}$$

The physical strain tensor component ε_{11} is therefore

$$\varepsilon_{11} = \frac{(\sqrt{\hat{a}_{11}}\ u_1)_{,1}}{\hat{a}_{11}} - \frac{\hat{a}_{11,1}\ u_1}{2\ \hat{a}_{11}\sqrt{\hat{a}_{11}}} + \frac{\hat{a}_{11,2}\ u_2}{2\sqrt{\hat{a}_{22}}\ \hat{a}_{11}} +$$

$$\frac{\hat{a}_{11,3}\ w}{2\ \hat{a}_{11}} + \frac{(w_{,1})^2}{2\ \hat{a}_{11}}$$

The remaining physical strain tensor components are found in the same manner. The nine (six independent) physical strain tensor components are

$$\varepsilon_{11} = \frac{(\sqrt{\hat{a}_{11}}\, u_1)_{,1}}{\hat{a}_{11}} - \frac{\hat{a}_{11,1}\, u_1}{2\sqrt{\hat{a}_{11}}\, \hat{a}_{11}} + \frac{\hat{a}_{11,2}\, u_2}{2\sqrt{\hat{a}_{22}}\, \hat{a}_{11}} +$$

$$\frac{\hat{a}_{11,3}\, w}{2\, \hat{a}_{11}} + \frac{(w_{,1})^2}{2\, \hat{a}_{11}} \qquad (3.34a)$$

$$\varepsilon_{22} = \frac{(\sqrt{\hat{a}_{22}}\, u_2)_{,2}}{\hat{a}_{22}} - \frac{\hat{a}_{22,2}\, u_2}{2\sqrt{\hat{a}_{22}}\, \hat{a}_{22}} + \frac{\hat{a}_{22,1}\, u_1}{2\sqrt{\hat{a}_{11}}\, \hat{a}_{22}} +$$

$$\frac{\hat{a}_{22,3}}{2\, \hat{a}_{22}}\, w + \frac{(w_{,2})^2}{2\, \hat{a}_{22}} \qquad (3.34b)$$

$$\varepsilon_{33} = 0 \qquad (3.34c)$$

$$\varepsilon_{12} = \varepsilon_{21} = \frac{[(\sqrt{\hat{a}_{11}}\, u_1)_{,2} + (\sqrt{\hat{a}_{22}}\, u_2)_{,1}]}{2\sqrt{\hat{a}_{11}\, \hat{a}_{22}}} -$$

$$\frac{[\frac{\hat{a}_{11,2}}{\sqrt{\hat{a}_{11}}}\, u_1 + \frac{\hat{a}_{22,1}\, u_2}{\sqrt{\hat{a}_{22}}}]}{2\sqrt{\hat{a}_{11}\, \hat{a}_{22}}} +$$

$$\frac{w_{,1}\, w_{,2}}{2\sqrt{\hat{a}_{11}\, \hat{a}_{22}}} \qquad (3.34d)$$

$$\varepsilon_{13} = \varepsilon_{31} = \frac{(\hat{a}_{11}\, u_1)_{,3}}{2\sqrt{\hat{a}_{11}}} + \frac{w_{,1}}{2\sqrt{\hat{a}_{11}}} - \frac{\hat{a}_{11,3}\, u_1}{2\, \hat{a}_{11}} \tag{3.34e}$$

$$\varepsilon_{23} = \varepsilon_{32} = \frac{(\sqrt{\hat{a}_{22}}\, u_2)_{,3}}{2\sqrt{\hat{a}_{22}}} + \frac{w_{,2}}{2\sqrt{\hat{a}_{22}}} - \frac{\hat{a}_{22,3}\, u_2}{\hat{a}_{22}} \tag{3.34f}$$

Further simplifications can be made through use of the Love-Kirchoff assumption that straight lines normal to the undeformed midsurface remain straight and normal to the deformed midsurface. The in-surface components of displacement u_α can be expressed in terms of the displacement $u_{\alpha 0}$ at the midsurface, the slope $(u_{\alpha,Z})_0$ of the rotated normal, and the directed distance Z of the point along the normal. That is

$$u_\alpha(\eta^1,\eta^2,Z) = u_{\alpha 0} + Z \cdot (u_{\alpha,Z})_0 \tag{3.35}$$

Recall that the surface metric tensor at height Z is related to the midsurface metric tensor by equation (3.24b).

$$\hat{a}_{\alpha\alpha} = a_{\alpha\alpha}\left(1 + \frac{Z}{R_\alpha}\right)^2 \tag{3.24b}$$

(no sum on α)

The rate of change of this tensor element with respect to Z is

$$\hat{a}_{\alpha\alpha,Z} = 2a_{\alpha\alpha}\left(1 + \frac{Z}{R_\alpha}\right)\frac{1}{R_\alpha} \qquad \text{(no sum on } \alpha) \tag{3.36}$$

The limitation of thin shells stipulates that

$$\frac{Z}{R_\alpha} \ll 1$$

and, therefore, that

$$1 + \frac{Z}{R_\alpha} \doteq 1.$$

Equations (3.24b) and (3.36) are simplified to

$$\hat{a}_{\alpha\alpha} = a_{\alpha\alpha} \tag{3.37a}$$

and

$$\hat{a}_{\alpha\alpha,Z} = \frac{2a_{\alpha\alpha}}{R_\alpha} \tag{3.37b}$$

Since the normals to the midsurface remain normal,

$$\varepsilon_{13} = \varepsilon_{23} = 0.$$

By carrying out the indicated operations of equation (3.34e) with the approximations of equation (3.37) and by evaluating the results at the midsurface (Z=0), one finds that

$$(u_{1,Z})_0 = -\frac{w_{,1}}{\sqrt{a_{11}}} + \frac{u_{10}}{R_1} \tag{3.38a}$$

and

$$(u_{2,Z})_0 = -\frac{w_{,2}}{\sqrt{a_{22}}} + \frac{u_{20}}{R_2} \tag{3.38b}$$

Substitution of equations (3.38) into equation (3.35) yields

$$u_1 = u_{10} + Z\left(\frac{u_{10}}{R_1} - \frac{w_{,1}}{\sqrt{a_{11}}}\right) \tag{3.39a}$$

and

$$u_2 = u_{20} + Z\left(\frac{u_{20}}{R_2} - \frac{w_{,2}}{\sqrt{a_{22}}}\right) \tag{3.39b}$$

Let us now substitute equations (3.39) along with equations (3.37) into the expression for ε_{11}, equation (3.34a), collecting those terms of which Z is a factor.

$$\varepsilon_{11} = \left[\frac{(\sqrt{a_{11}}\, u_{10})_{,1}}{a_{11}} - \frac{a_{11,1}\, u_{10}}{2\sqrt{a_{11}}\, a_{11}} + \frac{a_{11,2}\, u_{20}}{2\, a_{11}\sqrt{a_{22}}} + \frac{w}{R_1} + \frac{(w_{,1})^2}{2a_{11}}\right] + Z\left[\frac{\left(\frac{\sqrt{a_{11}}\, u_{10}}{R_1}\right)_{,1}}{a_{11}} - \frac{w_{,11}}{a_{11}} - \frac{a_{11,1}\, u_{10}}{2(a_{11})^{\frac{3}{2}} R_1} + \frac{a_{11,1}\, w_{,1}}{2(a_{11})^2} + \frac{a_{11,2}\, u_{20}}{2a_{11}\sqrt{a_{22}}\, R_2} - \frac{a_{11,2}\, w_{,2}}{2a_{11}\, a_{22}}\right] \tag{3.40}$$

This result and the similar results obtained from equations (3.34 b and d) will be expressed in terms of the commonly used generalized strains $\varepsilon_{\alpha 0}$ the midsurface normal strains, γ_0 the midsurface shear strain, κ_α the bending changes of shell curvature, and κ_{12} the twisting change in

shell curvature, which are defined by the following set of equations.

$$\varepsilon_{11} = \varepsilon_{10} + z\kappa_1 \tag{3.41a}$$

$$\varepsilon_{22} = \varepsilon_{20} + z\kappa_2 \tag{3.41b}$$

$$\varepsilon_{12} + \varepsilon_{21} = \gamma_0 + 2z\kappa_{12} \tag{3.41c}$$

Before writing the three strain expressions and the three curvature expressions, let us define two metric scale factors A and B such that

$$A(\eta^1,\eta^2) = [a_{11}(\eta^1,\eta^2)]^{\frac{1}{2}} \tag{3.42a}$$

and

$$B(\eta^1,\eta^2) = [a_{22}(\eta^1,\eta^2)]^{\frac{1}{2}} \tag{3.42b}$$

Proceeding as in equation (3.40) and using the notation of equations (3.42), the (midsurface) strain components and (change of) curvature components defined by equations (3.41) are found to be

$$\varepsilon_{10} = \frac{u_{10,1}}{A} + \frac{A_{,2}\, u_{20}}{AB} + \frac{w}{R_1} + \frac{(w_{,1})^2}{2A^2} \tag{3.43a}$$

$$\varepsilon_{20} = \frac{u_{20,2}}{B} + \frac{B_{,1}\, u_{10}}{AB} + \frac{w}{R_2} + \frac{(w_{,2})^2}{2B^2} \tag{3.43b}$$

$$\gamma_0 = \frac{A}{B}\left(\frac{u_{10}}{A}\right)_{,2} + \frac{B}{A}\left(\frac{u_{20}}{B}\right)_{,1} + \frac{w_{,1}\, w_{,2}}{AB} \tag{3.43c}$$

$$\kappa_1 = \frac{1}{A}\left(\frac{u_{10}}{R_1} - \frac{w_{,1}}{A}\right)_{,1} + \frac{A_{,2}}{AB}\left(\frac{u_{20}}{R_2} - \frac{w_{,2}}{B}\right) \tag{3.43d}$$

$$\kappa_2 = \frac{1}{B}\left(\frac{u_{20}}{R_2} - \frac{w_{,2}}{B}\right)_{,2} + \frac{B_{,1}}{AB}\left(\frac{u_{10}}{R_1} - \frac{w_{,1}}{A}\right) \tag{3.43e}$$

$$2\kappa_{12} = \frac{A}{B}\left(\frac{u_{10}}{AR_1} - \frac{w_{,1}}{A^2}\right)_{,2} + \frac{B}{A}\left(\frac{u_{20}}{BR_2} - \frac{w_{,2}}{B^2}\right)_{,1} \tag{3.43f}$$

It should be noted that retention of finite (moderately large) transverse deflections gives rise to the nonlinear term in ε_{10}, ε_{20} and γ_0. These nonlinear terms are missing if all deflections are infinitesimal.

The strain rate and curvature rate equations are obtained by differentiating each of equations (3.43) with respect to time. In the case of infinitesimal deflections, the strain and curvature equations are homogeneous with respect to time. If finite deflections are accounted for, the nonlinear term in each of the midsurface strains produces a nonlinear term in the corresponding strain rate equation.

The strain rate and curvature rate equations are

$$\dot{\varepsilon}_{10} = \frac{\dot{u}_{10,1}}{A} + \frac{A_{,2}\,\dot{u}_{20}}{AB} + \frac{\dot{w}}{R_1} + \frac{w_{,1}\,\dot{w}_{,1}}{A^2} \tag{3.44a}$$

$$\dot{\varepsilon}_{20} = \frac{\dot{u}_{20,2}}{B} + \frac{B_{,1}\,\dot{u}_{10}}{AB} + \frac{\dot{w}}{R_2} + \frac{w_{,2}\,\dot{w}_{,2}}{B^2} \tag{3.44b}$$

$$\dot{\gamma}_0 = \frac{A}{B}\left(\frac{\dot{u}_{10}}{A}\right)_{,2} + \frac{B}{A}\left(\frac{\dot{u}_{20}}{B}\right)_{,1} + \frac{\dot{w}_{,1}\, w_{,2}}{AB} + \frac{w_{,1}\, \dot{w}_{,2}}{AB} \qquad (3.44c)$$

$$\dot{\kappa}_1 = \frac{1}{A}\left(\frac{\dot{u}_{10}}{R_1} - \frac{\dot{w}_{,1}}{A}\right)_{,1} + \frac{A_{,2}}{AB}\left(\frac{\dot{u}_{20}}{R_2} - \frac{\dot{w}_{,2}}{B}\right) \qquad (3.44d)$$

$$\dot{\kappa}_2 = \frac{1}{B}\left(\frac{\dot{u}_{20}}{R_2} - \frac{\dot{w}_{,2}}{B}\right)_{,2} + \frac{B_{,1}}{AB}\left(\frac{\dot{u}_{10}}{R_1} - \frac{\dot{w}_{,1}}{A}\right) \qquad (3.44e)$$

$$2\dot{\kappa}_{12} = \frac{A}{B}\left(\frac{\dot{u}_{10}}{AR_1} - \frac{\dot{w}_{,1}}{A^2}\right)_{,2} + \frac{B}{A}\left(\frac{\dot{u}_{20}}{BR_2} - \frac{\dot{w}_{,2}}{B^2}\right)_{,1} \qquad (3.44f)$$

The fact that the strain and curvature expressions (and, therefore, the rate equations) derived in this chapter contain approximations should be reemphasized.

There have been many attempts to derive strain and curvature expressions for thin shells using the Love-Kirchoff assumption or something equivalent, and there are almost as many different results as there have been attempts. Differences creep into the curvature expressions due to the approximations made and due to the stage at which the approximations are made. The author has not found any disagreement in the expressions for (midsurface) strain.

Table 3.1 gives a comparison between some representative theories. The Table shows what terms, if any, must be added to the corresponding curvature expression of this thesis to bring it into agreement with the theory referenced. Symbols and directions have been changed to agree with those of this thesis.

Budiansky and Sanders [3-8] defined a pseudo-curvature in order to produce a symmetric tensor from which curvature could be found. The comparison in Table 3.1 was made with the curvature, not the pseudo-curvature.

The various curvature results would lead to differing results for the equilibrium equations as well. Only the set of equilibrium equations which is consistent with strain rate and curvature rate equations of this thesis will be presented. The finite deflections considered do not affect the curvature rate expressions.

TABLE 3.1

Comparison Between Curvature Expressions

(The terms listed are those which must be added to the corresponding curvature expression of this thesis to bring it into agreement with the theory referenced.)

Author and Reference	κ_1	κ_2	$2\kappa_{12}$
Novozhilov [3-3]	--	--	$\frac{u_{10,2}}{BR_1} - \frac{A_{,2}\, u_{10}}{ABR_2} + \frac{u_{20,1}}{AR_2} - \frac{B_{,1}\, u_{20}}{ABR_1}$
Wang [3-4]	--	--	--
Love [3-5]	--	--	$\frac{B_{,1}}{AB}\left(\frac{u_{20}}{R_2} - \frac{w_{,2}}{B}\right) - \frac{1}{B}\left(\frac{u_{10}}{R_1} - \frac{w_{,1}}{A}\right)_{,2} + \frac{A_{,2}\, u_{10}}{ABR_1} + \frac{A_{,2}\, w_{,1}}{A^2B} + \frac{1}{A}\left(\frac{u_{20}}{R_2} - \frac{w_{,2}}{B}\right)_{,1} - \frac{2u_{20,1}}{AR_1}$

Author and Reference	κ_1	κ_2	$2\kappa_{12}$
Koiter [3-6]	--	--	$(\frac{1}{R_2} - \frac{1}{R_1})(\frac{u_{20,1}}{A} - \frac{u_{10,2}}{B} - \frac{u_{10}A_{,2}}{AB} + \frac{u_{20}B_{,1}}{AB})$
Donnel [3-7]	$-\frac{1}{A}(\frac{u_{10}}{R_1})_{,1} - \frac{A_{,2}u_{20}}{ABR_2} + \frac{w}{R_1^2}$	$-\frac{1}{B}(\frac{u_{20}}{R_2})_{,2} - \frac{B_{,1}u_{10}}{ABR_1} + \frac{w}{R_2^2}$	$-\frac{B}{A}(\frac{u_{20}}{BR_2})_{,1} - \frac{A}{B}(\frac{u_{10}}{AR_1})_{,2}$
Budiansky and Sanders [3-8]	$\frac{1}{AR_1}(u_{10,1} + \frac{A_{,2}u_{20}}{B}) + \frac{w}{R_1^2}$	$\frac{1}{BR_2}(u_{20,2} + \frac{B_{,1}u_{10}}{A}) + \frac{w}{R_2^2}$	(Same as Novozhilov)
Kraus [3-9]	--	--	--

Section 4. Equilibrium Equations

Let us now investigate the equilibrium of a differential element of a thin shell. In order to ensure that the equilibrium equation results will have approximations consistent with the rate equations (3.44), the equilibrium equations are developed from an energy approach rather than from a strictly geometric approach [3-10].

In the theory of plates and shells the resultant forces and moments which act on the midsurface at an element face are normally used instead of the stresses themselves. The resultants are defined by a force or moment balance and are called generalized stresses.

A typical shell differential element is shown in Figure (3.2) and indicates the positive sense of stresses, forces, moments, and pressures used in this thesis.

Taking a force balance in the η^1 direction on the face perpendicular to η^1 yields

$$N_1 B d\eta^2 = \int_{-h/2}^{h/2} \sigma_1 \, B d\eta^2 \, \frac{R_2+Z}{R_2} \, dZ$$

A moment balance in the η^2 direction on the η^1 face yields

$$M_1 B d\eta^2 = \int_{-h/2}^{h/2} \sigma_1 \, B d\eta^2 \, Z \, \frac{R_2+Z}{R_2} \, dZ$$

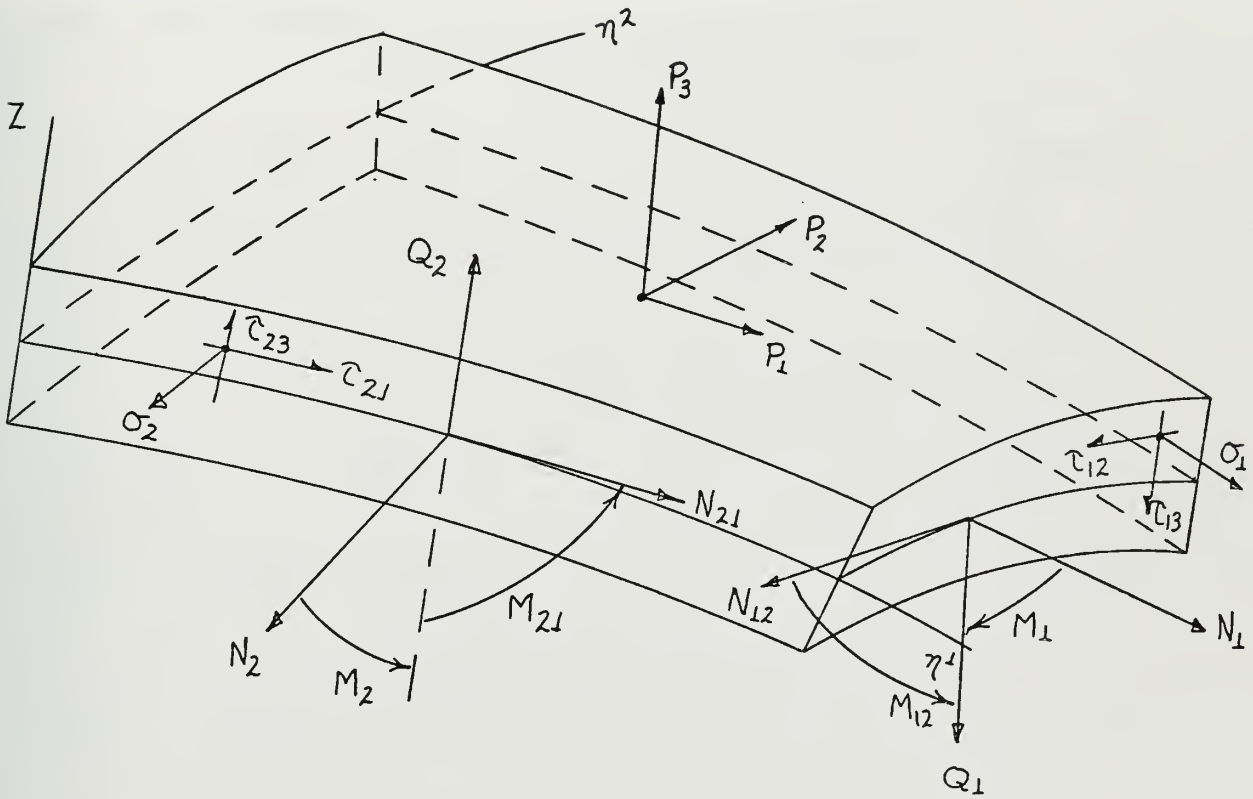
Z
η^2
P_3
P_2
P_1
Q_2
τ_{23}
τ_{21}
σ_2
N_{21}
M_{21}
N_2
M_2
τ_{12}
τ_{13}
σ_1
N_{12}
M_1
N_1
η^1
M_{12}
Q_1

Fig. 3.2

And a force balance in the Z direction on the η^1 face yields

$$Q_1 B d\eta^2 = \int_{-h/2}^{h/2} \tau_{13} \, B d\eta^2 \, \frac{R_2+Z}{R_2} \, dZ$$

Applying the same technique to the remaining forces and moments and using the thin shell assumption that $\frac{Z}{R} << 1$, the definitions of the generalized stresses become

$$N_1 = \int_{-h/2}^{h/2} \sigma_1 dZ \tag{3.45a}$$

$$N_2 = \int \sigma_2 dZ \tag{3.45b}$$

$$N_{12} = N_{21} = \int \tau_{12} dZ \tag{3.45c}$$

$$M_1 = \int \sigma_1 Z dZ \tag{3.45d}$$

$$M_2 = \int \sigma_2 Z dZ \tag{3.45e}$$

$$M_{12} = -M_{21} = \int \tau_{12} Z dZ \tag{3.45f}$$

$$Q_1 = \int \tau_{13} dZ \tag{3.45g}$$

$$Q_2 = \int \tau_{23} dZ \tag{3.45h}$$

The integration limits are the same in each definition.

Because of the Love-Kirchoff assumption that normals to the midsurface remain normal and straight, $\varepsilon_{13} = \varepsilon_{23} = 0$. Therefore there is no transverse shear strain energy, and Q_1 and Q_2 are considered to be reaction forces necessary for transverse equilibrium.

The affect of the shell thickness has been taken into account in the definitions of equation (3.45) and the resultant forces and moments are assumed to act on the shell midsurface.

Figure (3.3) illustrates the variation of the generalized stresses and reactions of a loaded shell element.

The principal of virtual velocities states that if any stress field which is in equilibrium with the applied loads acts in conjunction with any arbitrary, continuous virtual velocity field which satisfies the actual boundary conditions, then the external work rate (due to reaction forces and applied load) is equal to the internal energy dissipation rate.

Symbolically this is represented as

$$\dot{W}_{external} = \dot{W}_{internal} \tag{3.46}$$

The internal energy dissipation rate is determined by integrating the strain energy rate over the volume of the body. This result can also be obtained by integrating the product of the generalized stresses with the corresponding generalized strain rate over the undeformed midsurface area.

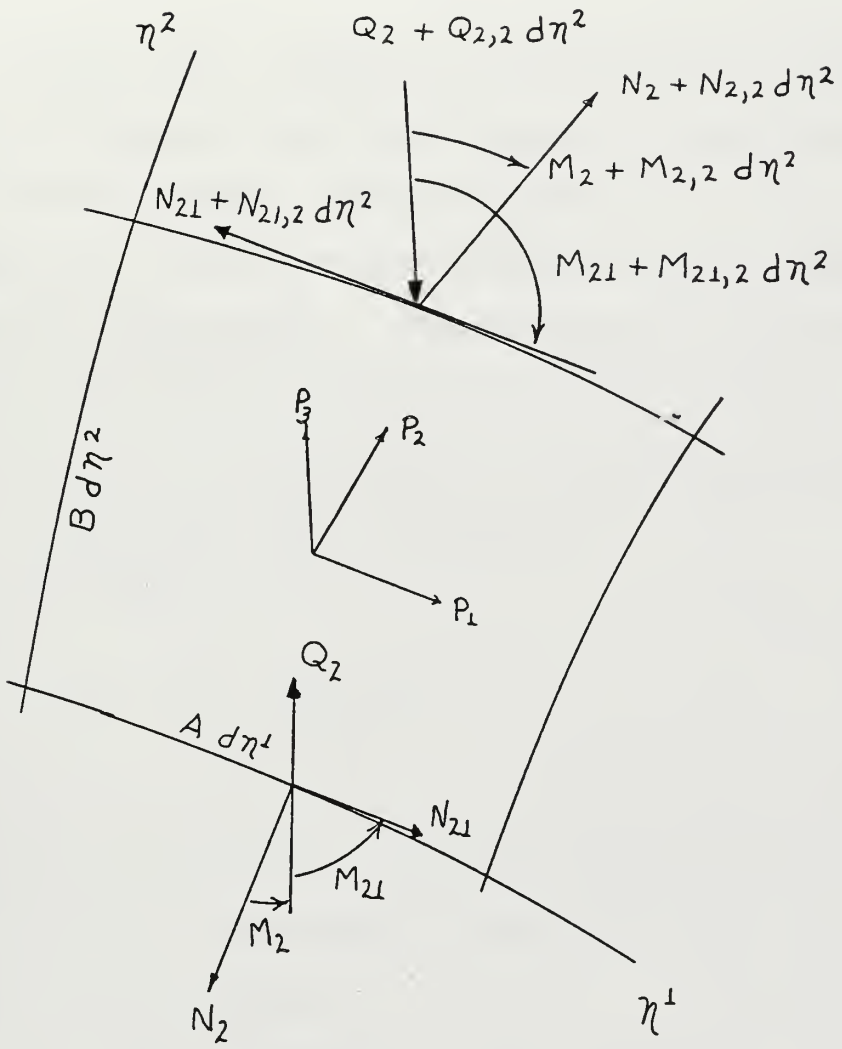
η^2
$Q_2 + Q_{2,2}\, d\eta^2$
$N_2 + N_{2,2}\, d\eta^2$
$M_2 + M_{2,2}\, d\eta^2$
$N_{21} + N_{21,2}\, d\eta^2$
$M_{21} + M_{21,2}\, d\eta^2$
P_3
P_2
P_1
$B\, d\eta^2$
Q_2
$A\, d\eta^1$
N_{21}
M_{21}
M_2
N_2
η^1

Fig. 3.3

$$\dot{W}_{int} = \int_S [N_1\dot{\varepsilon}_1 + N_2\dot{\varepsilon}_2 + N_{12}\dot{\gamma}_0 + M_1\dot{\kappa}_1 + M_2\dot{\kappa}_2 + 2M_{12}\dot{\kappa}_{12}]dS \tag{3.47a}$$

The external work consists of contributions from the work done by boundary forces and moments, by the D'Alembert forces (inertial forces), and by the load.

Figure (3.4) indicates the boundary forces, moments and associated displacement. The boundary is a curve and the boundary work rate is, therefore a line integral.

$$\dot{W}_{ext} = \int_{C_{boundary}} [\bar{N}_{\alpha\beta}\dot{t}_{\alpha\beta} + \bar{Q}_\alpha\dot{n}_\alpha + \bar{M}_{\alpha\beta}\dot{\phi}_{\alpha\beta}]dC +$$

$$\int_S P_i\dot{u}_i\, dA - \int_S \mu\ddot{u}_i\dot{u}_i dS \tag{3.47b}$$

First let us evaluate a representative term of equation (3.47a) by substituting equations (3.44) for the strain and curvature rates.

The first term of equation (3.47a) becomes

$$\int_S N_1\dot{\varepsilon}_{10}dS = \int_{\eta^1}\int_{\eta^2} [N_1\frac{\dot{u}_{10,1}}{A} + N_1\frac{\dot{u}_{20}A_{,2}}{AB} + \frac{N_1\dot{w}}{R_1} + \frac{N_1w_{,1}\dot{w}_{,1}}{A^2}] \cdot$$

$$(Ad\eta^1 Bd\eta^2) \tag{3.48}$$

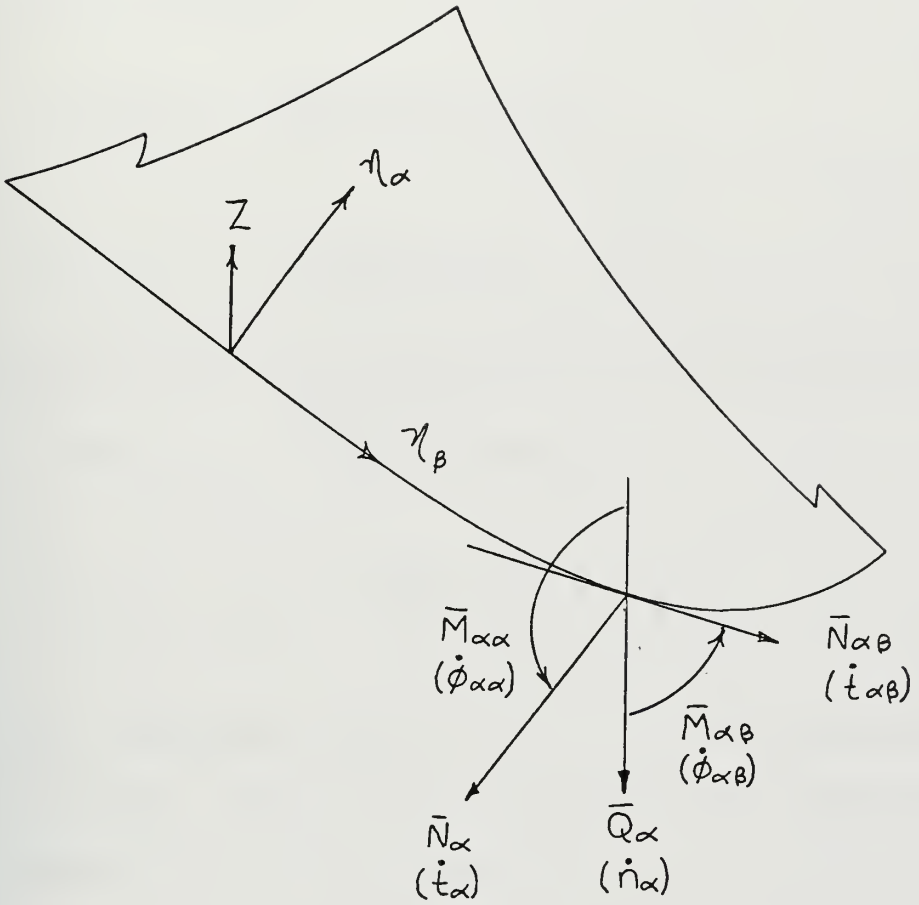
Z
η_α
η_β
$\bar{M}_{\alpha\alpha}$
$(\dot{\phi}_{\alpha\alpha})$
$\bar{N}_{\alpha\beta}$
$(\dot{t}_{\alpha\beta})$
$\bar{M}_{\alpha\beta}$
$(\dot{\phi}_{\alpha\beta})$
$\bar{N}_\alpha$
$(\dot{t}_\alpha)$
$\bar{Q}_\alpha$
$(\dot{n}_\alpha)$

Fig. 3.4

The first and last terms on the right hand side of equation (3.47) contain surface derivatives of displacement rates. Let us integrate those two terms by parts in order to produce a line integral at the boundary which can match that found in $\dot{W}_{ext}$.*

$$\int\int [\frac{N_1 \dot{u}_{10,1}}{A} + \frac{N_1 \dot{w}_{,1} w_{,1}}{A^2}] \, AB d\eta_1 d\eta_2 =$$

$$\int [\int (N_1 B \dot{u}_{10,1} + \frac{N_1 B w_{,1} \dot{w}_{,1}}{A}) d\eta_1] \, d\eta_2 =$$

$$\int \{ [N_1 B \dot{u}_{10}] + [\frac{N_1 B w_{,1}}{A} \dot{w}] \} \, d\eta_2 -$$

$$\int\int [(N_1 B)_{,1} \dot{u}_{10} + (\frac{N_1 B w_{,1}}{A}) \dot{w}_{,1}] \, d\eta_1 \, d\eta_2$$

where the expression within the {} is to be evaluated at the shell boundary. The integral involving that expression can be expressed as the line integral

$$\oint_{C_{boundary}} (N_1 B \dot{u}_{10} + \frac{N_1 B w_{,1} \dot{w}}{A} \, d\eta_2$$

The first term of equation (3.47) can therefore be written as

---

*For ease in presentation the η^α symbols will be typed as η_α and the integration paths will be omitted from the $\int\int$.

$$\int_S N_1 \dot{\varepsilon}_{10}\, dS = \oint_C (N_1 B \dot{u}_{10} + \frac{N_1 B w_{,1} \dot{w}}{A})\, d\eta_2 +$$

$$\int\int [N_1 A_{,2} \dot{u}_{20} + \frac{N_1 A B \dot{w}}{R_1} - (N_1 B)_{,1} \dot{u}_{10} -$$

$$(\frac{N_1 B w_{,1}}{A})_{,1} \dot{w}]\, d\eta_1\, d\eta_2 \qquad (3.49)$$

Next let us consider the components of motion at a shell boundary. Figure (3.5) shows a differential profile of a shell midsurface at a boundary before and after deformation and indicates the displacement rate components on the edge η_1 = constant.

The angle ϕ_1 is the sum of the angles a and b.

$$\phi_{11} = \frac{u_{10}}{R_1} - \frac{w_{,1}}{A} \qquad (3.50a)$$

The corresponding angle for the edge η_2 = constant is

$$\phi_{22} = \frac{u_{20}}{R_2} - \frac{w_{,2}}{B} \qquad (3.50b)$$

From Figure (3.5b) it is seen that

$$\dot{t}_{11} = \dot{u}_{10} \cos\phi_1 - \dot{w} \sin\phi_1 \qquad (3.51a)$$

$$\dot{n}_1 = -\dot{w} \cos\phi_1 - \dot{u}_{10} \sin\phi_1 \qquad (3.51b)$$

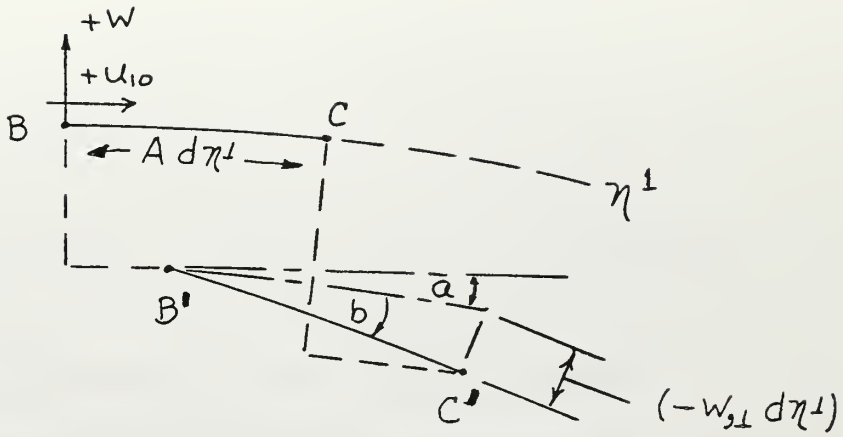

$$\measuredangle a = \frac{u_{10}}{R_1}$$

$$\measuredangle b = -\frac{w_{,1}}{A}$$

(a)

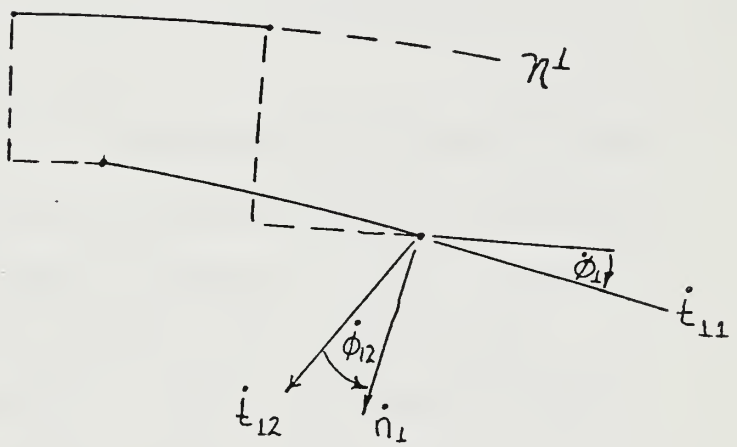

(b)

Fig. 3.5

Similarly,

$$\dot{t}_{22} = \dot{u}_{20} \cos\phi_2 - \dot{w} \sin\phi_2 \tag{3.51c}$$

$$\dot{n}_2 = -\dot{w} \cos\phi_1 - \dot{u}_{20} \sin\phi_2 \tag{3.51d}$$

Using small angle approximation and neglecting mixed products of the displacements one finds the components

$$\dot{t}_{11} = \dot{t}_{21} = \dot{u}_{10} + \frac{\dot{w}_{,1}}{A} \tag{3.52a}$$

$$\dot{n}_1 = -\dot{w} \tag{3.52b}$$

$$\dot{\phi}_{11} = \dot{\phi}_{21} = \frac{\dot{u}_{10}}{R_1} - \frac{\dot{w}_{,1}}{A} \tag{3.52c}$$

plus five other components which can be obtained by permutation of the indices.

The difference between the external and internal energy rates must be zero. If the procedure which led to equation (3.49) is applied to all terms of equation (3.47a) and the results subtracted from the external work rate (3.47b) formed with the aid of equations (3.52), the final result must equal zero.

Since the displacement rates are arbitrary, the coefficient of each displacement rate must be identically zero. The line integral terms, with two exceptions, simply show that the internal forces and moments at the boundary are equal to the

external forces and moments at the boundary. Since $Q_\alpha = \bar{Q}_\alpha$ at the boundary, the line integral terms which relate Q_α to the internal moments at the boundary are presumed to be valid everywhere within the shell

$$Q_1 = \frac{1}{AB}\left[M_2B_{,1} - (M_1B)_{,1} - (M_{12}A)_{,2} - M_{12}A_{,2}\right] \qquad (3.53a)$$

$$Q_2 = \frac{1}{AB}\left[M_1A_{,2} - (M_2A)_{,2} - (M_{12}B)_{,1} - M_{12}B_{,1}\right] \qquad (3.53b)$$

The area integral terms lead to the following results.

$$AB(P_1 - \mu\ddot{u}_{10}) - N_2B_{,1} + (N_{12}A)_{,2} + (N_1B)_{,1} +$$

$$N_{12}A_{,2} + \frac{(M_1B)_{,1}}{R_1} - \frac{M_2B_{,1}}{R_1} + \frac{(M_{12}A)_{,2}}{R_1} + \frac{M_{12}A_{,2}}{R_1} = 0 \qquad (3.53c)$$

$$AB(P_2 - \mu\ddot{u}_{20}) - N_1A_{,2} + (N_{12}B)_{,1} + (N_2A)_{,2} + N_{12}B_{,1} +$$

$$\frac{(M_2A)_{,2}}{R_2} - \frac{M_1A_{,2}}{R_2} + \frac{(M_{12}B)_{,1}}{R_2} + \frac{M_{12}B_{,1}}{R_2} = 0 \qquad (3.53d)$$

$$AB(P_3 - \mu\ddot{w}) - \frac{N_1AB}{R_1} - \frac{N_2AB}{R_2} + \left(\frac{N_1Bw_{,1}}{A}\right)_{,1} + \left(\frac{N_2Aw_{,2}}{B}\right)_{,2} +$$

$$(N_{12}w_{,2})_{,1} + (N_{12}w_{,1})_{,2} + \left[\frac{(M_1B)_{,1}}{A}\right]_{,1} + \left[\frac{(M_2A)_{,2}}{B}\right]_{,2} +$$

$$2\left(\frac{M_{12}A_{,2}}{A}\right)_{,1} + 2\left(\frac{M_{12}B_{,1}}{B}\right)_{,2} + 2M_{12,12} - \left(\frac{M_1A_{,2}}{B}\right)_{,2} -$$

$$\left(\frac{M_2B_{,1}}{A}\right)_{,1} = 0 \qquad (3.53e)$$

Retention of the nonlinear, finite deflection, terms in the strain rate equations leads to the terms involving the transverse deflection w in equation (3.53e), which is the equilibrium equation in the Z direction. These terms do not appear in the case of infinitesimal deflections.

The infinitesimal deflection equilibrium equations of this thesis have been compared with those of several authors for shells of revolution and have been found to be in exact agreement.

CHAPTER 4

THIN SHELL MATERIAL RELATIONS

Section 1. Yield Surfaces

It was noted in Chapter 2 that the yield surface and the associated flow rule for rigid-perfectly plastic thin shells are usually described in terms of the generalized stresses and generalized strain rates defined in Chapter 3.

One of the major assumptions of shell theory is that the transverse normal stress is negligible, and that the state of stress at a point on any parallel surface of the shell is essentially biaxial. The state of stress can be expressed, then, in terms of two principal, in-surface stresses, σ_1 and σ_2. The yield surface of a biaxial state of stress expressed in terms of the principal stresses was seen to be a plane, closed, convex curve (Figure 2.1).

Substitution of the principal stresses into the generalized stress definitions (equations 3.45) produces a yield criterion in terms of four principal generalized stresses, two membrane forces (N_1 and N_2) and two bending moments (M_1 and M_2). The corresponding yield surface is described in four-dimensional space, as is the generalized strain-rate vector. A generalized stress yield point is reached and generalized plastic strain can begin at a shell cross section only when the yield condition for stress at a point has been reached for every point of the cross section.

That is, plastic flow at a cross section is constrained if any level of the cross section remains rigid.

No mention has been made of the transverse shear forces, Q. Since the shell theory used here assumes that there is no transverse shear strain, it is assumed that the transverse shear stresses and the resultant transverse shear forces have no effect on yielding. The transverse shear forces are treated as reaction forces necessary for equilibrium.

If the principal generalized stresses are not known, the yield criterion will be expressed in terms of the six independent generalized stresses ($N_{\alpha\beta}$ and $M_{\alpha\beta}$). The yield surface is then described in six-dimensional generalized stress space.

The class of problems consisting of axisymmetric loading and response of thin shells of revolution is one for which the principal stress directions correspond to the coordinate directions. The four-dimensional generalized stress yield surface is, therefore, directly applicable. The yield surface based upon the Tresca yield condition was developed by Onat and Prager [4-1]. The VonMises yield surface in four-dimensional generalized stress space was developed by Hodge [4-2]. To the author's knowledge neither yield condition has as yet been extended to six-dimensional generalized stress space.

The VonMises yield condition for a shell of revolution is considerably more complex for analytical work than the Tresca condition. Onat and Prager's Tresca condition is

considered in this thesis to be the exact yield condition.

For problems in six-dimensional stress space,and often in four-dimensional stress space problems as well, approximate yield surfaces are used. These simplified yield surfaces may be necessary in order to make the resulting equations tractable. Although the results obtained from approximate yield conditions will, in general, be in error, the bounding theorems of limit analysis allow the exact results to be bounded with two approximate yield surfaces of the same shape, one of which circumscribes the exact surface and one of which inscribes the exact surface [4-3].

The two-moment limited interaction yield surface proposed by Hodge [4-4] and shown in Figure 4.1, for example, circumscribes the Tresca yield surface, while a similar surface with a scale 0.618 times that of the original inscribes the Tresca surface. The results which would be obtained through use of the Tresca surface must lie between the results obtained through use of the two limited interaction surfaces.

A two-direction limited interaction yield surface suggested by the Tresca yield surface of a curved beam [4-5] and shown in Figure 4.2 also circumscribes the exact Tresca surface. The inscribing surface also has a scale 0.618 times that of the circumscribing surface (Appendix A).

Closer bounding may be possible if the stress points of a given problem lie only on a small portion of the yield surface.

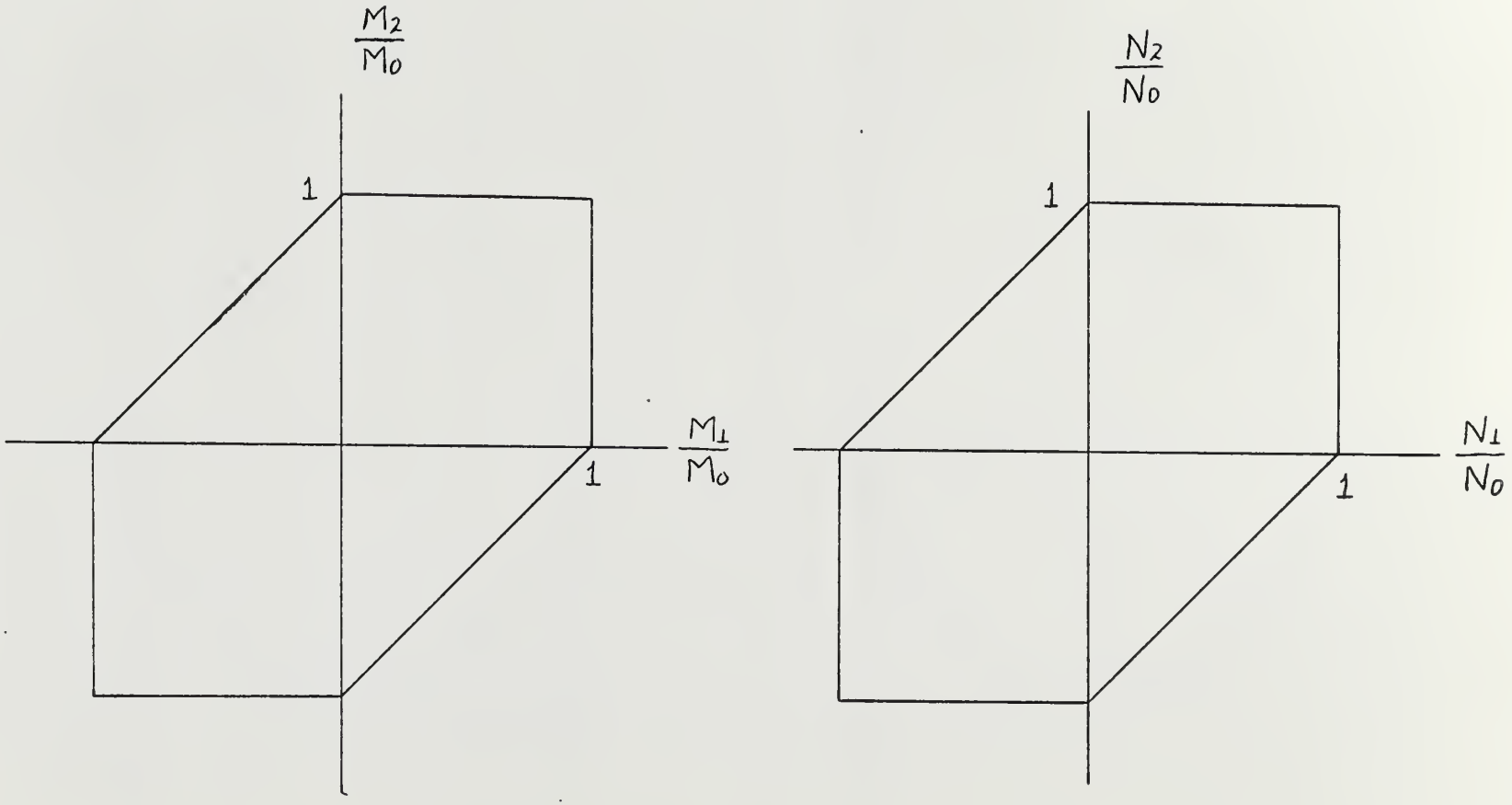

FIG. 4.1

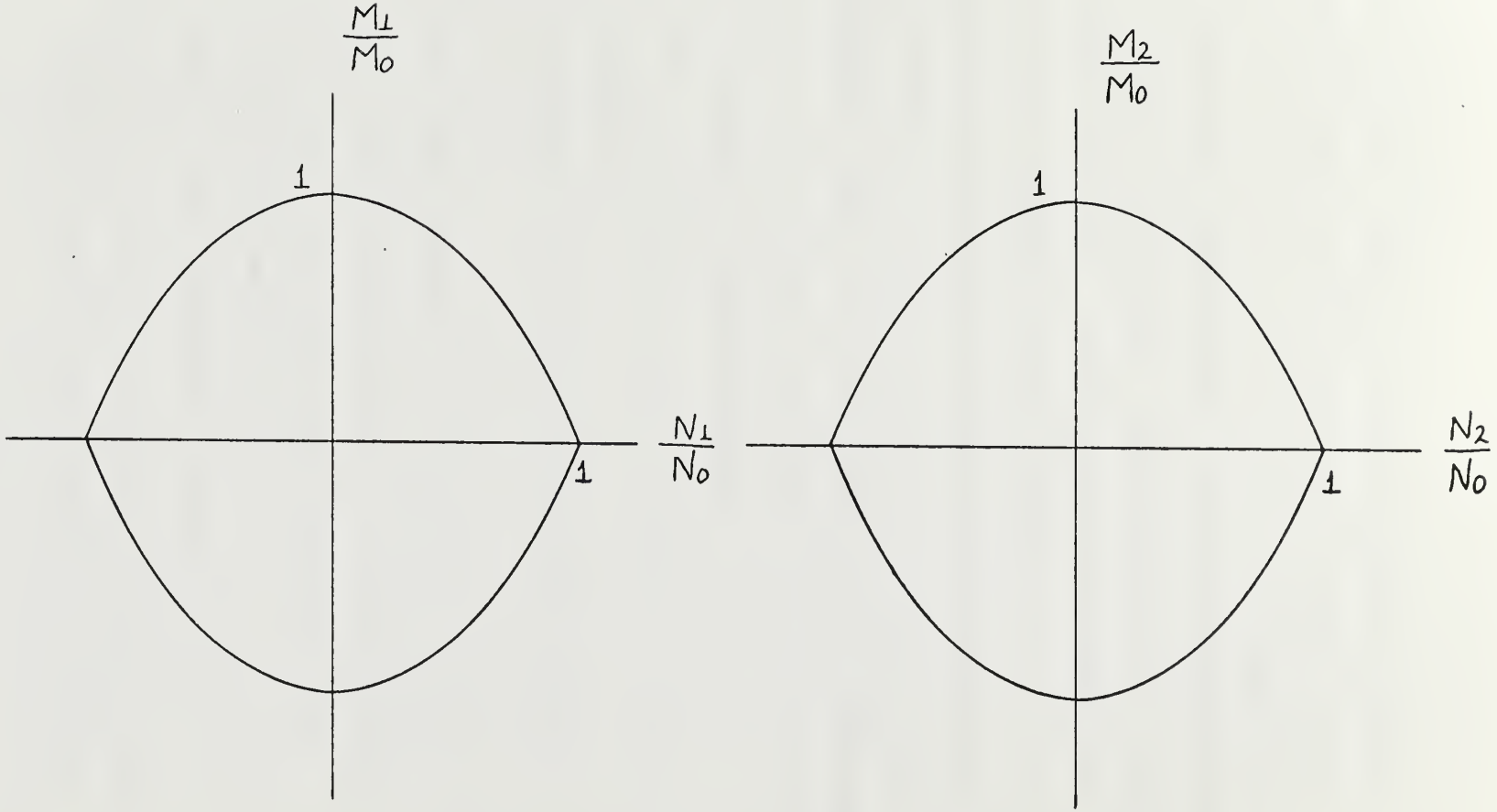

FIG. 4.2

Section 2. Discontinuities

In the mathematical theory of rigid-perfectly plastic shells, the possibility of discontinuities in displacement, displacement rate, and stress fields exists. It should be recognized of course that what may be a discontinuity in the rigid-perfectly plastic, midsurface representation of a shell would in the actual shell be a narrow zone across which the "discontinuous" field quantity varies rapidly.

Mathematical discontinuities and the associated notion of a generalized hinge are useful ideas in the model of an ideally plastic shell. Not all discontinuities are acceptable, however, and those which violate the assumptions of the shell theory should be identified and eliminated.

This examination extends the work of Hopkins on flat plates [4-7] to shells.

First let us examine displacements and displacement rates.

The in-surface displacements and displacement rates ($u_{\alpha 0}$ and $\dot{u}_{\alpha 0}$, α=1,2) may be discontinuous. Fracture is not considered in this thesis, and these discontinuities are interpreted as severe local deformation.

A discontinuity in the transverse displacement or displacement rate (w or $\dot{w}$) would correspond to severe transverse strain. The basic Love-Kirchoff assumption requires transverse strain to be zero. Therefore, w and $\dot{w}$ are assumed to be continuous.

The continuity of a quantity across a line in a shell imposes certain requirements on the derivatives of that quantity.

Figure 4.3a shows a simple curve $\Gamma(t)$ in the midsurface of a shell element. The s and n directions are tangent and normal to the curve, respectively. The curve Γ is shown in Figure 4.3b passing through a differential element of length ds and width dn centered on the point P(t). Γ divides the shell element into two regions as shown, R^+ and R^-. The points P', P_1', P_1, P_1'', P", P_2'', P_2, and P_2' lie on the boundary of the differential element.

Let us define the discontinuity of a field quantity G as one crosses the curve Γ at the point P as

$$[G]_P = G^+ - G^- \tag{4.1}$$

where

$$G^+ = \lim_{pp'' \to 0} G_{P''}$$

and

$$G^- = \lim_{pp' \to 0} G_{P'}$$

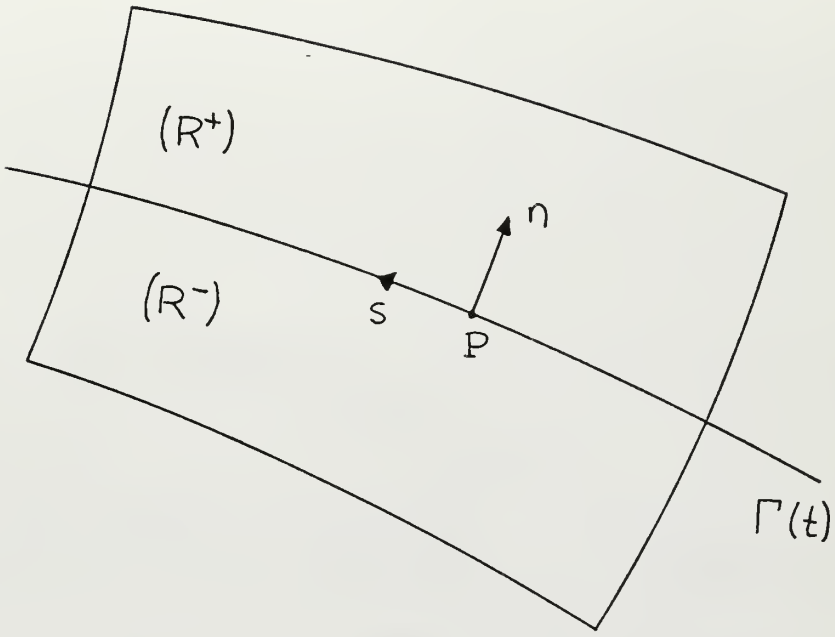

(a)

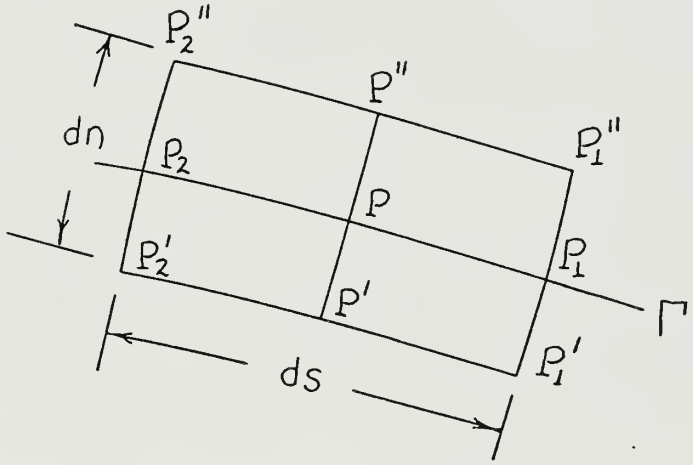

(b)

Fig. 4.3

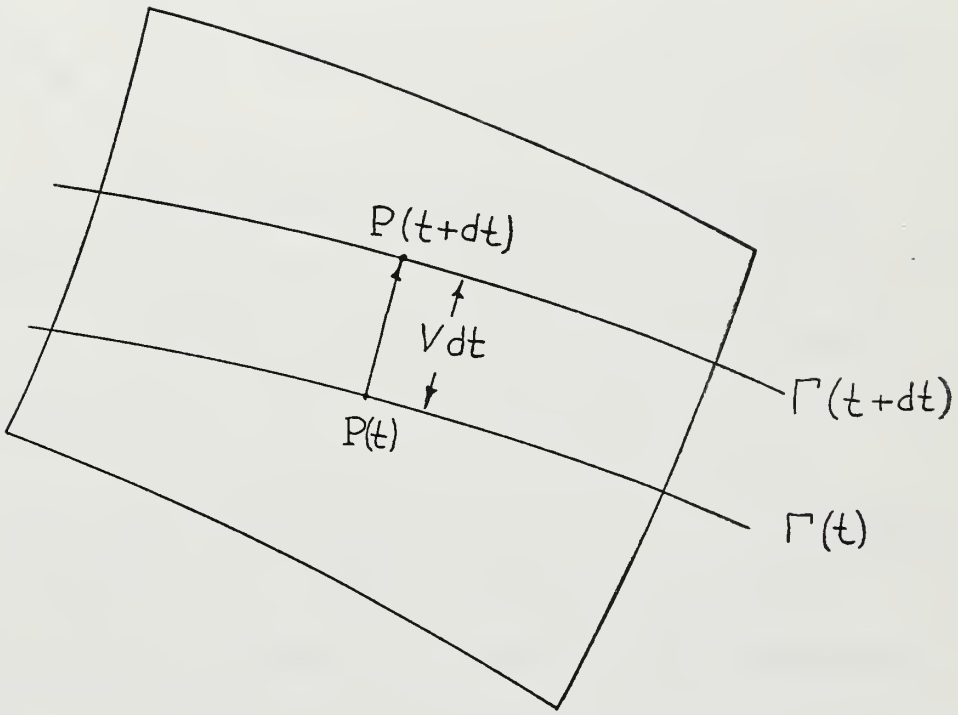

(c)

Fig. 4.3 (con't)

Let us suppose that [G] = 0 all along the curve Γ. Then

$$[G]_{P_1} = [G]_P = [G]_{P_2} = 0 \tag{4.2}$$

Therefore,

$$\lim_{ds \to 0} \frac{[G]_{P_2} - [G]_{P_1}}{ds} = [\frac{\partial G}{\partial s}] = 0 \tag{4.3}$$

That is, there is no discontinuity across Γ of the rate of change of G along Γ.

If we look at the position of Γ at two instants of time, t and t+dt, (Figure 4.3c)

$$[G]_{P(t)} = [G]_{P(t+dt)} = 0 \tag{4.4}$$

Since the curve Γ is assumed to be moving, the change in the discontinuity as a function of time is a function of both position and time, and leads to a substantial or material derivative [4-6].

$$\lim_{dt \to 0} \frac{[G]_{P(t+dt)} - [G]_{P(t)}}{dt} = V[\frac{\partial G}{\partial n}] + [\frac{\partial G}{\partial t}] = 0 \tag{4.5}$$

where V is the instantaneous velocity of Γ normal to the curve.

Equation (4.5) presents the following three possibilities:

If $V = 0$

$$[\frac{\partial G}{\partial t}] = 0$$

$[\frac{\partial G}{\partial n}]$ is not necessarily zero (4.6a)

If $V \neq 0$

either

$$[\frac{\partial G}{\partial n}] = [\frac{\partial G}{\partial t}] = 0 \quad (4.6b)$$

or

$$[\frac{\partial G}{\partial n}] = -\frac{1}{V}[\frac{\partial G}{\partial t}] \quad (4.6c)$$

Applying equations (4.3 and 4.6) to the continuous quantities w and $\dot{w}$ one finds (recalling that $\dot{w} = \frac{\partial w}{\partial t}$)

$$[\frac{\partial w}{\partial s}] = 0 \quad (4.7a)$$

$$[\frac{\partial \dot{w}}{\partial s}] = 0 \quad (4.7b)$$

If $V = 0$ (stationary hinge)

$[\frac{\partial w}{\partial n}]$ not necessarily zero (4.7c)

$[\frac{\partial \dot{w}}{\partial n}]$ not necessarily zero (4.7d)

$$[\ddot{w}] = 0 \quad (4.7e)$$

If $V \neq 0$ (travelling hinge)

$$[\frac{\partial w}{\partial n}] = 0 \tag{4.7f}$$

and either

$$[\frac{\dot{\partial w}}{\partial n}] = [\ddot{w}] = 0 \tag{4.7g}$$

or

$$[\frac{\dot{\partial w}}{\partial n}] = -\frac{1}{V}[\ddot{w}] \tag{4.7h}$$

The requirements for continuity of forces and moments across the line Γ at the point P are obtained by looking at the equilibrium of the differential element of Figure (4.3b). This element is redrawn in Figure (4.4) with the membrane and transverse shear forces indicated.

The condition of vertical force equilibrium can be expressed as

$$\left(\int_{P_1'}^{P_1''} - \int_{P_2'}^{P_2''}\right) Q_s \cos\omega \, dn + \left(\int_{P_1'}^{P_2''} - \int_{P_1''}^{P_2''}\right) Q_n \cos\delta \, ds$$

$$-\left(\int_{P_1'}^{P_2'} + \int_{P_1''}^{P_2''}\right) N_n \sin\delta \, ds - \left(\int_{P_1'}^{P_1''} + \int_{P_2'}^{P_2''}\right) N_s \sin\omega \, dn$$

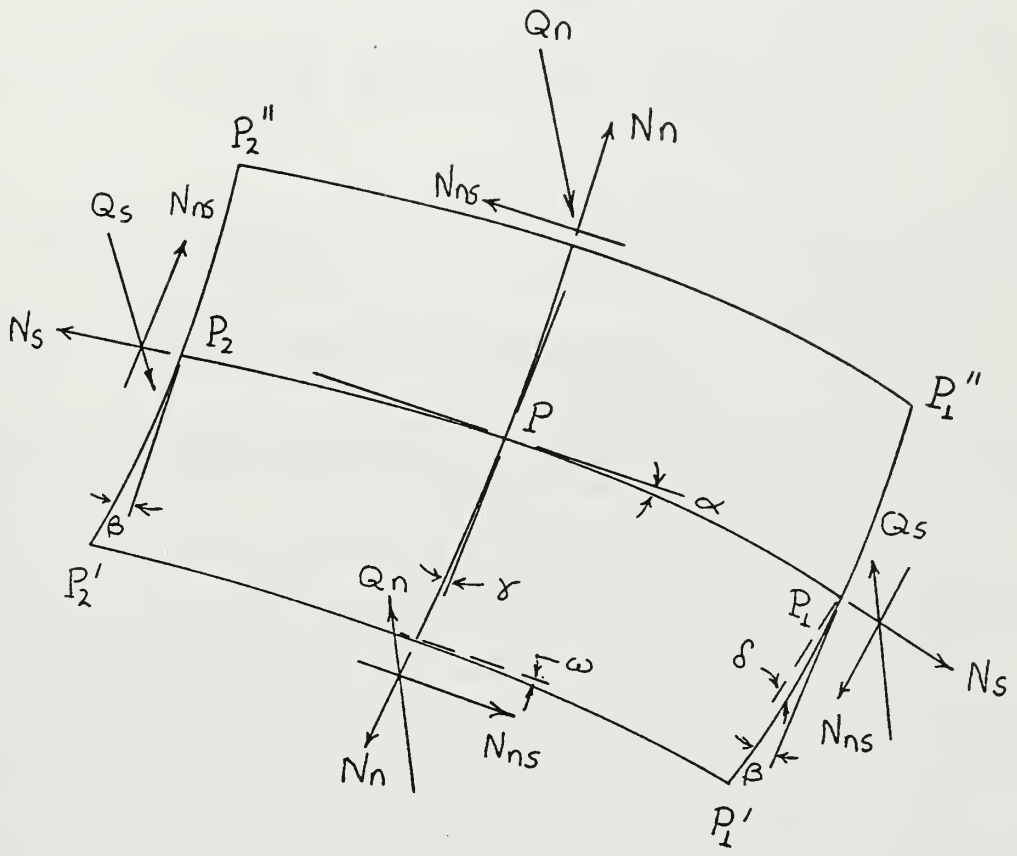

Fig. 4.4

$$+ \int_{P_1'}^{P_1''} \int_{P_2''}^{P_2'} (p_3 - \mu\ddot{w})\, dnds = 0 \qquad (4.8a)$$

If we now allow P_1' and P_1'' to approach P_1 and P_2' and P_2'' to approach P_2, dn and $d\phi$ approach zero. Then

$$\int_{P_1}^{P_2} [Q_n]\, ds = 0 \qquad (4.8b)$$

Finally, allow P_1 and P_2 to approach P to find that

$$[Q_n]_P = 0 \qquad (4.8c)$$

Similar operations with the force and moment equilibrium requirements in the s and n directions yield the following results.

$$[M_n]_P = [M_{ns}]_P = [N_n]_P = [N_{ns}]_P = 0 \qquad (4.8d)$$

The conclusion, therefore, is that only Q_s, N_s and M_s may be discontinuous across the curve Γ.

CHAPTER 5

RESPONSE OF ARBITRARY THIN SHELL TO DYNAMIC LOAD

Experience has shown that bodies which have been plastically deformed often have regions with little or no permanent strain separated by relatively narrow regions which have been severely strained. Although the regions of severe deformation have a finite width, they are often narrow enough to suggest the appearance of a line. These lines, or hinges, are normally thought of in conjunction with severe bending, which causes a discontinuity in the slope of the body. It was noted in Chapter 4, however, that discontinuities in other quantities can also occur in a body. The term "hinge" in this thesis will be construed to mean any line across which an allowable discontinuity in the stress field or the displacement field (or their derivatives) exists.

Although line hinges, that is, hinges of zero width, do not actually occur, the representation of such a hinge can be mathematically consistent within the framework of the thin shell assumptions so far introduced.

Since hinges appear to be lines, one would expect the dissipation of energy at a line hinge to be represented by a line integral. Such was the representation of the external work rate at a shell boundary used in Chapter 3 (equation 3.47b). It should therefore be instructive to look for line integral representations of shell energy dissipation expressions.

If there is no dissipation of energy at the shell boundary

(a restriction which will not be maintained for long), the external energy dissipation rate for a shell is the work rate of the external forces acting on the shell.

$$D_E = \int_S \{(P_1 - \mu\ddot{u}_{10})\dot{u}_{10} + (P_2 - \mu\ddot{u}_{20})\dot{u}_{20} + (P_3 - \mu\ddot{w})\dot{w}\}dS \qquad (5.1)$$

Each expression within parenthesis may be replaced by an expression involving the generalized stresses. The resulting equation, which will not be reproduced here, is simply obtained by use of equilibrium equations (3.53c, d and e).

Each term of the resulting expression can be integrated by parts over any region within which the term is continuous. This process leads to a line integral along the curve bounding the region and an area integral within the region.

Let us carry out the integration of a typical term, the first term in the $\dot{u}_{10}$ integrand, over a region of the mid-surface bounded by the curve C (Figure 5.1).

$$\int_{\eta_2\eta_1} [\int N_2 B_{,1} \dot{u}_{10} d\eta_1] d\eta_2 = \int \{N_2 B \dot{u}_{10}\}_{\eta_1} d\eta_2 - \int\int B(N_2 \dot{u}_{10})_{,1} d\eta_1 d\eta_2 \qquad (5.2)$$

where $\{\}_{\eta_1}$ indicates that the bracketed quantity is to be evaluated at the η_1 limits. For a given curve C the values of η_1 and η_2 are not independent, and the η_1 limits must be

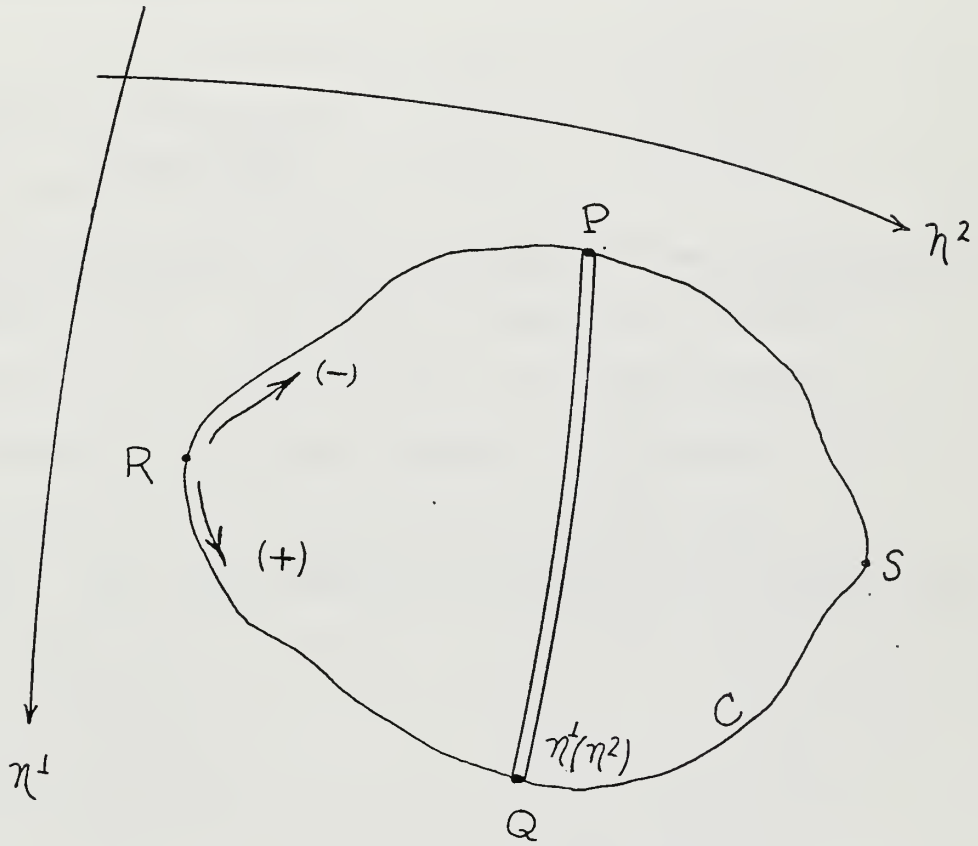

Fig. 5.1

expressed in terms of η_2 in order to continue integration of the first term on the right hand side of equation (5.2). This integration process is indicated schematically in Figure (5.1). The narrow strip indicates the integration over η_1 and the arrows indicate the η_2 integration. The η_2 integration can be thought of as

$$\underset{\text{(Path RQS)}}{\int\{N_2B\dot{u}_{10}\}d\eta_2} - \underset{\text{(Path RPS)}}{\int\{N_2B\dot{u}_{10}\}d\eta_2}$$

The sign of the second term is changed if the integration path is reversed to SPR. The entire integration is then in the counter-clockwise direction around the closed curve C and may be represented as a line integral. A counter-clockwise integration path is considered positive by convention [5-1]. The same reasoning applied to an integral of the form

$$\int\{F\}_{\eta_2}\, d\eta_1$$

leads to a clockwise integration path which, by convention, is considered negative.

The final result for the dissipation term being considered is

$$\int\int N_2B_{,1}\dot{u}_{10}d\eta_1d\eta_2 = \oint_C N_2B\dot{u}_{10}d\eta_2 - \int\int B(N_2\dot{u}_{10})_{,1}d\eta_1d\eta_2 \qquad (5.3)$$

The closed curve C would be chosen as a line across which a discontinuity in $(N_2\dot{Bu}_{10})$ exists. There may be several curves of discontinuity for each term of the dissipation integral. The contribution from each term is the sum of its associated area and line integrals from (and around) each region. Not all terms would, in general, have discontinuities at the same curves. Each term considered might have its own particular regions of continuity and hinge lines. Therefore each term should be separately summed. For simplicity in presenting the results of converting the dissipation integral to the sum of line and area integrals, only one summation index will be used, merely to serve as a reminder that summation of the contribution from the different regions is required. If the procedure described above is applied to each term of the dissipation integral which can have an allowable discontinuity, the final result is

$$D_E = \sum_n [\emptyset\{[N_2 - N_1 - \frac{M_1}{R_1} + \frac{M_2}{R_1}]\dot{Bu}_{10} - 2(N_{12} + \frac{M_{12}}{R_2})\dot{Bu}_{20} -$$

$$[\frac{N_1 B\dot{w},1}{A} + N_{12}\dot{w},2 + \frac{(M_1 B),1}{A} + M_{12,2} + \frac{2M_{12}A,2}{A} - \frac{M_2 B,1}{A_1}]\dot{w}$$

$$+ (N_1 w + M_1)\frac{B}{A}\dot{w},1 + (N_{12}w + M_{12})\dot{w},2\}d\eta_2$$

$$- \emptyset\{[N_1 - N_2 - \frac{M_2}{R_2} + \frac{M_1}{R_2}]A\dot{u}_{20} - 2(N_{12} + \frac{M_{12}}{R_1})A\dot{u}_{10} -$$

$$[\frac{N_2 A w}{B},_2 + N_{12}w,_1 + \frac{(M_2 A)}{B},_2 + M_{12},_1 + \frac{2M_{12}B}{B},_1 - \frac{M_1 A}{B},_2]\,\dot{w}$$

$$+ (N_2 w + M_2)\frac{A}{B}\,\dot{w},_2 + (N_{12}w + M_{12})\,\dot{w},_1\}d\eta_1$$

$$+\int\int\{-B(N_2\dot{u}_{10}),_1 + N_1 B\dot{u}_{10},_1 + M_1 B(\frac{\dot{u}_{10}}{R_1}),_1 - B(\frac{M_2\dot{u}_{10}}{R_1}),_1$$

$$+ N_{12}B\dot{u}_{20},_1 + B(N_{12}\dot{u}_{20}),_1 + M_{12}B(\frac{\dot{u}_{20}}{R_2}),_1$$

$$+ B(\frac{M_{12}\dot{u}_{20}}{R_2}),_1 + N_{12}A\dot{u}_{10},_2 + A(N_{12}\dot{u}_{10}),_2$$

$$+ M_{12}A(\frac{\dot{u}_{10}}{R_1}),_2 + A(\frac{M_{12}\dot{u}_{10}}{R_1}),_2 - A(N_1\dot{u}_{20}),_2 + N_2 A\dot{u}_{20},_2$$

$$+ M_2 A(\frac{\dot{u}_{20}}{R_2}),_2 + A(\frac{M_1\dot{u}_{20}}{R_2}),_2 + AB(\frac{N_1}{R_1} + \frac{N_2}{R_2})\dot{w} + M_{12},_2\dot{w},_1$$

$$+ M_{12},_1\dot{w},_2 + \frac{2M_{12}A,_2\dot{w},_1}{A} - \frac{M_2 B,_1\dot{w},_1}{A} + \frac{2M_{12}B,_1\dot{w},_2}{B}$$

$$- \frac{M_1 A,_2\dot{w},_2}{B} - (\frac{N_1 B\dot{w},_1}{A}),_1 w - (N_{12}\dot{w},_2),_1 w - M_1 B(\frac{\dot{w},_1}{A}),_1$$

$$-(\frac{N_2 A\dot{w},_2}{B}),_2 w - (N_{12}\dot{w},_1),_2 w - M_2 B(\frac{\dot{w},_2}{B}),_2\}\,d\eta_1 d\eta_2 \quad (5.4)$$

If the external energy dissipation rate expressed in terms of external load and displacement rates (equation 5.1) were equated to the external dissipation rate expressed in terms of the generalized stresses and the displacement rates (equation 5.4), and if the generalized stresses were expressed in terms of the displacements and the displacement rates through use of the material yield surface and the rule of normality, then the displacement field could be found as a function of time, in principle. The extreme complexity of such an endeavor has precluded exact solution of such a problem except for very simple cases.

In the next chapter the general results of this chapter will be specialized to a shell of revolution, and an approximate solution of the shell response to dynamic load will be presented.

It should be noted that the general dissipation equation (5.4) can include hinge lines which coincide with the physical boundaries of the shell. Therefore, the external work done at a shell boundary can also be accounted for, effectively removing the restriction imposed before equation (5.1).

CHAPTER 6

AN APPROXIMATE METHOD FOR DETERMINING THE RESPONSE OF A THIN SHELL OF REVOLUTION TO AXISYMMETRIC DYNAMIC LOAD

In Chapter 5 the external energy dissipation rate of a general, thin shell of uniform thickness was developed in terms of area and line integrals involving the generalized stresses, the displacement rates, the transverse displacement (if deflections are finite), and their derivatives. The line integrals represent mathematically the possibility of hinges in a rigid-perfectly plastic material.

In this chapter the general results indicated in Chapter 5 are specialized to the case of a thin shell of revolution which is subjected to an axisymmetric dynamic load. Neither buckling nor nonsymmetric response is considered.

A commonly used coordinate system for shells of revolution is indicated in Figure 6.1 along with the positive directions of transverse and meridional load and displacement. It is assumed that there are no loads or displacements in the circumferential direction.

Table 6.1 relates the symbols used for general shells in previous chapters to the symbols commonly used for this axisymmetric class of problems.

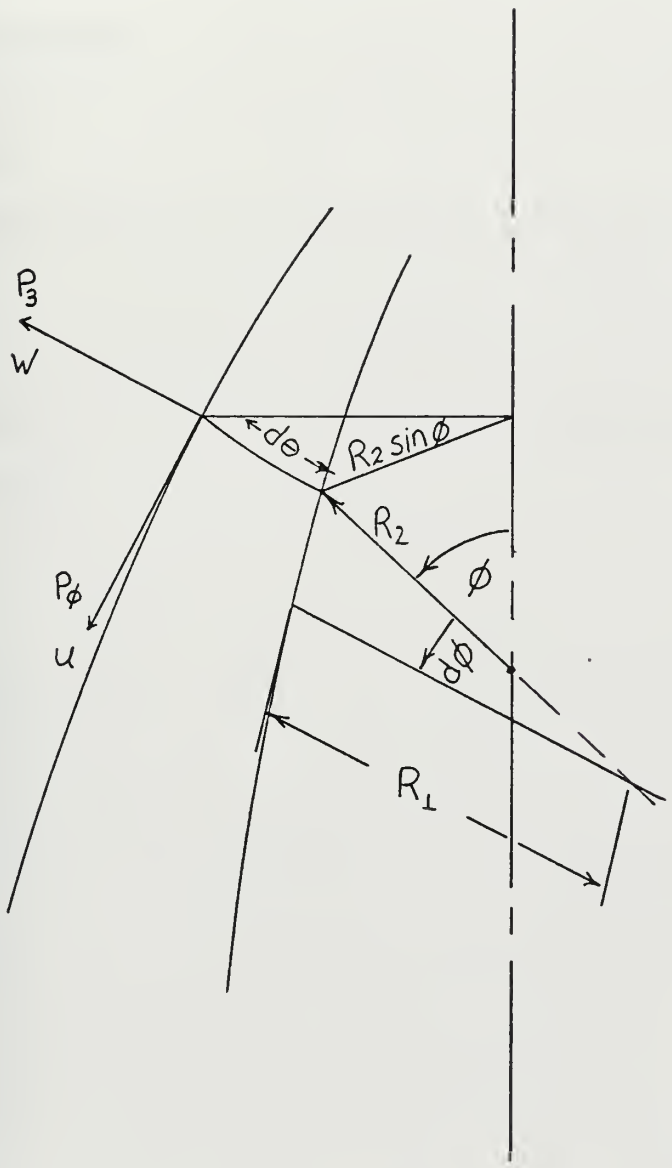

Fig. 6.1

TABLE 6.1

AXISYMMETRIC SHELL PROBLEM SYMBOLS

AND THEIR GENERAL SHELL PROBLEM COUNTERPARTS

Axisymmetric	General
z	z
ϕ	η_1
θ	η_2
R_1	R_1
R_2	R_2
R_1	A
$R_2 \sin\phi$	B
u	u_{10}
w	w
ε_ϕ	ε_{10}
ε_θ	ε_{20}
γ_0	γ_0
κ_ϕ	κ_1
κ_θ	κ_2
$\kappa_{\phi\theta}$	κ_{12}
$M_\phi;\ N_\phi;\ Q_\phi$	$M_1;\ N_1;\ Q_1$
$M_\theta;\ N_\theta;\ Q_\theta$	$M_2;\ N_2;\ Q_2$
P_ϕ	P_1
P_3	P_3

Since the geometry of this class of shells does not vary with θ, the derivatives of all geometric quantities with respect to θ are identically equal to zero.

Because of the assumed axisymmetry of the load (and the shell response) the derivatives of all stresses and displacements with respect to θ are also identically equal to zero.

The non-zero rate equations (3.44a, b, d, e) reduce to

$$\dot{\varepsilon}_\phi = \frac{1}{R_1}\left(\dot{u}' + \dot{w} + \frac{w'\dot{w}'}{R_1}\right) \tag{6.1a}$$

$$\dot{\varepsilon}_\theta = \frac{1}{R_2}\left(\dot{u}\cot\phi + \dot{w}\right) \tag{6.1b}$$

$$\dot{\kappa}_\phi = \frac{1}{R_1^2}\left[\dot{u}' - \dot{w}'' + \frac{(\dot{w}'-\dot{u})R_1'}{R_1}\right] \tag{6.1c}$$

$$\dot{\kappa}_\theta = \frac{\cot\phi}{R_1 R_2}\left(\dot{u}-\dot{w}'\right) \tag{6.1d}$$

where

$$(\,)' \equiv \frac{d(\,)}{d\phi}$$

The equilibrium equations (3.53) reduce to

$$R_1R_2\sin\phi(P_\phi - \mu\ddot{u}) - N_\theta R_1\cos\phi + (N_\phi R_2\sin\phi)' + \frac{(M_\phi R_2\sin\phi)'}{R_1} - M_\theta\cos\phi = 0 \tag{6.2a}$$

$$R_1R_2 \sin\phi(P_3 - \mu\ddot{w}) - N_\phi R_2 \sin\phi - N_\theta R_1 \sin\phi +$$

$$\left(\frac{N_\phi R_2 \sin\phi\, w'}{R_1}\right)' + \left[\frac{(M_\phi R_2 \sin\phi)'}{R_1}\right]' - (M_\theta \cos\phi)' = 0 \qquad (6.2b)$$

$$Q_\phi = \frac{\cot\phi}{R_2}(M_\theta - M_\phi) - \frac{M'_\phi}{R_1} \qquad (6.2c)$$

Noting that the differential midsurface area, dS, is

$$dS = (2\pi R_2 \sin\phi)\, R_1 d\phi$$

and neglecting external work at the shell boundary, the external energy dissipation rate can be expressed in terms of external loads as

$$D_E = 2\pi \int [(P_\phi - \mu\ddot{u})\dot{u} + (P_3 - \mu\ddot{w})\dot{w}]\, R_1R_2 \sin\phi d\phi \qquad (6.3)$$

The dissipation rate in terms of area integrals and line integrals may be obtained from the general results (equation 5.4) or by applying the procedure of Chapter 5 to equation (6.3). Application of the procedure to a portion of the dissipation integral is demonstrated in this chapter.

Symmetry limits hinge curves in the rigid perfectly-plastic material to circles (ϕ = constant), and the regions of continuity for each term of the dissipation integral are

therefore each bounded by two circles. Since there is no variation with θ, the problem is essentially one-dimensional.

Regions in which a typical term of the dissipation integrand (expressed in terms of the generalized stresses) is continuous are indicated in Figure 6.2.

Integration by parts of such a typical term gives

$$\int(-N_\phi R_2 \sin\phi)' \dot{u}\, d\phi = \sum_n \int N_\phi R_2 \sin\phi \dot{u}' d\phi - \sum_n \{N_\phi R_2 \sin\phi \dot{u}\} \quad (6.4)$$

where { } indicates that the expression is to be evaluated between the upper and lower limits ϕ_m corresponding to the nth region.

Indicating the value of $(N_\phi R_2 \sin\phi\dot{u})$ evaluated by approaching ϕ_m from below as $(\ )_m^-$ and from above as $(\ )_m^+$, the second term on the right hand side of equation (6.4) can be expressed as

$$-\sum_n \{N_\phi R_2 \sin\phi \dot{u}\} = -\sum_m [(\ )_{m+1}^- - (\ )_m^+] \quad (6.5)$$

If the summation over m is expanded and the terms grouped according to the plastic hinge index m, this becomes

$$-\sum_n \{N_\phi R_2 \sin\phi \dot{u}\} = -[(\ )_1^- - (\ )_1^+] - [(\ )_2^- - (\ )_2^+] -$$

$$\cdots = +\sum_m [N_\phi R_2 \sin\phi \dot{u}]_m \quad (6.6)$$

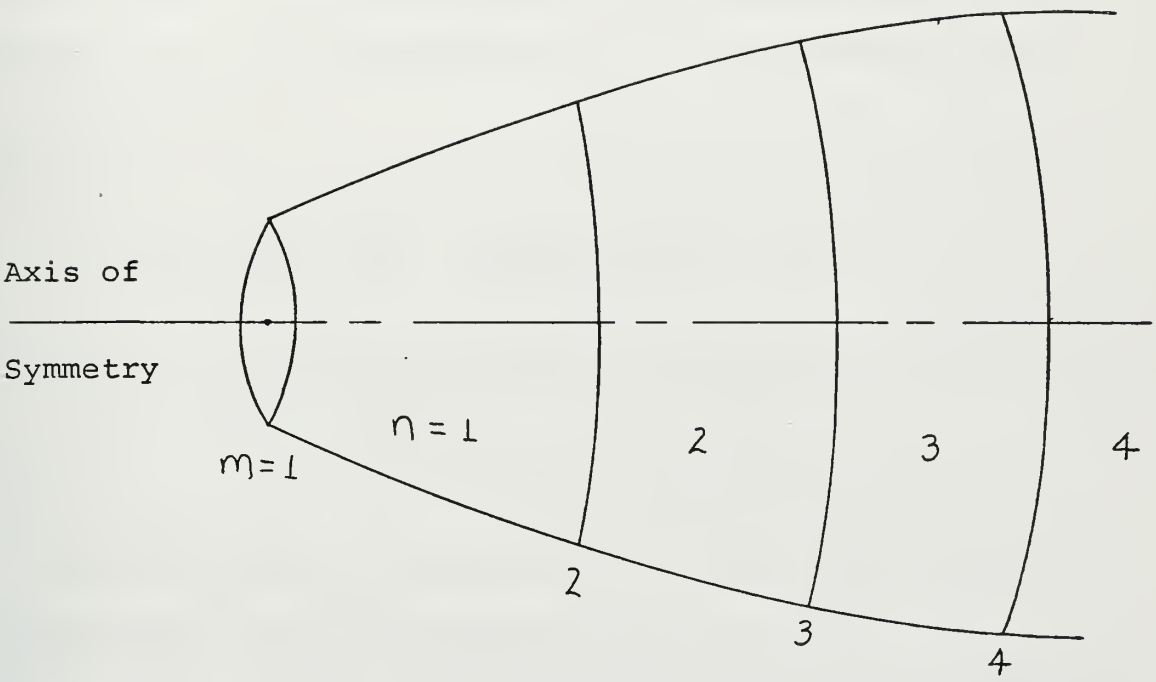

Fig. 6.2

where $[F]_m$ indicates the discontinuity in F across the hinge circle $\phi = \phi_m$. That is, $[F]_m = F_m^+ - F_m^-$.

If attention is restricted to shells with smooth generators, geometrical factors such as $R_2 \sin\phi$ are not discontinuous. Let the notation $(G)_m$ indicate that the function G is to be evaluated at ϕ_m. Then equation (6.4) can be written as

$$\int(-N_\phi R_2 \sin\phi)' \dot{u} d\phi = \sum_n \int N_\phi R_2 \sin\phi \, \dot{u}' \, d\phi$$

$$+ \sum_m (R_2 \sin\phi)_m [N_\phi \dot{u}]_m \qquad (6.7)$$

Investigation of discontinuities across the hinge circles based on the assumption that the w and $\dot{w}$ are continuous everywhere and based on the interpretation that a mathematical discontinuity in u merely represents a very large local strain yields the following results (c.f. Chapter 4).

$$[M_\phi] = [N_\phi] = [Q_\phi] = 0 \qquad (6.8a)$$

[w'] may be different from zero at a stationary hinge. (6.8b)

$[\dot{w}']$ may be different from zero at a travelling hinge. (6.8c)

Since $[M_\phi]$ and $[Q_\phi]$ are both zero, equation (6.2c) shows that

$$[M_\phi'] = \frac{R_1 \cot\phi}{R_2} [M_\theta] \tag{6.9}$$

With the discontinuity results of equations (6.8) and (6.9) and the notation of equation (6.7), the external dissipation rate expression for the axisymmetric case may be written as

$$\frac{D_E}{2\pi} = -\int_\phi \{\sum_i N_\theta' R_2 \sin\phi + \sum_g (\frac{M_\theta}{R_1})' R_2 \sin\phi + \sum_m \frac{M_\phi R_1' R_2 \sin\phi}{R_1^2}\} \dot{u} d\phi$$

$$+\int_\phi \{\sum_n N_\phi R_2 \sin\phi - \sum_i N_\theta R_2 \sin\phi + \sum_m \frac{M_\phi R_2 \sin\phi}{R_1}$$

$$- \frac{M_\theta R_2 \sin\phi}{R_1}\} \dot{u}' d\phi + \int_\phi \{N_\phi R_2 + N_\theta R_1\} \sin\phi \, \dot{w} d\phi$$

$$+\int_\phi \{\sum_\kappa \frac{R_1' R_2 \sin\phi}{R_1^2} (N_\phi w + M_\phi) - \sum_\kappa (N_\phi R_2 \sin\phi)' \frac{w}{R_1}$$

$$- M_\theta \cos\phi\} \dot{w}' d\phi - \int_\phi \{\sum_\kappa \frac{R_2 \sin\phi}{R_1} (N_\phi w + M_\phi)\} \dot{w}'' d\phi$$

$$+ \sum_q \{R_2 \sin\phi (N_\phi + \frac{M_\phi}{R_1})\}_q [\dot{u}]_q - \sum_p (R_2 \sin\phi)_p [N_\theta \dot{u}]_p$$

$$- \sum_y (\frac{R_2 \sin\phi}{R_1})_y [M_\theta \dot{u}]_y - \sum_\kappa (\frac{R_2 \sin\phi \{N_\phi w + M_\phi\}}{R_1})_\kappa [\dot{w}']_\kappa$$

$$+ \sum_{\kappa} \left(\frac{R_2 \sin\phi N_\phi \dot{w}}{R_1}\right)_\kappa [w']_\kappa \qquad (6.10)$$

It should be noted that the nonlinear terms in w appear only if finite deflections are considered. One of these, the final term of equation (6.10), can be shown to be zero.

Continuity considerations revealed that [w'] could be different from zero at a stationary hinge only. Now $[w'] \neq 0$ implies that w" and $\dot{w}$" are infinite and, therefore, that $\dot{\kappa}_\phi$ is infinite. For the exact Tresca yield surface of shells of revolution (Onat and Prager [6-1]), normality requires the ratio $\dot{\kappa}_\phi/\dot{\varepsilon}_\phi$ to be finite unless N_ϕ is zero. Finite deflections give rise to membrane forces and, therefore, $\dot{\varepsilon}_\phi$ would also be infinite. If the shell stretched at a hinge with an infinite rate for a finite period of time, infinite thinning would occur. The finite deflection term involving [w'] is therefore zero.

Solution of equation (6.10) in terms of displacements as functions of time and position is a very complex problem, and is made more so because of the presence of travelling hinges.

In order to simplify the problem, let us restrict our attention to problems with transverse loading only.

For the remainder of this chapter it will be assumed that $P_\phi = 0$ and that $\ddot{u} = 0$. Therefore, the integrals and hinge terms involving $\dot{u}$ are identically zero.

Another approximation, suggested by Sawczuk [6-2] and by Jones [6-3] for the static and dynamic response, respectively, of flat plates, is also used.

Although the discontinuity [$\dot{w}'$] can only exist at a travelling hinge, let us treat such a hinge as if it is in fact stationary and formed at the same location at which a static collapse hinge would form. Identical displacement profiles for static collapse and for dynamic response have been found for cases such as square plates [6-4], circular plates [6-5], and cylindrical shells [6-6], if the applied load does not greatly exceed the static collapse load.

If the external dissipation rate expression for the transverse load problem in terms of generalized stresses is equated to the dissipation rate expression in terms of external load, the result is

$$\frac{D_E}{2\pi} = \int_\phi \{N_\phi R_2 \sin\phi + N_\theta R_1 \sin\phi\}\dot{w}d\phi +$$

$$\sum_k \int_\phi \{\frac{R_1' R_2 \sin\phi}{R_1^2} (N_\phi w + M_\phi) - (N_\phi R_2 \sin\phi)' \frac{w}{R_1}\} \dot{w}'d\phi -$$

$$\int_\phi M_\theta \cos\phi \, \dot{w}'d\phi - \sum_k \int_\phi \frac{R_2 \sin\phi}{R_1} (N_\phi w + M_\phi) \, \dot{w}''d\phi \; -$$

$$\sum_\kappa \{\frac{R_2 \sin\phi}{R_1} (N_\phi w + M_\phi)\}_\kappa [\dot{w}']_\kappa = \int_\phi R_1 R_2 \sin\phi (P_3 - \mu\ddot{w})\dot{w}d\phi \quad (6.11)$$

where boundary loading has been omitted for simplicity.

To use equation (6.11) in estimating the permanent deflection of a shell of revolution subjected to an axisymmetric, transverse dynamic load, one begins by assuming a kinematically admissible velocity profile whose shape is time independent. The static collapse profile is suggested, if known.

$$\dot{w}(\phi,t) = \dot{w}_0(t) \cdot f(\phi) \tag{6.12}$$

where $f(\phi)$ is the deformation velocity mode and $\dot{w}_0(t)$ is the velocity mode amplitude.

The velocity profile of the assumed mode of deformation is used with equations (6.1) to determine the strain and curvature rates.

The rate equations are used in conjunction with the assumed yield surface and its associated flow rule (normality) in order to determine the values of the corresponding generalized stresses.

The expressions derived for the generalized stresses are entered into equation (6.11) and the indicated summations and integrations performed. The result, after factoring out common coefficients, is a second order differential equation in w_0 and time. The equation will be nonlinear if finite deflections have been retained.

The exact formulation of this differential equation is dependent upon several factors such as shell geometry, assumed deformation mode, and assumed yield surface. Specific examples are given in Chapter 8.

The method of solving the differential equation depends upon its formulation and upon whether or not the pressure pulse shape is known. If the shape of the pulse is not known or if it is a high pressure, short duration pulse, the problem can be treated as impulsive loading.

If the time history of the pressure pulse is to be used, the initial conditions are

$$w_0(t=0) = \dot{w}_0(t=0) = 0.$$

If, however, impulsive loading is assumed, the initial conditions are

$$w_0(t=0) = 0$$

$$\dot{w}_0(t=0) = \nu V_0$$

where V_0 is the actual impulsive velocity at the location of $\dot{w}_0$, and ν is the Martin and Symonds mode factor for optimum matching of the actual impulsive problem with the mode approximation (time independent profile) [6-7]. Equation (6.11) reduces to the flat plate approximation of Jones [6-3].

CHAPTER 7

APPROXIMATE RESPONSE OF NON-SYMMETRIC SHELL TO DYNAMIC LOAD

The solution technique of Chapter 5 can be applied, in principle, to any shell which satisfies the usual thin shell theory assumptions. In this chapter, however, an approximate technique is investigated which is not derived from the previous results. The technique for dynamic loads developed here is a simple extension of a static collapse method proposed by Janas for the limit analysis of non-symmetric shells [7-11]. Finite deflections have not been included.

The basic assumption used in this approach is that the body deforms as several rigid regions separated by narrow plastic hinges. The plastic hinges are viewed mathematically as curves. The results of severe membrane strain, twisting, and bending rates are viewed in terms of discontinuities in velocities and relative rotation rates between rigid regions at the hinge curves. All internal energy dissipation occurs in the plastic hinges, and, according to the principle of virtual velocities, the external work rate must equal the internal energy dissipation rate. The dissipation rate can be expressed as a function of the hinge discontinuities.

Consider a hinge separating rigid regions I and II to have a small width λ, as shown in Figure 7.1. Because transverse shear strain is assumed to be zero, there can be no discontinuity in the transverse displacement rate $\dot{w}$. The only displacement rate discontinuities

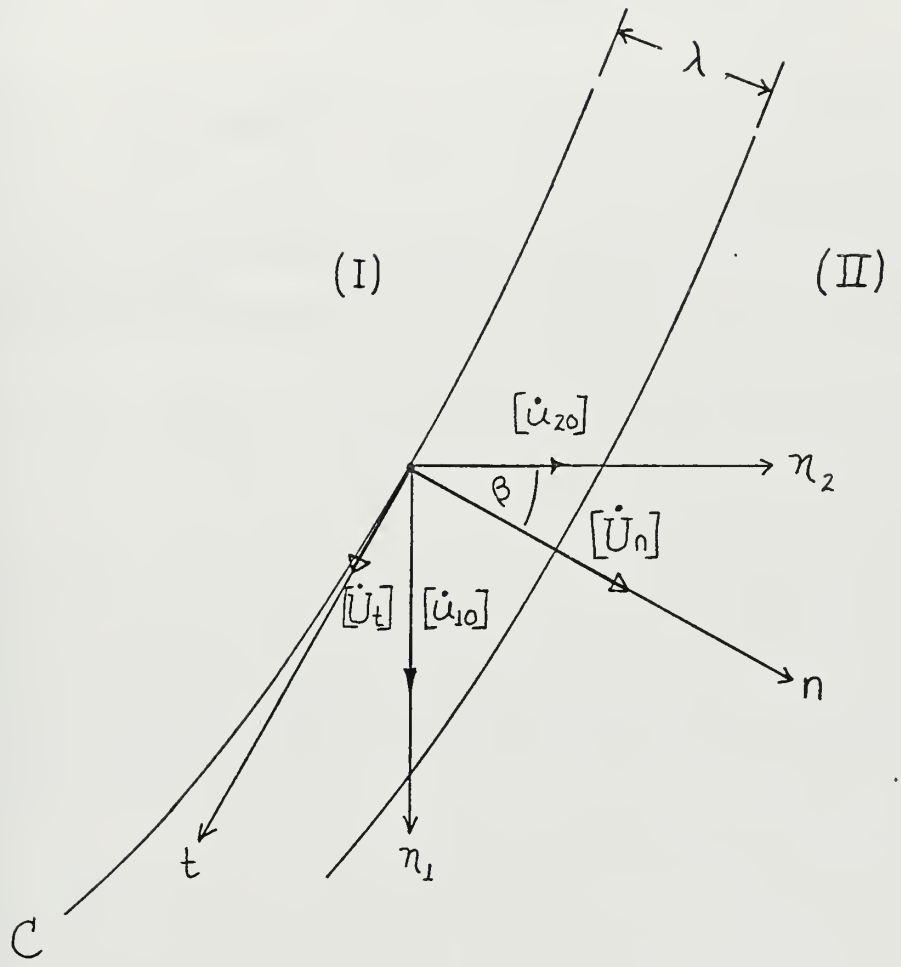

Fig. 7.1

then are $[\dot{u}_{10}]$ and $[\dot{u}_{20}]$ corresponding to the shell coordinate axes η_1 and η_2.

The velocity discontinuity components normal to and tangent to the hinge curve C are seen to be

$$[\dot{U}_n] = [\dot{u}_{20}] \cos\beta + [\dot{u}_{10}] \sin\beta \tag{7.1a}$$

and

$$[\dot{U}_t] = [\dot{u}_{10}] \cos\beta - [\dot{u}_{20}] \sin\beta \tag{7.1b}$$

where β is the angle between the normal to the hinge curve and the coordinate axis η_2.

Regions I and II are rigid and the length of the hinge curve can not change. Therefore,

$$\dot{\varepsilon}_t = 0 \tag{7.2a}$$

If one assumes that the displacement rates vary linearly across the width,

$$\dot{\varepsilon}_n = \frac{[\dot{U}_n]}{\lambda} \tag{7.2b}$$

and

$$\dot{\gamma}_{nt} = \frac{[\dot{U}_t]}{\lambda} \tag{7.2c}$$

By transformation of axes it can be shown that

$$\dot{\varepsilon}_{10} = \frac{[\dot{u}_{10}]}{\lambda} \sin\beta \tag{7.3a}$$

$$\dot{\varepsilon}_{20} = \frac{[\dot{u}_{20}]}{\lambda} \cos\beta \tag{7.3b}$$

$$\dot{\gamma}_0 = \frac{[\dot{u}_{10}] \cos\beta + [\dot{u}_{20}] \sin\beta}{\gamma} \tag{7.3c}$$

By similar reasoning one finds the curvature rates across the plastic hinge.

$$\dot{\kappa}_1 = \frac{\dot{\Omega}_1}{\lambda} \sin\beta \tag{7.4a}$$

$$\dot{\kappa}_2 = \frac{\dot{\Omega}_2}{\lambda} \cos\beta \tag{7.4b}$$

$$2\dot{\kappa}_{12} = \frac{\dot{\Omega}_1 \cos\beta + \dot{\Omega}_2 \sin\beta}{\lambda} \tag{7.4c}$$

where $\dot{\Omega}_\alpha$ is the η_α component of the relative rotation rate between rigid regions I and II.

The internal dissipation rate is

$$D_i = \int_{\substack{S \\ \text{hinge}}} (N_1 \dot{\varepsilon}_{10} + N_2 \dot{\varepsilon}_{20} + N_{12} \dot{\gamma}_0 + M_1 \dot{\kappa}_1 + M_2 \dot{\kappa}_2 + 2M_{12} \dot{\kappa}_{12}) \, dS \tag{7.5}$$

If it is assumed that the generalized stress values are uniform across the hinge zone, and if it is noted that

$$dS = \lambda dC$$

then equation (7.5) can be written in the form

$$D_i = \int_C \{N_1[\dot{u}_{10}] \sin\beta + N_2[\dot{u}_{20}] \cos\beta + N_{12}[\dot{u}_{10}] \cos\beta + N_{12}[\dot{u}_{20}] \sin\beta + M_1 \dot{\Omega}_1 \sin\beta + M_2 \dot{\Omega}_2 \cos\beta + 2M_{12} \dot{\Omega}_1 \cos\beta + 2M_{12} \dot{\Omega}_2 \sin\beta\} dC \qquad (7.6)$$

A limited interaction yield surface is assumed which reduces to the two moment limited interaction yield surface (c.f. Chapter 4) for $N_{12} = M_{12} = 0$. It is assumed that membrane shear strain can occur only if $N_{12} = \frac{1}{2} N_0$ and that twisting can occur only if $M_{12} = \frac{1}{2} M_0$. The factor of one half arises from the fact that the yield stress for shear is one half the yield stress in simple tension.

The limited interaction yield surface is shown in Figure 7.2.

The scale of the similar yield surface which would inscribe the exact six-dimensional Tresca yield surface is not known because the six-dimensional Tresca yield surface has not

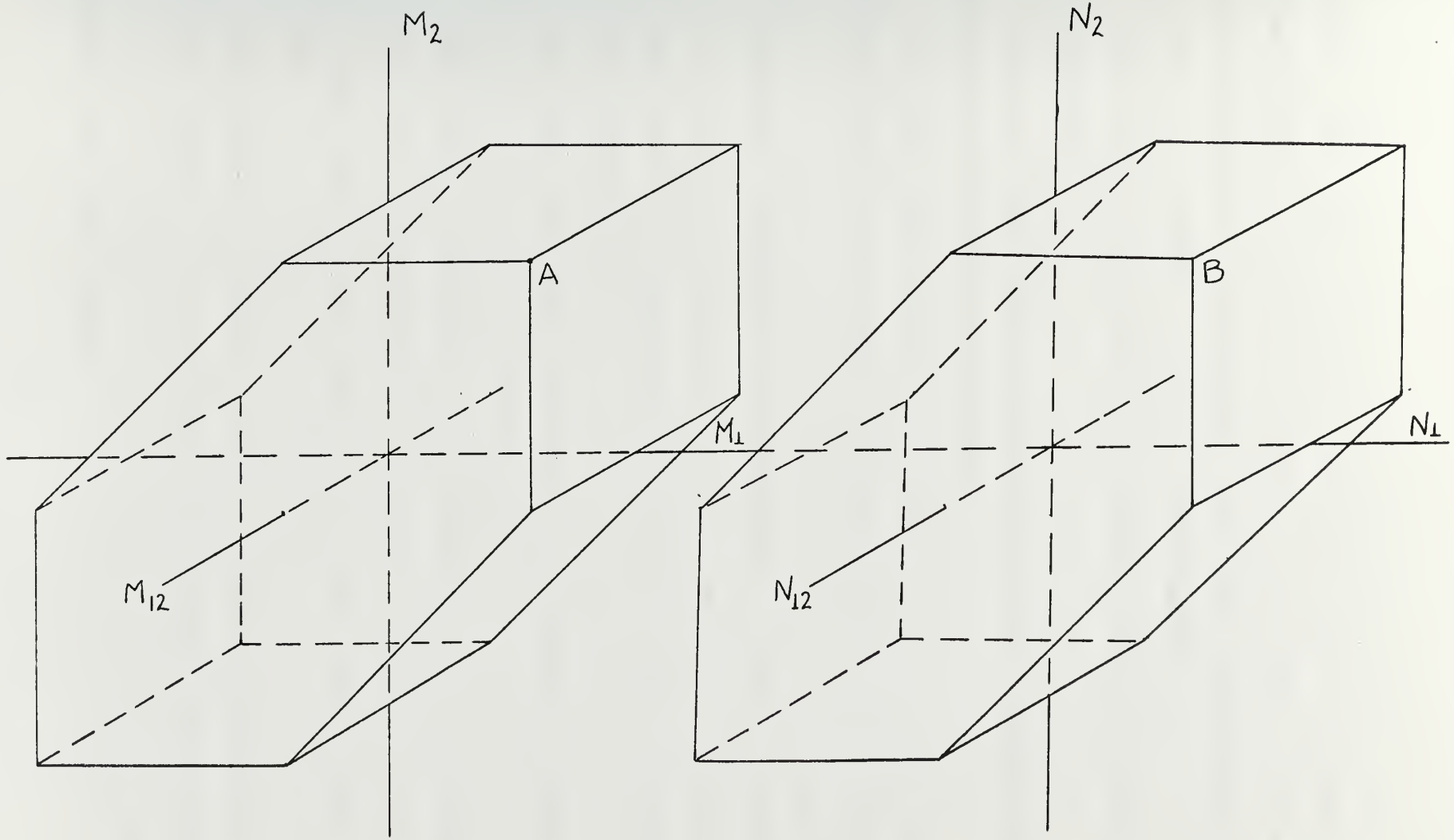

FIG. 7.2

been developed. The scale of the inscribing surface can be no larger than 0.618, which is the scale of the two moment limited interaction surface inscribed in the Tresca surface in four-dimensional stress space. The value 0.618 is used in this thesis as the best available scale factor.

The solution to a particular problem would be carried out as follows.

First a collapse mode is postulated which involves rigid body motion of one or more regions.

The rigid body equations of motion for each region are examined at each hinge curve to determine the velocity discontinuities and the relative rotation rates between regions. The condition of continuity of transverse velocity $\dot{w}$ may be used to determine the equation of one or more hinge curves. All velocities may be expressed in terms of a characteristic transverse velocity $\dot{w}_0$.

The strain rates and curvature rates are used to determine the corresponding generalized stresses.

The internal dissipation rate (equation 7.6) is equated to the external dissipation rate (equation 5.1). The resultant second order differential equation in w_0 and time can then be solved for the permanent deformation w_0.

The procedure indicated in this chapter has been used to solve the problem of a cylindrical panel loaded impulsively over a portion of the shell inner surface. The results are reported in the next chapter.

Extension of this technique to include finite deflections is not conceptually difficult. The major difference is that the path of a point in the midsurface of a shell region undergoing rigid body rotation must be recognized as the arc of a circle rather than assumed to be the tangent to the arc.

Rigid body motion cannot be limited, in general, such that transverse displacements are much larger than in-surface displacements. Non-linear terms involving all of the displacements could therefore be expected to arise in finite deflection problems.

CHAPTER 8

APPLICATION OF GENERAL METHODS TO PARTICULAR CASES

Section 1: Complete Spherical Shell Subjected to Uniformly Distributed, Exponentially Decaying Pressure

As a first example let us examine the case of a complete spherical shell of radius R and thickness h subjected to a uniformly distributed, exponential internal pressure, p_3. Comparison will be made with the infinitesimal deflection, two-moment limited interaction (Figure 4.1) solution of Sankaranarayanan [8.1].

The deformation field for this trivial problem is one of uniform radial expansion.

The velocity field is

$$\dot{w}(\phi,t) = \dot{w}_0(t) \geq 0 \tag{8.1}$$

There is no bending ($M_\phi = M_\theta = 0$); therefore, normality requires that

$$N_\phi = N_\theta = N_0 \tag{8.2}$$

where

$$N_0 = \sigma_0 h$$

Dissipation equation (6.11) reduces to

$$2\int_0^{\frac{\pi}{2}} 2R\sin\phi \quad N_0 \dot{w}_0 \, d\phi = 2\int_0^{\frac{\pi}{2}} R^2\sin\phi \, (p_3 - \mu\ddot{w}_0)\dot{w}_0 \, d\phi \qquad (8.3)$$

Letting

$$p_3 = P_0 e^{-t/t_0}$$

and evaluating equation (8.3), one finds that

$$\mu\ddot{w}_0 = P_0 e^{-t/t_0} - P_c \qquad (8.4)$$

where $P_c = \frac{2N_0}{R}$ = the uniform static collapse pressure of a complete spherical shell

and t_0 is the decay time constant.

Integrating, one finds that

$$\mu\dot{w}_0 = -P_0 t_0 e^{-t/t_0} - P_c t + P_0 t_0 \qquad (8.5)$$

since

$$\dot{w}_0(t=0) = 0.$$

Motion will cease at time t_f, obtained from the positive root of

$$-P_0 t_0 e^{-t_f/t_0} - P_c t_f + P_0 t_0 = 0 \qquad (8.6)$$

Integrating equation (8.5) with the initial condition $w_0(t=0) = 0$ and evaluating at $t=t_f$ yields the final displacement

$$w_{0f} = \frac{1}{\mu}[P_0 t_0^2 (e^{-t_f/t_0} + \frac{t_f}{t_0} - 1) - \frac{P_c t_f^2}{2}] \tag{8.7a}$$

or through use of equation (8.6),

$$w_{0f} = \frac{1}{\mu}[(P_0 - P_c) t_f t_0 - \frac{P_c t_f^2}{2}] \tag{8.7b}$$

These results are in complete agreement with those of reference [8.1].

Section 2: Clamped Circular Cylinder Subjected to Uniform Impulsive Load

Consider one bay of a rigid-plastic cylinder which is reinforced periodically with rigid circumferential stiffeners. Because of symmetry the boundary conditions at each stiffener are those of the clamped condition.

Hodge investigated the response of such a shell section for infinitesimal deflections when subjected to axisymmetric dynamic pressures [8-2].

Jones considered the response of the same cylinder when subjected to an axisymmetric impulsive load with and without the effect of finite transverse deflections [8-3]. This solution included travelling hinges and for the infinitesimal case is much simpler than the corresponding dynamic pressure pulse analysis of Hodge [8-2].

In reducing the strain rate equations (6.1), equilibrium equations (6.2), and the energy dissipation rate equation (6.11) to the case of a circular cylinder with transverse velocity field, it should be noted that ϕ is $\pi/2$ radians, R_1 is infinite, and $d\phi$ is zero. The product $R_1 d\phi$ is, however, the differential longitudinal element dx. Using the notation

$$( )^* \equiv \frac{( )'}{R_1} \equiv \frac{d( )}{dx}$$

and assuming $\dot{u}$ to be zero, the strain rate equations (6.1), take the form

$$\dot{\varepsilon}_x = w^* \dot{w}^* \tag{8.8a}$$

$$\dot{\varepsilon}_\theta = \frac{\dot{w}}{R} \tag{8.8b}$$

$$\dot{\kappa}_x = -\dot{w}^{**} \tag{8.8c}$$

$$\dot{\kappa}_\theta = 0$$

The consistent set of equilibrium equations (6.2) reduces to

$$Q_x = -M_x^* \tag{8.9a}$$

$$(p_x - \mu\ddot{u}) = N_x^* = 0 \tag{8.9b}$$

$$(p_3 - \mu\ddot{w}) = \frac{N_\theta}{R} - (N_x w^*)^* - M_x^{**} \tag{8.9c}$$

when M_θ is assumed to be zero.

Equation (8.9b) is a consequence of the assumption that $\dot{u} = 0$ when $p_x = 0$.

The approximate energy dissipation equation (6.11) reduces to the form

$$\frac{D_E}{2\pi R} = \sum_i \int \{\frac{N_\theta \dot{w}}{R} - N_x^* w \dot{w}^* - (N_x w + M_x)\dot{w}^{**}\} dx$$

$$- \sum_j (N_x w + M_x)_j [\dot{w}^*]_j = \int (p_3 - \mu \ddot{w})\dot{w} dx \qquad (8.10)$$

where the summations are taken over i continuous regions and over j hinges.

The velocity profile is assumed to be symmetric about the midspan of the cylinder (Figure 8.1).

$$\dot{w}(x,t) = \dot{w}_0(t) \frac{x}{L} \qquad \text{for } 0 \leq x \leq L \qquad (8.11)$$

where $\dot{w}_0$ is the velocity at $x = L$.

Using the velocity profile (8.11), symmetry about $x = L$, and the equilibrium result that $N_x^* = 0$, equation (8.10) reduces to

$$2 \int_0^L \frac{N_\theta \dot{w}_0 x}{RL} dx - 2(M_x)_{x=0} \frac{\dot{w}_0}{L} - (N_x w + M_x)_{x=L} \left(\frac{-2\dot{w}_0}{L}\right) =$$

$$2 \int_0^L (p_3 - \frac{\mu \ddot{w}_0 x}{L}) \frac{\dot{w}_0 x}{L} dx \qquad (8.12)$$

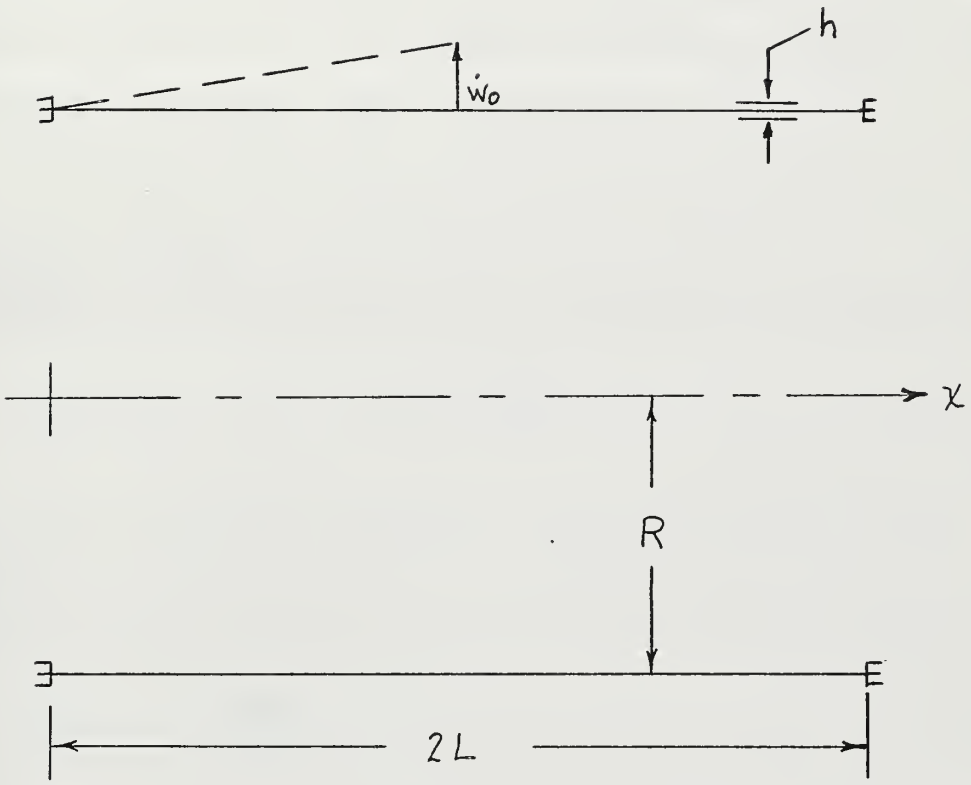

Fig. 8.1

From the two-direction limited interaction yield surface (Figure 4.2) it is seen that, since $M_\theta = 0$, $N_\theta = N_0$ for $\dot{w} > 0$.

If one assumes that the central hinge is twice the length of the end hinges and that the longitudinal strain is concentrated equally in each of the three hinges, it can be shown that the ratio of the average longitudinal strain rate to the average curvature rate in the hinges is

$$\frac{\dot{\varepsilon}_x \text{ avg.}}{\dot{\kappa}_x \text{ avg.}} = \pm \frac{w_0}{2} \tag{8.13}$$

where (+) is used at the clamped ends and (-) at x=L when $\dot{w} > 0$.

The equation of the x-direction portion of the yield surface is

$$M_x = \pm M_0 \left[1 - \left(\frac{N_x}{N_o}\right)^2\right] \tag{8.14}$$

By normality

$$\frac{dM_x}{dN_x} = - \frac{\dot{\varepsilon}_x}{\dot{\kappa}_x} \tag{8.15a}$$

Therefore,

$$\pm\frac{w_0}{2} = \pm\frac{2N_x M_0}{N_0^2} = \pm\frac{2N_x N_0 h}{N_0^2 \quad 4} \tag{8.15b}$$

from which

$$N_x = N_0 \frac{w_0}{h} \tag{8.15c}$$

However, N_x cannot exceed N_0 and the final result is

$$N_x = N_0 \frac{w_0}{h} \qquad \text{for } \frac{w_0}{h} \leq 1 \tag{8.16a}$$

$$N_x = N_0 \qquad \text{for } \frac{w_0}{h} \geq 1 \tag{8.16b}$$

$$M_x = \pm M_0 [1 - (\frac{w_0}{h})^2] \qquad \text{for } \frac{w_0}{h} \leq 1 \tag{8.16c}$$

$$M_x = 0 \qquad \text{for } \frac{w_0}{h} \geq 1 \tag{8.16d}$$

where (+) is used at the central hinge when $\dot{w} > 0$.

These results are the same as those of [8-3] for a clamped beam.

If equations (8.16) are substituted into equation (8.12) along with the fact that $N_\theta = N_0$ and the spatial integrations are then performed, the results, after some simplification, are

$$\frac{2M_0}{Rh} + \frac{2M_0}{L^2}\left(1 + \frac{w_0^2}{h^2}\right) = \frac{p_3}{2} - \frac{\mu \ddot{w}_0}{3} \qquad \text{while } \frac{w_0}{h} \leq 1 \tag{8.17a}$$

and then become

$$\frac{2M_0}{Rh} + \frac{4M_0}{L^2}\frac{w_0}{h} = \frac{p_3}{2} - \frac{\mu \ddot{w}_0}{3} \qquad \text{when } \frac{w_0}{h} \text{ exceeds 1.} \tag{8.17b}$$

It should be noted that there are no longitudinal membrane stress and no longitudinal membrane strain rate if the transverse deflections are considered to be infinitesimal. The kinematically admissible velocity profile (8.11) would require M_x to be $+M_0$ and $-M_0$ at the central hinge and at the boundary hinges, respectively.

From equation (8.9c) it can be verified that the generalized stress field

$$N_\theta = N_0$$

and

$$M_x = M_0 \left(-1 + \frac{4x}{L} - \frac{2x^2}{L^2}\right)$$

is statically admissible.

The upper and lower bound static collapse pressures, P_c, coincide.

$$P_c = \frac{N_0}{R} + \frac{4M_0}{L^2} \tag{8.18a}$$

or

$$P_c = 4M_0 \left(\frac{1}{Rh} + \frac{1}{L^2}\right) \tag{8.18b}$$

or

$$P_c = \frac{2M_0}{L^2} (2 + c^2) \tag{8.18c}$$

where

$$c^2 = \frac{2L^2}{Rh}.$$

P_c is the same as equation (11) of [8-2].

The dissipation equation (8.12) yields the following results for dynamic infinitesimal behavior

$$\frac{2M_0}{Rh} + \frac{2M_0}{L^2} = \frac{p_3}{2} - \frac{\mu\ddot{w}_0}{3} \tag{8.19}$$

Equation (8.19) is an ordinary linear second order differential equation in $w_0(t)$. Equation (8.17) is a pair of ordinary second order differential equations, one of which is nonlinear and governs the motion until $\frac{w_o}{h}$ reaches unity, and the other of which is linear and governs the motion if and when $\frac{w_0}{h}$ exceeds unity.

For the case of impulsive loading, p_3 is considered to be zero. The impulse delivered to the shell is accounted for by the initial conditions of the mode approximation.

$$w_0(t=0) = 0 \tag{8.20a}$$

and

$$\dot{w}_0(t=0) = \nu V_0 \tag{8.20b}$$

where ν is the Martin and Symonds [8-4] mode factor (defined below) and V_0 is the characteristic initial velocity determined from the applied impulse by the conservation of momentum.

$$[\ \int p\,dt = \mu V_0\ ]$$

Martin and Symonds showed for infinitesimal deflections of an impulsively loaded rigid-perfectly plastic structure that the best agreement between the physical deformation process and a mode approximation (time-independent velocity profile) results when the characteristic mode initial velocity $\dot{w}_0$ is equal to a certain multiple of the exact characteristic impulsive initial velocity [8-4]. It is assumed herein that the same factor is valid for finite deflection problems. The factor, ν, is shown to be [8-4]

$$\nu = \frac{\int_S \mu \dot{u}_i \, V_i \, dS}{\int_S \mu \dot{u}_i \, \dot{u}_i \, dS} \tag{8.21}$$

where μ is mass per unit area, $\dot{u}_i$ are the mode approximation initial velocity profiles, $\dot{u}_i = V_0 f_i(x)$, and V_i are the actual impulsive initial velocities $V_i = V_0 \, g_i(x)$.

For this particular problem, only $\dot{u}_3$ and V_3 are different from zero.

$$\dot{u}_3 = V_0 \frac{x}{L}$$

and

$$V_3 = V_0$$

Substituting these values into equation (8.21), the mode factor is found to be $\nu = 1.5$.

The motion equations (8.19) and (8.17) can be rewritten in the following form for the impulsive case

$$\ddot{w}_0 = -\frac{3P_c}{2\mu} \qquad \text{for infinitesimal deflections} \tag{8.22a}$$

or, for finite deflections

$$\ddot{w}_0 + \frac{6M_0}{\mu L^2}\frac{w_0^2}{h^2} + \frac{3P_c}{2\mu} = 0 \tag{8.22b}$$

while

$$\frac{w_0}{h} \leq 1$$

and

$$\ddot{w}_0 + \frac{12M_0}{\mu L^2}\frac{w_0}{h} = -\frac{3P_c}{2\mu} + \frac{6M_0}{\mu L^2} = -\frac{6M_0}{\mu Rh}$$

when

$$\frac{w_0}{h} \text{ exceeds } 1 \tag{8.22c}$$

where P_c is given by equation (8.18) and the initial conditions for (8.22 a and b) are given by equations (8.20).

The infinitesimal problem is easily solved by integrating equation (8.22a) twice and recognizing that motion ceases when $\dot{w}_0 = 0$.

The ratio of the final central deflection w_{0f} to the shell thickness h is

$$\frac{w_{0f}}{h} = \frac{3\mu\ V_0^2\ RhL^2}{16M_0h\ (Rh+L^2)} \tag{8.23a}$$

or

$$\frac{w_{0f}}{h} = \frac{3\lambda}{2(2+c^2)} \tag{8.23b}$$

where λ is the loading parameter $\frac{\mu V_0^2 L^2}{4M_0h}$.

Solution of the finite deflection problem is more involved. Solution of the nonlinear equation (8.22b) with its initial conditions (8.20) is sufficient so long as

$$\frac{w_{0f}}{h} \leq 1.$$

If the solution yields

$$\frac{w_{0f}}{h} > 1,$$

then equation (8.22c) must be solved for the second stage of motion. The initial conditions for the second stage of motion are that the displacement equals h and that the velocity equals the velocity at the end of the first stage of motion.

Let us write the first stage finite deflection equation in the form

$$\ddot{w}_0 + \beta_1 w_0^2 + \beta_2 = 0 \tag{8.24}$$

where $\beta_1 = \frac{6M_0}{\mu L^2 h^2}$ and $\beta_2 = \frac{3P_c}{2\mu} = \frac{3M_0(2+c^2)}{\mu L^2}$

Note by use of the Chain Rule that

$$\ddot{w}_0 = \dot{w}_0 \frac{d\dot{w}_0}{dw_0}.$$

Substitute this expression into equation (8.24) and integrate between the displacement limits 0 and w_0 to find

$$\tfrac{1}{2} \{\dot{w}_0^2(w_0) - \dot{w}_0^2(0)\} = -(\frac{\beta_1 w_0^3}{3} + \beta_2 w_0) \tag{8.25}$$

Recalling that

$$\dot{w}_0(0) = \nu V_0$$

and that w_0 is maximum when $\dot{w}_0 = 0$, we see that

$$w_{0m}^3 + \frac{3\beta_2}{\beta_1} w_{0m} - \frac{3\nu^2 V_0^2}{2\beta_1} = 0 \tag{8.26}$$

Using the definitions of β_1, β_2, P_c, λ, and the value of ν for this particular problem along with the formula for solution of a cubic equation [8-5], it can be shown that

$$\frac{w_{0m}}{h} = [\frac{9\lambda}{8} + \sqrt{(\frac{2+c^2}{2})^3 + (\frac{9\lambda}{8})^2}\,]^{\frac{1}{3}}$$

$$+ [\frac{9\lambda}{8} - \sqrt{(\frac{2+c^2}{2})^3 + (\frac{9\lambda}{8})^2}\,]^{\frac{1}{3}} \tag{8.27}$$

(First stage of motion)

Now,

$$\frac{w_{0f}}{h} = \frac{w_{0m}}{h}$$

if less than unity.

If, on the other hand, the value of $\frac{w_{0m}}{h}$ calculated from equation (8.27) is greater than unity, find from equation (8.25) that the velocity when $\frac{w_0}{h} = 1$ is

$$v_1 \equiv \dot{w}_0(h) = \dot{w}_0(\tau=0) = [\nu^2 V_0^2 - \frac{2\beta_1 h^3}{3} - 2\beta_2 h]^{\frac{1}{2}} \qquad (8.28)$$

where τ is time of second stage motion (i.e., $\tau=0$ when $w_0=h$).

For this particular problem equation (8.28) can be expressed as

$$\dot{w}_0(h) = \dot{w}_0(\tau=0) = V_0[\frac{9}{4} - \frac{2+3\ (2+c^2)}{2\lambda}] \qquad (8.29)$$

The finite deflection, second stage equation (8.22c) can be written in the form

$$\ddot{w}_0 + \beta_3 w_0 + \beta_4 = 0 \qquad (8.30)$$

where

$$\beta_3 = \frac{12M_0}{\mu L^2 h}$$

and

$$\beta_4 = \frac{6M_0}{\mu Rh}$$

with initial conditions

$$w_0(\tau=0) = h$$

and

$\dot{w}_0(\tau=0)$ is given by (8.29).

The solution is

$$w_0(\tau) = \frac{v_1}{f} \sin f\tau + (h+\frac{\beta_4}{\beta_3}) \cos f\tau - \frac{\beta_4}{\beta_3} \qquad (8.31a)$$

and the velocity is

$$\dot{w}_0(\tau) = v_1 \cos f\tau - f(h+\frac{\beta_4}{\beta_3}) \sin f\tau \qquad (8.31b)$$

where

$$f \equiv \sqrt{\beta_3}$$

In terms of this particular problem, the second stage solution can be expressed as

$$\frac{w_0(\tau)}{h} = \sqrt{\frac{3\lambda}{4} - \frac{(8+3c^2)}{6}} \sin f\tau + \frac{4+c^2}{4} \cos f\tau - \frac{c^2}{4} \qquad (8.32a)$$

and

$$\frac{\dot{w}_0(\tau)}{h} = f\sqrt{\frac{3\lambda}{4} - \frac{(8+3c^2)}{6}} \cos f\tau - \frac{(4+c^2)f}{4} \sin f\tau \qquad (8.32b)$$

If the shell does enter the second stage of motion, the final displacement-thickness ratio is

$$\frac{w_{0f}}{h} = \sqrt{\frac{3\lambda}{4} - \frac{(8+3c^2)}{6}} \sin f\tau_1 + \frac{4+c^2}{4} \cos f\tau_1 - \frac{c^2}{4} \qquad (8.33)$$

where τ_1 is the first positive root obtained from setting the second stage velocity equal to zero.

That is,

$$f\tau_1 = \arctan \left\{ \frac{4\sqrt{\frac{3\lambda}{4} - \frac{(8+3c^2)}{6}}}{4+c^2} \right\} \qquad (8.34)$$

For the simply supported case with finite deflections it may be shown that

$$N_x = 2N_0 \frac{w_0}{h} \qquad \text{for } \frac{w_0}{h} \leq \frac{1}{2} \qquad (8.35a)$$

and

$$N_x = N_0 \qquad \text{for } \frac{w_0}{h} \geq \frac{1}{2} \qquad (8.35b)$$

The factor β_1 in equation (8.24) becomes

$$\beta_1' = \frac{12M_0}{\mu L^2 h^2} \tag{8.36a}$$

and β_2 becomes

$$\beta_2' = \frac{3M_0\ (1+c^2)}{\mu L^2} \tag{8.36b}$$

The final displacement-thickness ratio becomes

$$\frac{w_0}{h} = \left[\frac{9\lambda}{16} + \sqrt{\left(\frac{1+c^2}{4}\right)^3 + \left(\frac{9\lambda}{16}\right)^2}\ \right]^{\frac{1}{3}} + \left[\frac{9\lambda}{16} - \sqrt{\left(\frac{1+c^2}{4}\right)^3 + \left(\frac{9\lambda}{16}\right)^2}\ \right]^{\frac{1}{3}} \tag{8.37a}$$

for $\frac{w_0}{h} \leq \frac{1}{2}$

or

$$\frac{w_0}{h} = \sqrt{\frac{3\lambda}{4} - \frac{(4+3c^2)}{12}}\ \sin f\tau_1 + \frac{2+c^2}{4}\ \cos f\tau_1 - \frac{c^2}{4} \tag{8.37b}$$

for $\frac{w_0}{h} \geq \frac{1}{2}$

where $f\tau_1 = \arctan\left\{\frac{4\sqrt{\frac{3\lambda}{4} - \frac{4+3c^2}{12}}}{2+c^2}\right\}$

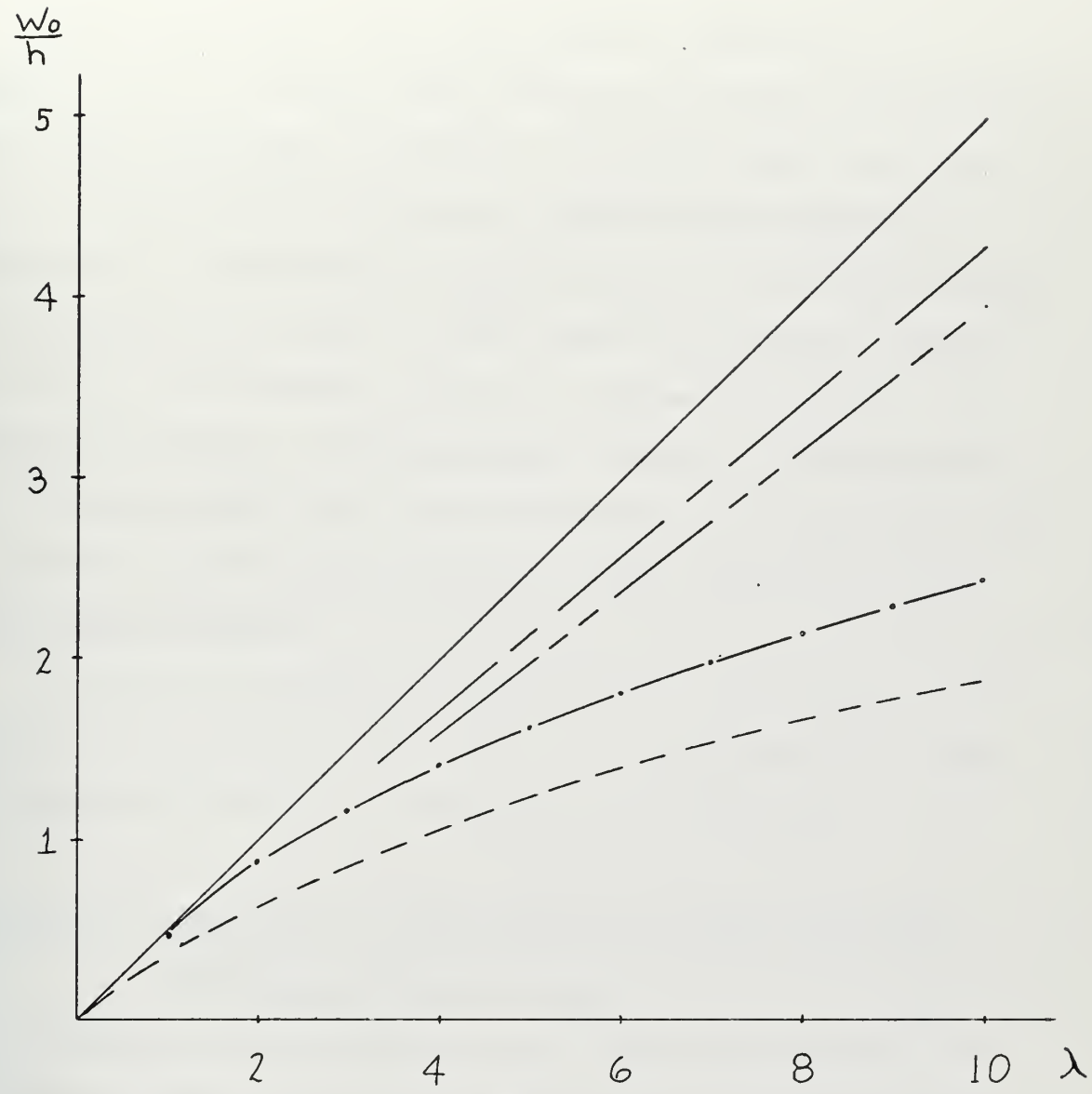

——————— Equation (8.23)

——— – ——— Jones (infinitesimal)[8-3]

——— – – ——— Hodge (rectangular pulse 10X static collapse pressure)[8-3]

———·——— Equations (8.27 & 8.33)

— — — — Jones (finite deflection)[8-3]

Fig. 8.2

Figure 8.2 shows the infinitesimal results of equation (8.23) and the finite deflection results of equations (8.27) and (8.33) for a clamped cylindrical shell for which $c = 1$. Also plotted are Hodge's infinitesimal deflection results for a rectangular pressure pulse of the same impulse with peak pressure equal to ten times the collapse pressure and Jone's infinitesimal and finite deflection results for impulsive loading. The approximate results of this section are slightly higher than the corresponding results from [8-3]. All results are for yield surfaces which circumscribe the exact yield surface.

It should be noted that the analyses of Hodge and Jones are valid only for $c^2 < 6$. There is no limitation on c for the approximate analysis performed in this section.

Section 3: Cylindrical Panel Subjected to Non-Uniformly Distributed Impulsive Load

Reference [8-6] reported some experimental results on the non-axisymmetric dynamic loading of cylindrical panels. Of interest here are some results for aluminum 6061T6 panels having clamped longitudinal boundaries and free circumferential boundaries which were plastically deformed by detonating sheet explosive which covered a portion of the inner surface. The midsurface configuration is shown in Figure 8.3.

Nominal test specimen dimensions are shown in Table 8.1.

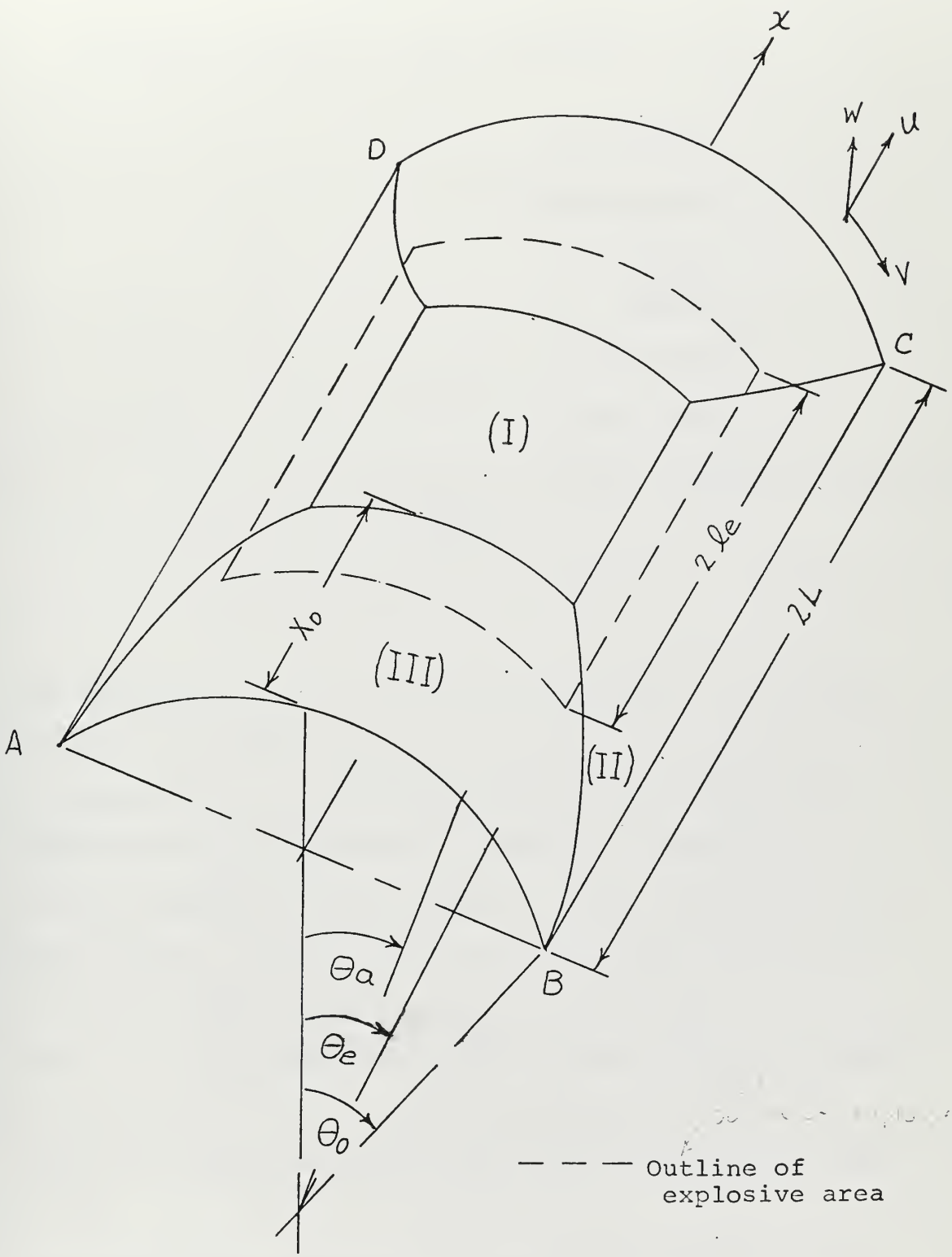

Fig. 8.3

Table 8.1

Nominal Cylindrical Panel Dimensions [8-6]

L	3.0 inches
θ_0	45.0 degrees
ℓ_e	1.5 inches
θ_e	33 degrees*
h	0.125 inches
	0.091 inches
	0.082 inches

*Varied slightly with thickness

The dimensions x_0 and θ_a are mode parameters and define the regions I, II, and III.

An approximate, infinitesimal deflection solution has been obtained using the general procedure of Chapter 7.

It was assumed that each region (I, II, III) experienced rigid body motion. Region I was assumed to rise vertically with a characteristic velocity of $\dot{w}_0$ at $x=L$, $\theta=0$.

Region II was assumed to rotate rigidly about the support line BC (or AD).

Region III was assumed to rotate rigidly about the line AB (or DC).

Because of symmetry about the curves $x=L$ and $\theta=0$, only one quadrant ($0 \leq x \leq L$; $0 \leq \theta \leq \theta_0$) need be analyzed.

With the requirement that w and $\dot{w}$ be continuous at the hinge curves between regions, the displacement rates for each region are found to be

Region I

$$\dot{u} = 0 \tag{8.38a}$$

$$\dot{v} = -\dot{w}_0 \sin\theta \tag{8.38b}$$

$$\dot{w} = \dot{w}_0 \cos\theta \tag{8.38c}$$

Region II

$$\dot{u} = 0 \tag{8.38d}$$

$$\dot{v} = \eta_a \dot{w}_0 \{1 - \cos(\theta_0 - \theta)\} \tag{8.38e}$$

$$\dot{w} = \eta_a \dot{w}_0 \sin(\theta_0 - \theta) \tag{8.38f}$$

where $\eta_a = \dfrac{\cos\theta_a}{\sin(\theta_0 - \theta_a)}$

Region III

$$\dot{u} = -\frac{Rx\ \dot{w}_0}{x_0} (\cos\theta - \cos\theta_0) \tag{8.38g}$$

$$\dot{v} = -\frac{x}{x_0} \dot{w}_0 \sin\theta \tag{8.38h}$$

$$\dot{w} = \frac{x}{x_0} \dot{w}_0 \cos\theta \tag{8.38i}$$

The positive directions of u, v, and w are indicated in Figure 8.3.

Continuity of w and $\dot{w}$ also determines the equation of the hinge curve C_{23} between regions II and III.

$$x_{23} = x_0 \eta_a \frac{\sin(\theta_0-\theta)}{\cos\theta} \tag{8.39}$$

Equations (8.38 and 8.39) agree with the results of Janas [8-7] for the static collapse mode velocities and hinge curve of a shallow cylindrical panel before shallow shell approximations were made.

From equations (8.38) the in-surface velocity discontinuities and transverse velocity derivative discontinuities are found to be:

Between regions I and II:

$$[\dot{u}] = 0 \tag{8.40a}$$

$$[\dot{v}] = \{\eta_a - \eta_a \cos(\theta_0-\theta_a) + \sin\theta_a\} \dot{w}_0 \tag{8.40b}$$

$$[\dot{w}'] = 0 \tag{8.40c}$$

$$[\dot{w}^*] = \{\sin\theta_a - \eta_a\cos(\theta_0-\theta_a)\} \dot{w}_0 \tag{8.40d}$$

where

$$\dot{w}' \equiv \frac{\partial \dot{w}}{\partial x}$$

and

$$\dot{w}^* \equiv \frac{\partial \dot{w}}{\partial \theta}$$

Between regions II and III:

$$[\dot{u}] = \frac{R}{x_0} (\cos\theta - \cos\theta_0)\, \dot{w}_0 \tag{8.40e}$$

$$[\dot{v}] = \eta_a\{1 - \cos(\theta_0-\theta) + \tan\theta \ \sin(\theta_0-\theta)\}\, \dot{w}_0 \tag{8.40f}$$

$$[\dot{w}'] = -\frac{\dot{w}_0}{x_0} \cos\theta \tag{8.40g}$$

$$[\dot{w}^*] = -\eta_a\{\cos(\theta_0-\theta) - \tan\theta \ \sin(\theta_0-\theta)\}\, \dot{w}_0 \tag{8.40h}$$

Between regions I and III:

$$[\dot{u}] = \frac{R}{x_0} (\cos\theta - \cos\theta_0)\, \dot{w}_0 \tag{8.40i}$$

$$[\dot{v}] = 0 \tag{8.40j}$$

$$[\dot{w}'] = -\frac{\dot{w}_0}{x_0} \cos\theta \tag{8.40k}$$

$$[\dot{w}^*] = 0 \tag{8.40l}$$

At the clamped boundary:

$$[\dot{u}] = [\dot{v}] = [\dot{w}'] = 0 \tag{8.40m}$$

$$[\dot{w}^*] = -\eta_a \dot{w}_0 \tag{8.40n}$$

If the curvature rates for a cylinder are found from equations (6.1) and then integrated across a hinge, the relative rotation rate components can be shown to be:

$$\dot{\Omega}_x = [\dot{w}'] \tag{8.41a}$$

and

$$\dot{\Omega}_\theta = \frac{[\dot{v}] - [\dot{w}^*]}{R} \tag{8.41b}$$

which may be evaluated using equations (8.40).

With the six-dimensional approximate yield surface described in Chapter 7 (Figure 7.2) normality considerations for $\dot{w}_0 > 0$ require the following generalized stress values.

Between regions I and II:

$$M_\theta = M_0;\ N_\theta = N_0$$

$$M_x = N_x = M_{x\theta} = N_{x\theta} = 0 \tag{8.42a}$$

Between regions I and III:

$$M_x = M_0;\ N_x = N_0$$

$$M_\theta = N_\theta = M_{x\theta} = N_{x\theta} = 0 \tag{8.42b}$$

Between regions II and III:

$$M_x = M_\theta = 2M_{x\theta} = M_0$$

$$N_x = N_\theta = 2N_{x\theta} = N_0 \tag{8.42c}$$

At the clamped boundary:

$$M_\theta = -M_0$$

$$M_x = N_x = M_{x\theta} = N_{x\theta} = N_\theta = 0 \tag{8.42d}$$

If the appropriate deformation rates (8.40 and 8.41) and generalized stress values (8.42) are substituted into the internal energy dissipation rate expression (equation 7.6) and the integration is carried out, it may be shown that the dissipation rate for one quadrant of the panel divided by the characteristic velocity, $\dot{w}_0$, and the yield moment, M_0 is

$$\frac{D_i}{\dot{w}_0 M_0} = (L-x_0)\left\{\frac{4}{h}(\eta_a[1-\cos(\theta_0-\theta_a)]+\sin\theta_a)+\frac{\eta_a}{R}\right\}$$

$$+\frac{4R^2}{x_0 h}(\sin\theta_0-\theta_0\cos\theta_0)+\frac{R}{x_0}\sin\theta_0+\frac{L\eta_a}{R}$$

$$+\frac{2R\eta_a}{h}\{(\theta_0-\theta_a)-\cos^2\theta_0(\tan\theta_0-\tan\theta_a)\}+\frac{\eta_a}{2}\{(\theta_0-\theta_a)$$

$$+\cos\theta_0\ \ln\left(\frac{\sec\theta_0+\tan\theta_0}{\sec\theta_a+\tan\theta_a}\right)\}\ +\frac{x_0}{R}\ \eta_a^2\cos\theta_0\{\tan\theta_0-\tan\theta_a\}$$

$$+\frac{4x_0}{h}\ \eta_a^2\cos\theta_0\{(\tan\theta_0-\tan\theta_a)-\tfrac{1}{2}\cos\theta_0\cdot$$

$$\left[\ln\left(\frac{\sec\theta_0+\tan\theta_0}{\sec\theta_a+\tan\theta_a}\right)+\tan\theta_0\ \sec\theta_0-\tan\theta_a\ \sec\theta_a\right]\}\qquad(8.43)$$

Let us call the right hand side of this expression F.

$$F = F(L,\ x_0,\ \theta_0,\ \theta_a)\qquad(8.44a)$$

and

$$D_i = F\ M_0\ \dot{w}_0\qquad(8.44b)$$

The external energy dissipation rate (equation 5.1) becomes

$$D_E = \int_{S \text{ quadrant}} [(p_3 - \mu\ddot{w})\dot{w} - \mu\ddot{u}\dot{u} - \mu\ddot{v}\dot{v}] \, dS \tag{8.45}$$

The indicated integration must be performed in each region, and the expressions for the pressure and velocities within each region depend on the assumed size of the central region (Region I) relative to the loaded area (defined by ℓ_e and θ_e).

Since $\dot{u}$ and $\dot{v}$ are defined in terms of $\dot{w}_0$, equation (8.45) can be expressed as

$$D_E = (p_3 g - \mu e \ddot{w}_0)\dot{w}_0 \tag{8.46}$$

where

$$g = g(L, x_0, \ell_e, \theta_0, \theta_a, \theta_e)$$

and

$$e = e(L, x_0, \ell_e, \theta_0, \theta_a, \theta_e)$$

The governing equation of motion is found by equating the internal and external energy dissipation rates and has the form

$$FM_0 = p_3 g - \mu e \ddot{w}_0 \tag{8.47}$$

The upper bound collapse pressure is

$$P_c = \frac{FM_0}{g}$$

which for a given panel with fixed loading geometry varies with the mode shape parameters x_0 and θ_a.

The pressure p_3 is zero everywhere outside of the loading area (Figure 8.3) and g is found by evaluating the integral

$$g = \int_{S_e} \dot{w} \, d \, S_e \tag{8.48}$$

where S_e indicates the loaded portion of the midsurface area.

Equation (8.48) consists of contributions from each region, and the limits of integration within each region depend on the parameters x_0 and θ_a. The form of the equation for the values of x_0 and θ_a indicated in Figure 8.3, for example, would be

$$g = \int_0^{\theta_a} \int_{x_0}^{L} R \, \dot{w}_I \, dx \, d\theta + \int_{\theta_a}^{\theta_e} \int_{x_{23}}^{L} R \, \dot{w}_{II} \, dx \, d\theta$$

$$+ \left\{ \int_0^{\theta_a} \int_{x_0}^{L} + \int_{\theta_a}^{\theta_e} \int_{x_0}^{x_{23}} \right\} R \, \dot{w}_{III} \, dx \, d\theta \tag{8.49}$$

where the subscript I indicates region I, etcetera. Equation (8.39) is used to define x_{23} in the limits of integration.

The optimum values of the mode parameters are those which give the lowest static collapse pressure. Because of the complicated forms of F and g, parameter optimization was accomplished by computing the collapse pressure for discreet combinations of x_0 and θ_a. In all cases it was found that the minimum collapse pressure occurred for x_0=L and for θ_a somewhat less than θ_e. Region I degenerated into a curve as shown in Figure 8.4.

Now e may be determined as

$$e = \frac{1}{\dot{w}_0 \ddot{w}_0} \left[\int_0^{\theta_a} \int_0^{L} + \int_{\theta_a}^{\theta_0} \int_0^{x_{23}} \right] (\dot{u}\ddot{u} + \dot{v}\ddot{v} + \dot{w}\ddot{w})_{III} \, R \, dx \, d\theta$$

$$+ \frac{1}{\dot{w}_0 \ddot{w}_0} \int_{\theta_a}^{\theta_0} \int_{x_{23}}^{L} (\dot{u}\ddot{u} + \dot{v}\ddot{v} + \dot{w}\ddot{w})_{II} \, R \, dx \, d\theta \qquad (8.50)$$

where the mode velocities and accelerations for the first set of integrals are those of region III and those of the final integral are of region II. Evaluation of this expression leads to

$$\frac{e}{RL} = \frac{\theta_a}{3} + \frac{R^2}{L^2}\left(\frac{\theta_a}{2} + \tfrac{1}{4} \sin 2\theta_a - 2\cos\theta_0 \sin\theta_a + \theta_a \cos^2\theta_0\right)$$

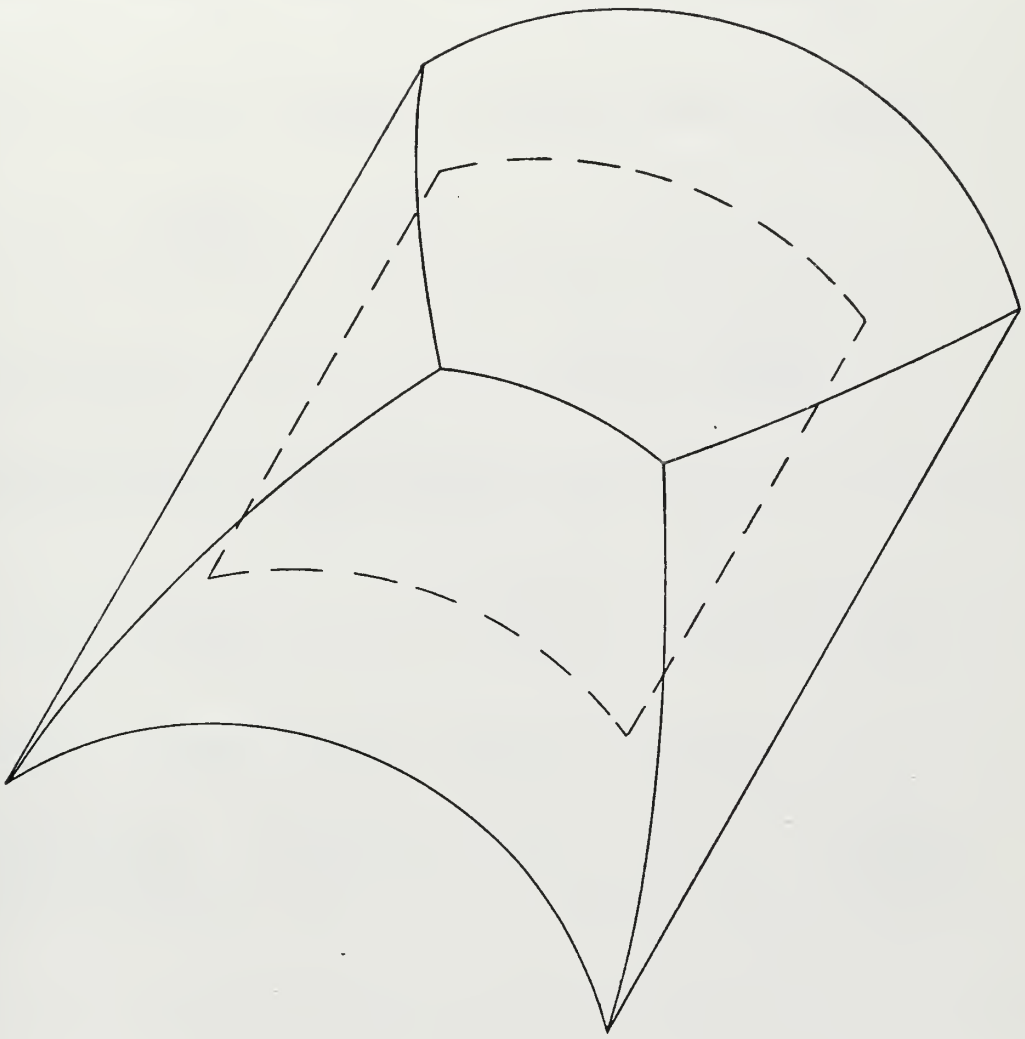

Fig. 8.4

$$+\frac{\eta_a R^2}{L^2}\left[\tfrac{1}{2}(\theta_0-\theta_a)\sin\theta_0+\frac{\sin\theta_0}{4}(\sin2\theta_0-\sin2\theta_a)\right.$$

$$-\sin2\theta_0(\sin\theta_0-\sin\theta_a)+(\theta_0-\theta_a)\sin\theta_0\cos^2\theta_0$$

$$+\frac{\cos\theta_0}{4}(\cos2\theta_0-\cos2\theta_a)-2\cos^2\theta_0(\cos\theta_0-\cos\theta_a)$$

$$\left.-\cos^3\theta_0\,\ell n\frac{\sec\theta_0}{\sec\theta_a}\right]+2\eta_a^2\left[\theta_0-\theta_a-\sin(\theta_0-\theta_a)\right.$$

$$+\eta_a^3\left\{\tfrac{1}{3}(\theta_0-\theta_a)\sin^3\theta_0-\sin^2\theta_0\cos\theta_0\;\ell n\frac{\sec\theta_0}{\sec\theta_a}\right.$$

$$+\sin\theta_0\cos^2\theta_0(\tan\theta_0-\tan\theta_a-\theta_0+\theta_a)$$

$$-2(\theta_0-\theta_a)\sin\theta_0+2\cos\theta_0\;\ell n\frac{\sec\theta_0}{\sec\theta_a}+2\sin2\theta_0(\sin\theta_0-$$

$$\sin\theta_a)+2\cos2\theta_0(\cos\theta_0-\cos\theta_a)-\sin2\theta_0\cdot$$

$$\left.\left.\ell n\frac{\sec\theta_0+\tan\theta_0}{\sec\theta_a+\tan\theta_a}-\frac{\cos^3\theta_0}{3}\left[\tfrac{1}{2}(\tan^2\theta_0-\tan^2\theta_a-\ell n\frac{\sec\theta_0}{\sec\theta_a}\right]\right\}\right.$$

(8.51)

From the definition of the Martin and Symonds mode factor, ν, equation (8.21) it can be seen that for constant density, μ, the denominator of ν is $\mu e V_0^2$. The impulsive velocity, V_0, is equal to the explosive impulse divided by the mass of the panel portion included within a radial projection of the sheet explosive boundaries.

For the degenerate mode shape shown in Figure 8.4, the numerator of ν is

$$\mu J V_0^2 = \left[\int_0^{\theta_a} \int_{L-\ell_e}^{} + \int_{\theta_a}^{\theta_e} \int_{L-\ell_e}^{x_{23}} \right] (\mu V_{i_{III}}^{+} V_i) \, R dx \, d\theta$$

$$+ \int_{\theta_a}^{\theta_e} \int_{x_{23}}^{L} \mu V_{i_{II}}^{+} V_i \, R dx \, d\theta \qquad (8.52)$$

where the $V_{i_A}^{+}$ are the mode velocity components in region A and the V_i are the actual impulsive velocity components.

Performing the indicated integration, one finds that

$$J = \frac{R}{2L} \{L^2\theta_a - (L-\ell_e)^2 \theta_e\} + RL\eta_a \{(\theta_e-\theta_a) \sin\theta_0$$

$$+ \cos\theta_e - \cos\theta_a - \eta_a [\tfrac{1}{2}(\sin^2\theta_0 - \cos^2\theta_0)(\theta_e-\theta_a)$$

$$+ \sin\theta_0 (\cos\theta_e - \cos\theta_a) + \cos\theta_0 (\sin\theta_a - \sin\theta_e)$$

$$+ \cos\theta_0 \ln\frac{\sec\theta_e + \tan\theta_e}{\sec\theta_a + \tan\theta_a} + \frac{\cos^2\theta_0}{2} (\tan\theta_e - \tan\theta_a)]\} \qquad (8.53)$$

For the impulsive solution p_3 is assumed zero and the initial characteristic velocity is assumed to be

$$\dot{w}_0(t=0) = \nu V_0$$

where $\nu = \frac{J}{e}$

The equation of motion (8.54) becomes

$$\ddot{w}_0 = -\frac{FM_0}{\mu e} \tag{8.55}$$

$$\dot{w}_0 = -\frac{FM_0}{\mu e} t + \nu V_0 \tag{8.56}$$

Motion ceases at t_f when

$$\dot{w}_0(t_f) = 0$$

and

$$t_f = \frac{\mu e \nu V_0}{FM_0} \tag{8.57}$$

$$w_0 = -\frac{FM_0}{\mu e}\frac{t^2}{2} + \nu V_0 t \tag{8.58}$$

The final displacement-thickness ratio is found by evaluating (8.58) at t_f.

$$\frac{w_{0f}}{h} = \frac{\mu J^2 \quad V_0^2}{2eFM_0 h} \tag{8.59}$$

Figure 8.5 shows the final central permanent displacement-thickness ratios observed during the experiments on the fourteen aluminum panels reported in [8-6] plotted as a function of a non-dimensional impulse parameter, ψ.

$$\psi \equiv \frac{\mu R \; V_0^2}{M_0} \tag{8.60}$$

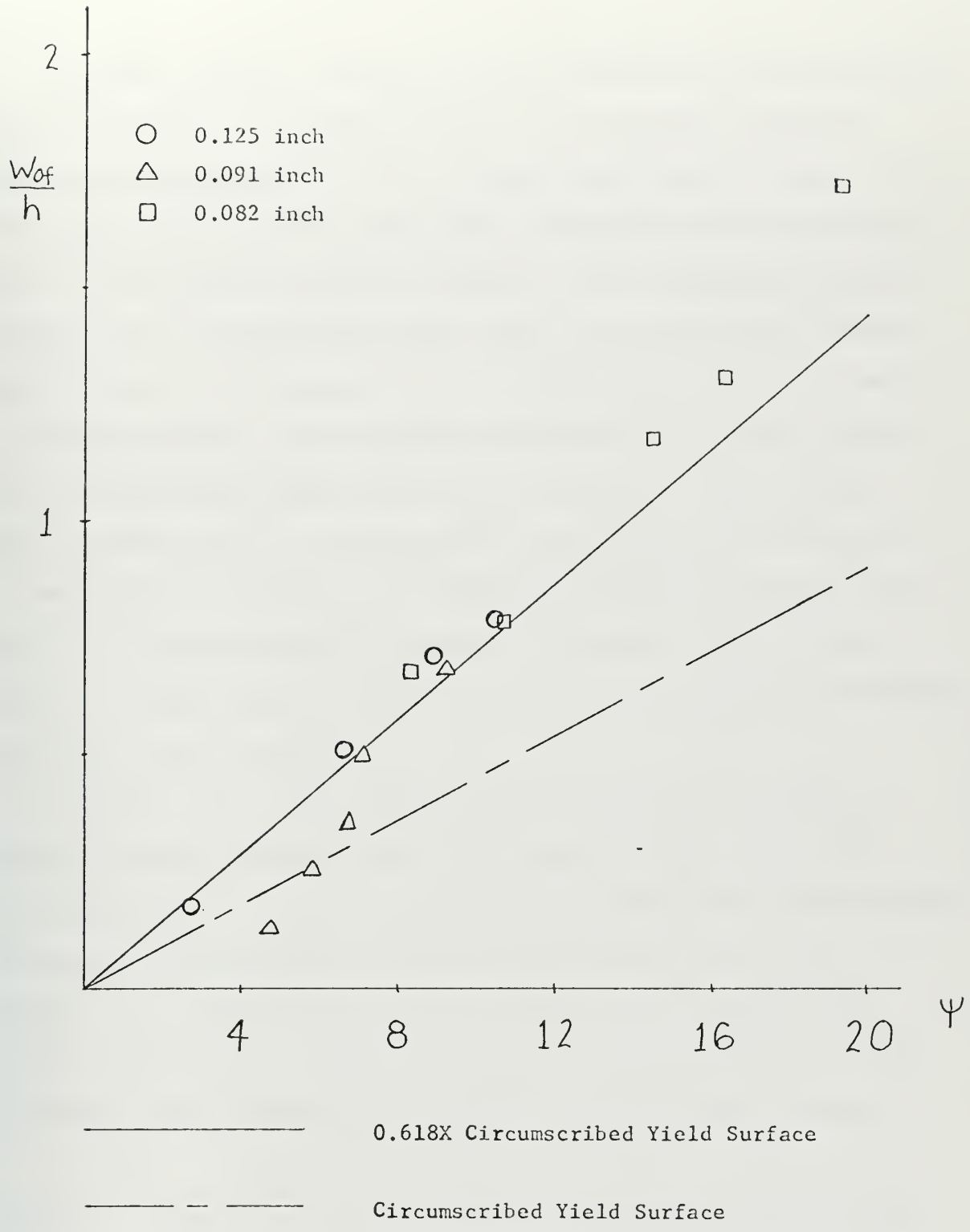
2
1
$\frac{W_{of}}{h}$
0.125 inch
0.091 inch
0.082 inch
4
8
12
16
20
Ψ
0.618X Circumscribed Yield Surface
Circumscribed Yield Surface

Fig. 8.5

The same figure contains a plot of points calculated from equation (8.59) for panels of the three different nominal thicknesses reported in [8.6]. Within plotting accuracy, all calculated points fell on the same straight line. The lower line of calculated results is based on the approximate yield surface which circumscribes the exact six-dimensional Tresca yield surface. The upper line of calculated results is based on the approximate yield surface whose scale is 0.618 that of the circumscribing approximate yield surface. The smaller yield surface may not inscribe the exact yield surface, but, as was noted in Chapter 7, no approximate yield surface which reduces to the two-moment limited interaction yield surface and has a scale factor greater than 0.618 can possibly inscribe the Tresca yield surface.

The fact that the smaller yield surface gave better results for this problem than the larger yield surface is not surprising. A large portion of the hinges has generalized stresses corresponding to the corners marked A and B in Figure 7.2. Corners of a circumscribed yield surface lie outside of the exact yield surface, while the corners of the inscribed yield surface may lie on the exact yield surface.

Section 4: Spherical Cap Subjected to Uniformly Distributed Impulsive Load

As a final example let us consider the case of a deep spherical cap with clamped boundary subjected to a transverse dynamic pressure load.

Giannotti [8-8] reported the results of some experiments on clamped spherical caps which were loaded by detonating sheet explosive which covered most of the internal surface. Of interest here are the results of some experiments on 6061T6 aluminum caps. Nominal dimensions are listed in Table 8.2 and indicated in Figure 8.6.

Table 8.2

Nominal Spherical Cap Dimensions [8-8]

ϕ_0 (degrees)	ϕ_e (degrees)	R (inches)	h (inches)
90	89	2.58	0.115
90	89	2.58	0.176
90	89	2.58	0.237
60	59	2.58	0.117
45	44	2.58	0.119

Onat and Prager considered the static collapse problem of a deep clamped shell subjected to a uniformly distributed pressure [8-9]. With an assumed velocity profile of the form

$$\dot{w}_0(\phi,t) = \frac{\dot{w}_0(t)\ (\cos\phi - \cos\phi_0)}{(1 - \cos\phi_0)} \tag{8.61a}$$

$$\dot{u} = 0 \tag{8.61b}$$

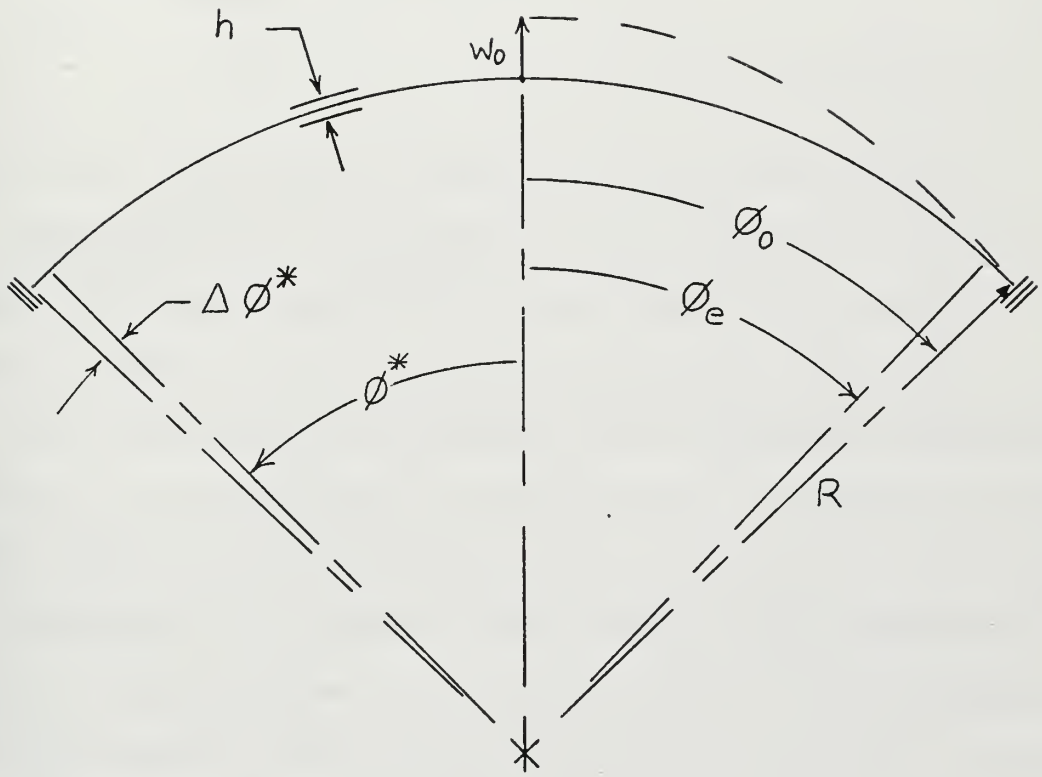

Fig. 8.6

where $\dot{w}_0$ is the transverse velocity at $\phi=0$, and as a consequence of using the Tresca yield surface, the state of generalized stress was found to be membrane (i.e., $M_\phi = M_\theta = 0$) except in a narrow region near the boundary, $\phi^* \leq \phi \leq \phi_0$. The angle ϕ^* is defined by the relation

$$\cos\phi^* = \frac{2\cos\phi_0}{2 - \frac{h}{R}} , \tag{8.62}$$

derived from the normality requirements of plasticity.

The upper and lower bound collapse pressures obtained by Onat and Prager for shells in the range of ϕ_0 and $\frac{R}{h}$ listed in Table 8.2 agreed within 15 percent or better.

The loading used by Giannotti [8-8] appeared sufficiently similar to uniform loading to use the Onat and Prager collapse profile (equation 8.61).

For comparison purposes the spherical cap problem was solved for infinitesimal deflections and for finite deflections. Two infinitesimal solutions with the Onat and Prager velocity profile were obtained, one using the Tresca yield surface and one using the two-moment limited interaction approximate yield surface (Figure 4.1). Lower bounds on the final displacement were also obtained using the method of Morales and Nevill [8-11] for a perfectly plastic material.

First let us examine the finite deflection solution.

In order to simplify the finite deflection analysis, the two-direction limited interaction yield surface (Figure 4.2) was utilized in place of the exact Tresca yield surface.

The strain rate and curvature rate equations (6.1) for a spherical cap with the velocity field of equation (8.61) reduce to

$$\dot{\varepsilon}_\phi = \frac{\dot{w}_0}{R(1-\cos\phi_0)} \{\cos\phi - \cos\phi_0 + \frac{w_0 \sin^2\phi}{1-\cos\phi_0}\} \tag{8.63a}$$

$$\dot{\varepsilon}_\theta = \frac{\dot{w}_0(\cos\phi - \cos\phi_0)}{R(1-\cos\phi_0)} \tag{8.63b}$$

$$\dot{\kappa}_\phi = \dot{\kappa}_\theta = \frac{\dot{w}_0 \cos\phi}{R^2(1-\cos\phi_0)} \tag{8.63c}$$

The last term of equation (8.63a) is the only finite deflection contribution.

If we assume that the two hinges' rotation rates can be represented by average curvature rates, each one averaged over one half of the arc $R\Delta\phi^*$, in conjunction with a meridional strain rate averaged over the arc $R\Delta\phi^*$, it can be shown from the normality requirements of plasticity that

$$\left(\frac{N_\phi}{N_0}\right)_A = \frac{R}{h} \frac{\sin\phi_0 - \sin\phi^* - \Delta\phi^* \cos\phi_0}{\sin\phi_0}$$

$$+ \frac{w_0}{h} \frac{\frac{\Delta\phi^*}{2} - \frac{\sin 2\phi_0 - \sin 2\phi^*}{4}}{\sin\phi_0(1-\cos\phi_0)} \tag{8.64a}$$

and

$$\left(\frac{N_\phi}{N_0}\right)_B = \frac{R}{h}\ \frac{\sin\phi_0 - \sin\phi^* - \Delta\phi^*\cos\phi_0}{\sin\phi^*}$$

$$+\ \frac{w_0}{h}\ \frac{\frac{\Delta\phi^*}{2} - \frac{\sin 2\phi_0 - \sin 2\phi^*}{4}}{\sin\phi^*\ (1-\cos\phi_0)} \qquad (8.64b)$$

where A and B refer to hinges A and B of Figure 8.7.

The bending moment associated with each hinge may be found from the yield surface equations

$$\frac{M_\phi}{M_0} = \pm\left(1 - \frac{N_\phi^2}{N_0^2}\right) \qquad (8.64c)$$

where (-) is used for hinge A and (+) for hinge B when $\dot{w}_0 > 0$.

For $\phi \leq \phi^*$

$$N_\phi = N_0 \qquad (8.64d)$$

and

$$M_\phi = 0 \qquad (8.64e)$$

Circumferential bending is important only in the same region as meridional bending and it can be shown that for $\dot{w}_0 > 0$.

$$\frac{N_\theta}{N_0} = \frac{2R}{h}\left(1 - \frac{\cos\phi_0}{\cos\phi}\right) \qquad (8.65a)$$

and

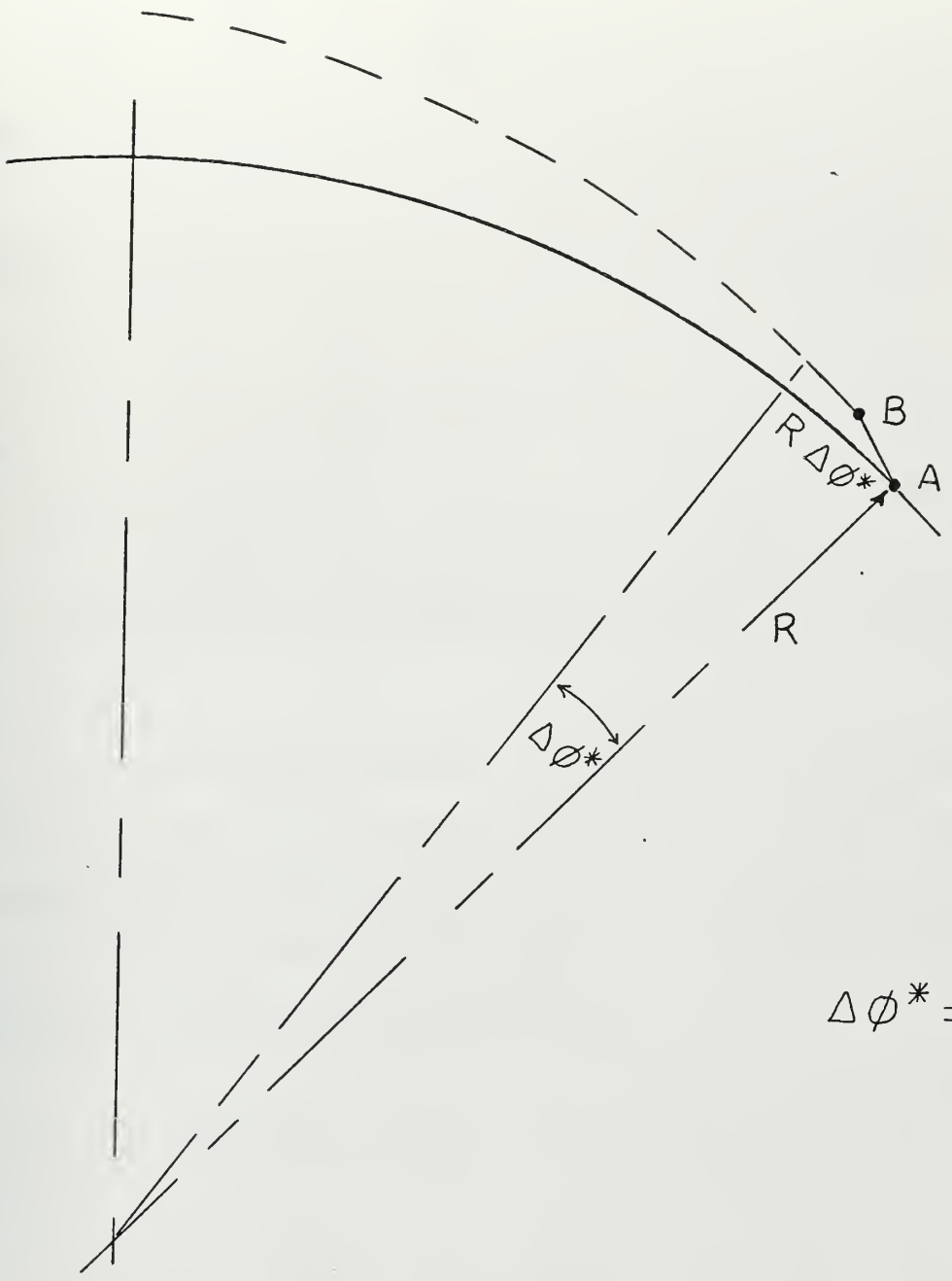

$$\Delta\phi^* = \phi_0 - \phi^*$$

Fig. 8.7

$$\frac{M_\theta}{M_0} = 1 - \frac{4R^2}{h^2} \left(1 - \frac{\cos\phi_0}{\cos\phi}\right)^2 \qquad (8.65b)$$

for $\phi^* \leq \phi \leq \phi_0$

while

$$N_\theta = N_0 \qquad (8.66a)$$

and

$$M_\theta = 0 \qquad (8.66b)$$

for $\phi \leq \phi^*$

If the velocity profile (equation 8.61), pressure, and the generalized stress values (equations 8.65 and 8.66) are substituted into the external dissipation rate expression for shells of revolution (equation 6.11), and the indicated integration performed, it can be shown that

$$P_c \{a_1+a_3+a_4+a_6[1-\{\frac{Rc_1}{h(1-\gamma)}\}^2] + a_7[1-(\frac{Rc_1}{h})^2]\}$$

$$+ P_c\{a_2+a_5 \frac{Rc_1}{h(1-\gamma)} - 2a_6 \frac{Rc_1c_2}{h(1-\gamma)^2} - 2a_7 \frac{Rc_1c_2}{h}\} \; w_0$$

$$+ P_c \{a_5 \frac{c_2}{h(1-\gamma)} - a_6[\frac{c_2}{h(1-\gamma)}]^2 - a_7 \frac{c_2^2}{h^2}\} \; w_0^2 =$$

$$a_8 p_3 - a_9 \ddot{w}_0 \qquad (8.67)$$

where

P_c is the Onat and Prager lower bound collapse pressure $\frac{8M_0}{Rh}$.

$$\gamma = \frac{\sin\phi^*}{\sin\phi_0}$$

$$c_1 = \frac{\sin\phi_0 - \sin\phi^* - \Delta\phi^* \cos\phi_0}{\sin\phi_0}$$

$$c_2 = \frac{\frac{\Delta\phi^*}{2} - \frac{\sin 2\phi_0 - \sin 2\phi^*}{4}}{\sin\phi_0(1-\cos\phi_0)}$$

$$a_1 = \frac{1-\cos^2\phi^*}{2} + \cos\phi_0 \cos\phi^* - \cos\phi_0$$

$$a_2 = \frac{1}{R(1-\cos\phi_0)} \left[\frac{1-\cos^3\phi^*}{3} + \frac{\cos\phi_0(\cos\phi^*-1)}{2}\right]$$

$$a_3 = \frac{R}{h} \left[\tfrac{1}{2}(3\cos^2\phi_0 + \cos^2\phi^*) - 2\cos\phi_0 \cos\phi^* + \cos^2\phi_0 \cdot \ell n\frac{\cos\phi^*}{\cos\phi_0}\right]$$

$$a_4 = \frac{h}{8R}\left[\tfrac{1}{2}(\cos^2\phi^* - \cos^2\phi_0) - \frac{4R}{h} a_3\right]$$

$$a_5 = \frac{\sin\phi^* (\sin\phi_0 - \sin\phi^*)(\cos\phi^* - \cos\phi_0)}{2R(1-\cos\phi_0)}$$

$$a_6 = \frac{h}{8R} \sin\phi^* (\sin\phi_0 - \sin\phi^*)$$

$$a_7 = \frac{h \sin^2\phi_0}{8R}$$

$$a_8 = \tfrac{1}{2}(1-\cos\phi_0)^2$$

$$a_9 = \frac{\mu}{3} \quad (1-\cos\phi_0)^3$$

and

μ is the mass density per unit midsurface area .

By defining new constants, equation (8.67) can be written in the form

$$\ddot{w}_0 + P_c b_2 w_0 - P_c b_3 w_0^2 = p_3 b_4 - P_c b_1 \tag{8.68}$$

where

$a_9 b_1$ is the coefficient of P_c,

$a_9 b_2$ is the coefficient of $P_c w_0$,

and $a_9 b_3$ is the coefficient of $P_c w_0^2$ on the left hand side of equation (8.67).

$$b_4 = \frac{a_8}{a_9}$$

Equation (8.68) has been solved for the impulsive loading case by the method of successive approximations [8-10].

The pressure p_3 is assumed to be zero and the initial characteristic velocity is

$$\dot{w}_0(t=0) = \nu V_0 \tag{8.69}$$

For the partial loading of the spherical cap in conjunction with the assumed velocity profile (equation 8.61) the Martin and Symonds mode factor becomes

$$\nu = \tfrac{3}{2}\left\{1-\left(\frac{\cos\phi_e - \cos\phi_0}{1 - \cos\phi_0}\right)^2\right\} \tag{8.70}$$

The actual impulsive initial velocity, V_0, is equal to the explosive impulse divided by the mass of the spherical cap included within a radial projection of the sheet explosive boundary.

Using the second approximation to the solution of equation (8.68) one finds

$$w_0(t) = J_1 \sin At + J_2 \cos At + J_3 \sin^2 At + J_4 \cos^2 At$$

$$+ J_5 \sin 2At + J_6\, t \sin At + J_7\, t \cos At + J_8 \tag{8.71}$$

where

$$A = \sqrt{P_c b_2}$$

$$J_1 = \frac{\nu V_0}{A}\left(1 - \frac{b_1 b_3}{b_2^2}\right)$$

$$J_2 = \frac{b_1}{b_2} - \frac{4b_1^2 b_3}{3b_2^3} - \frac{2b_3 \nu^2 V_0^2}{3b_2 A^2}$$

$$J_3 = \frac{b_3}{3b_2} \left(\frac{\nu^2 V_0}{A^2} + \frac{2b_1^2}{b_2^2}\right)$$

$$J_4 = \frac{b_3}{3b_2} \left(\frac{2\nu^2 V_0^2}{A^2} + \frac{b_1^2}{b_2^2}\right)$$

$$J_5 = - \frac{b_1 b_3 \nu V_0}{3b_2^2 A}$$

$$J_6 = -\frac{b_1^2 b_3 A}{b_2^3}$$

$$J_7 = \frac{b_1 b_3 \nu V_0}{b_2^2}$$

and

$$J_8 = - \frac{b_1}{b_2} + \frac{b_1^2 b_3}{b_2^3}$$

The velocity, $\dot{w}_0(t)$, can be found by differentiating equation (8.71) with respect to time. Motion ceases at the time, t_f, when $\dot{w}_0 = 0$. The time t_f is thus the first positive root of the transcendental equation obtained by setting $\dot{w}_0$ equal to zero.

The final central displacement, w_{0f}, is obtained by evaluating equation (8.71) at time t_f.

Computed results show less than one percent difference between the first and second approximations.

These approximate analytic results are themselves quite complicated, due primarily to the presence of finite deflection terms. In order to determine whether or not the additional complexity is justified, the problem was also solved for infinitesimal deflections alone.

If the same velocity field and the exact Tresca yield surface are assumed, and if a hinge is allowed at ϕ_0, the dissipation rate expression for shells of revolution (equation 6.11) produces the following infinitesimal results

$$P_c(a_1 + 2a_3 + 2a_4 + a_7) = a_8 p_3 - a_9 \ddot{w}_0 \tag{8.72}$$

Equation (8.72) is a linear, ordinary second order differential equation.

For the impulsive case, $p_3 = 0$. Integrating twice with respect to time and using the initial conditions that

$$\dot{w}_0(t=0) = vV_0$$

and

$$w_0(t=0) = 0,$$

one finds that

$$w_o(t) = - \frac{P_c(a_1+2a_3+2a_4+a_7)t^2}{2a_9} + vV_0 t \tag{8.73}$$

Finding t_f from the fact that motion ceases when $\dot{w}_0(t_f)=0$ and substituting into (8.73) leads to the final permanent central displacement-thickness ratio

$$\frac{w_{0f}}{h} = \frac{a_9\ \nu^2\ V_0^2}{2P_c h(a_1+2a_3+2a_4+a_7)} \tag{8.74}$$

If the Onat and Prager velocity profile is used in conjunction with the two-moment limited interaction yield surface the following infinitesimal deflection results are found

$$P_c\ \{\frac{(1-\cos\phi_0)^2}{2} + \frac{h}{4R}\ (1-\cos^2\phi_0)\} = (\frac{p_3}{2} - \frac{\mu\ddot{w}_0}{3})(1-\cos\phi_0)^2 \tag{8.75}$$

The impulsive final central displacement-thickness ratio is

$$\frac{w_{0f}}{h} = \frac{\mu\ \nu^2\ \ V_0^2}{3P_c h(1+\frac{h}{2R}\ \frac{1+\cos\phi_0}{1-\cos\phi_0})} \tag{8.76}$$

Morales and Nevill [8-11] have developed a lower bound displacement technique for rigid-plastic structures subjected to impulsive loading. The method is based on the use of a kinematically admissible velocity field.

The lower displacement bound obtained from the Onat and Prager velocity field and the Tresca yield surface is

$$\frac{w_{0f}}{h} \geq \frac{a_9 \nu^2 V_0^2}{3P_c h(a_1+2a_3+2a_4+a_7)} \tag{8.77}$$

The lower bound is seen to be two-thirds the value predicted by the Tresca yield surface infinitesimal solution.

Comparison of experimental and approximate theoretical results are shown in Figures 8.8 through 8.13. These figures show final permanent central displacement-thickness plotted as a function of impulse parameter λ.

$$\lambda = \frac{\mu R^2 V_0^2}{M_0 h} = \frac{4\rho R^2 V_0^2}{\sigma_0 h^2} \tag{8.78}$$

where ρ is density based on volume.

Figure 8.13 is a combined plot of the information from Figures 8.8, 8.9, and 8.10. This figure shows that if one combines the experimental results for the individual series of 90 degree caps the complete set of results approximates a curve.

Each figure (except 8.13) has a plot of experimental results, Tresca infinitesimal results, two-moment limited interaction infinitesimal results, Tresca lower displacement bound, and finite deflection results.

It is immediately obvious that in the range of observed displacement-thickness ratios the effect of finite deflections on the analytic solution is negligible.

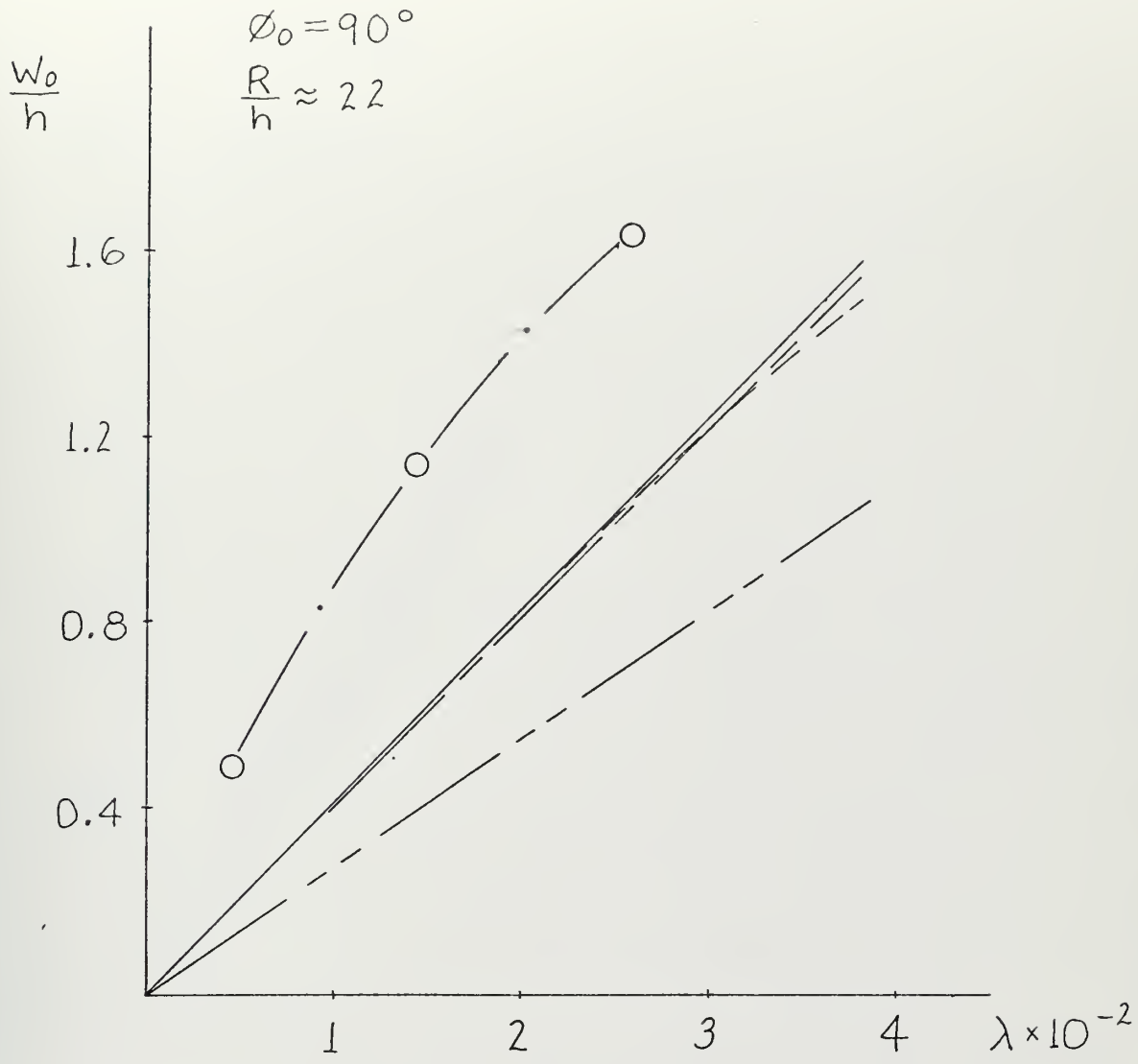

——————— Equation (8.73)

— — — — — Finite deflection (from 8.71)

——— – ——— Equation (8.76)

——— • ——— Experimental results

——— – – ——— Lower bound

Fig. 8.8

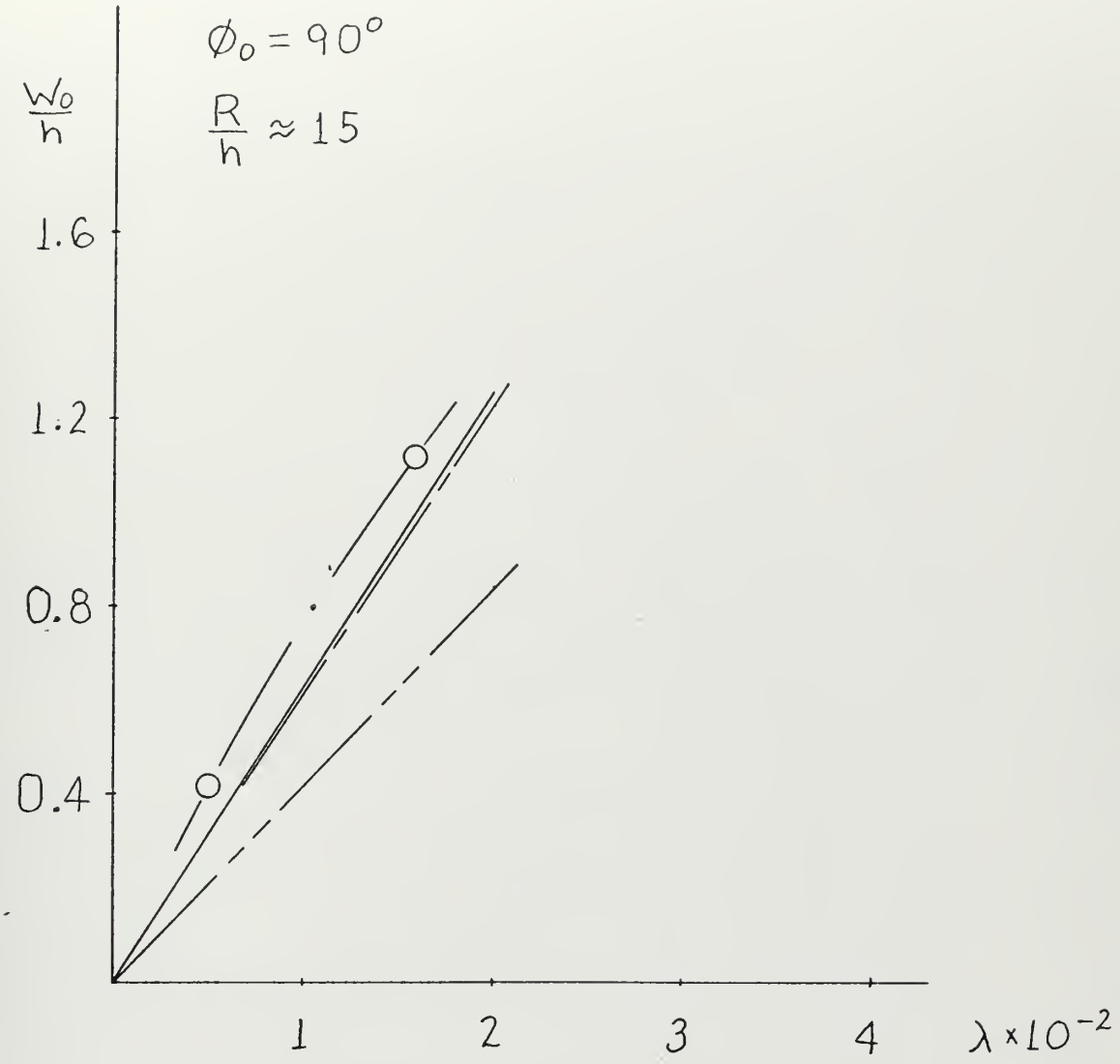

——————— Equation (8.73) and finite deflection

——— — ——— Equation (8.76)

——— · ——— Experimental results

——— – – ——— Lower bound

Fig.8.9

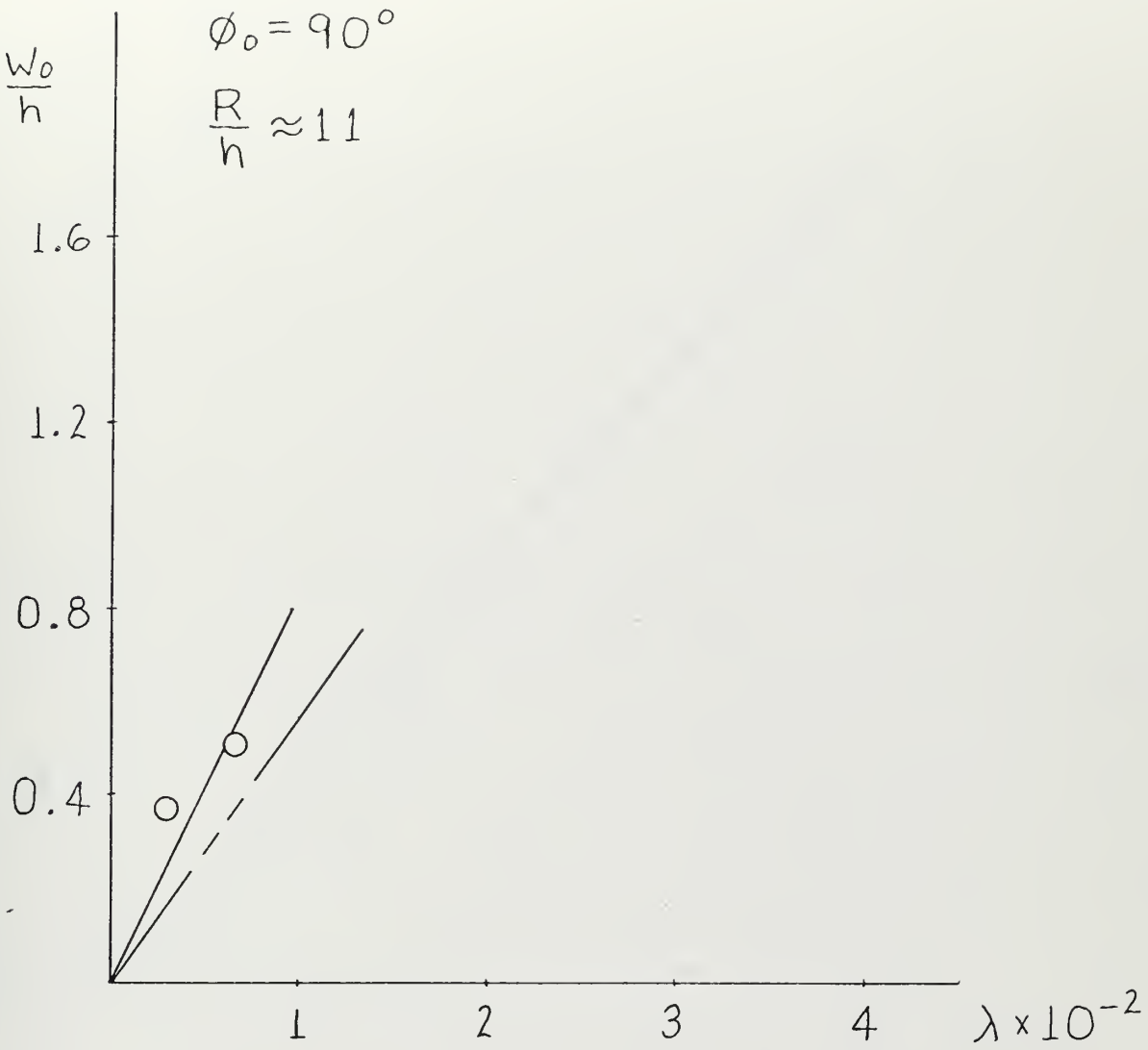

——————— Equations (8.73 and 8.76) and finite deflection

○ Experimental results

——— — — ——— Lower bound

Fig. 8.10

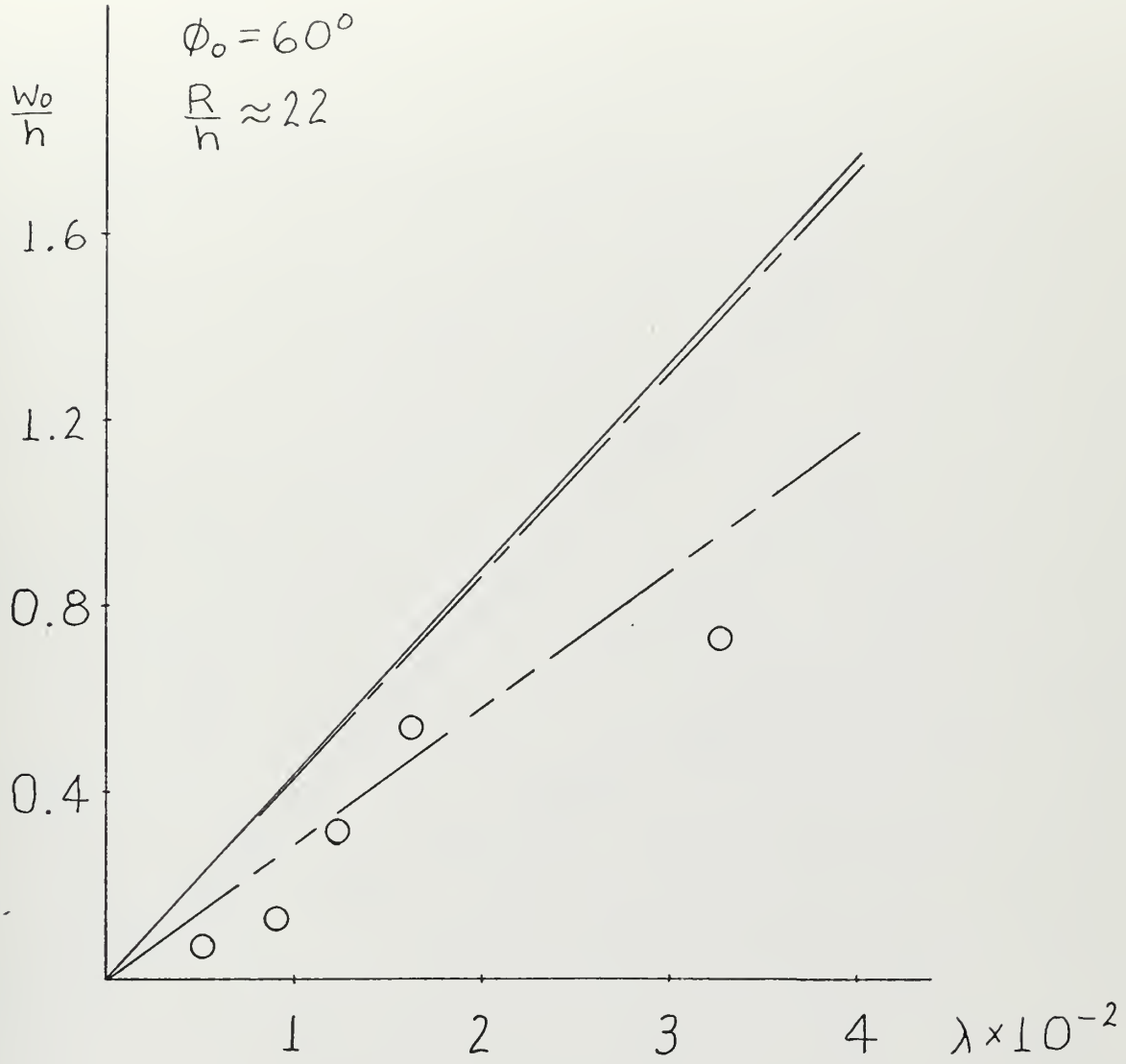

Equation (8.73) and finite deflection

Equation (8.76)

Experimental results

Lower bound

Fig. 8.11

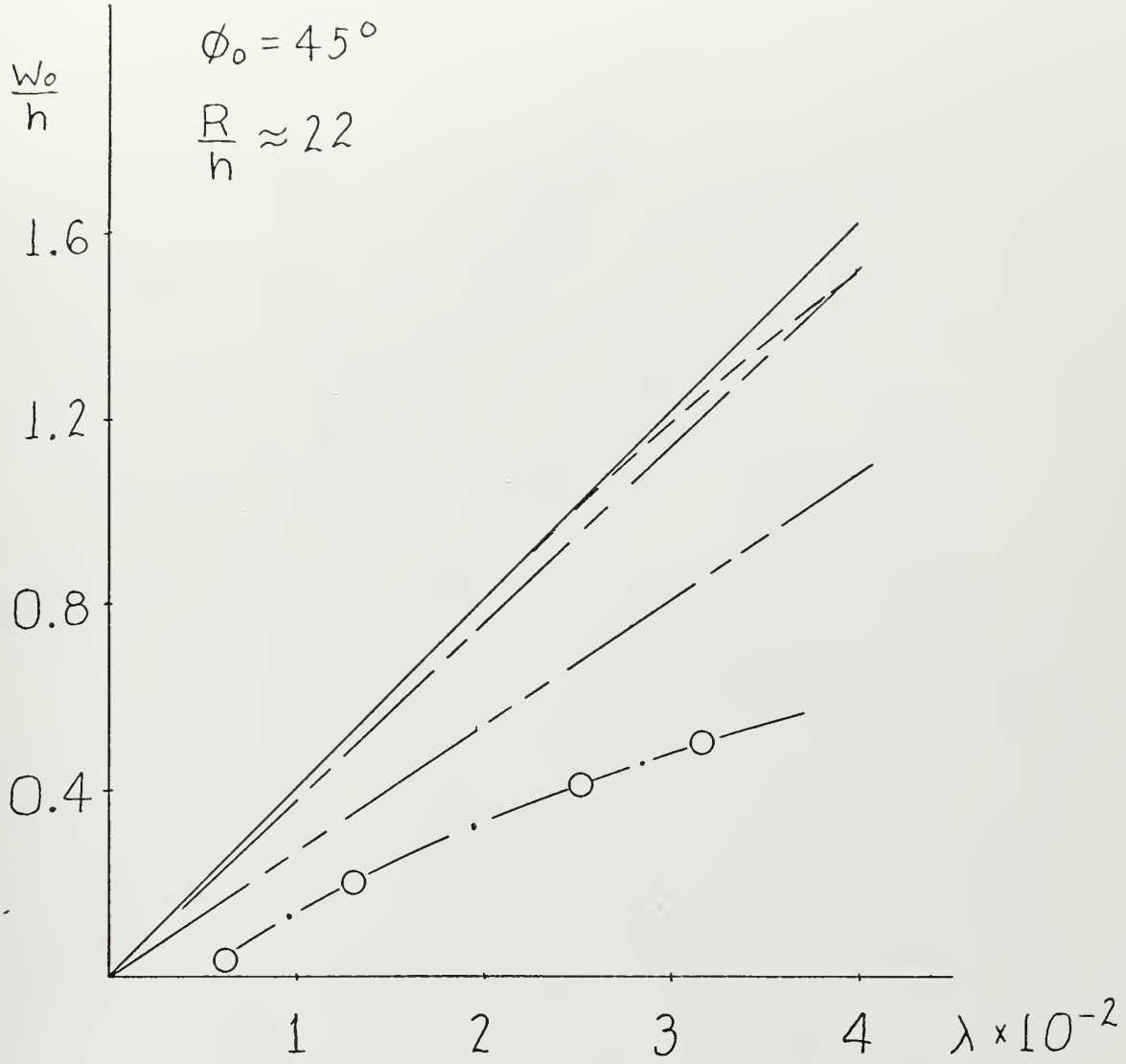

——————— Equation (8.73)

– – – – – – Finite deflection (from 8.71)

——— – ——— Equation (8.76)

——— · ——— Experimental results

——— – – ——— Lower bound

Fig. 8.12

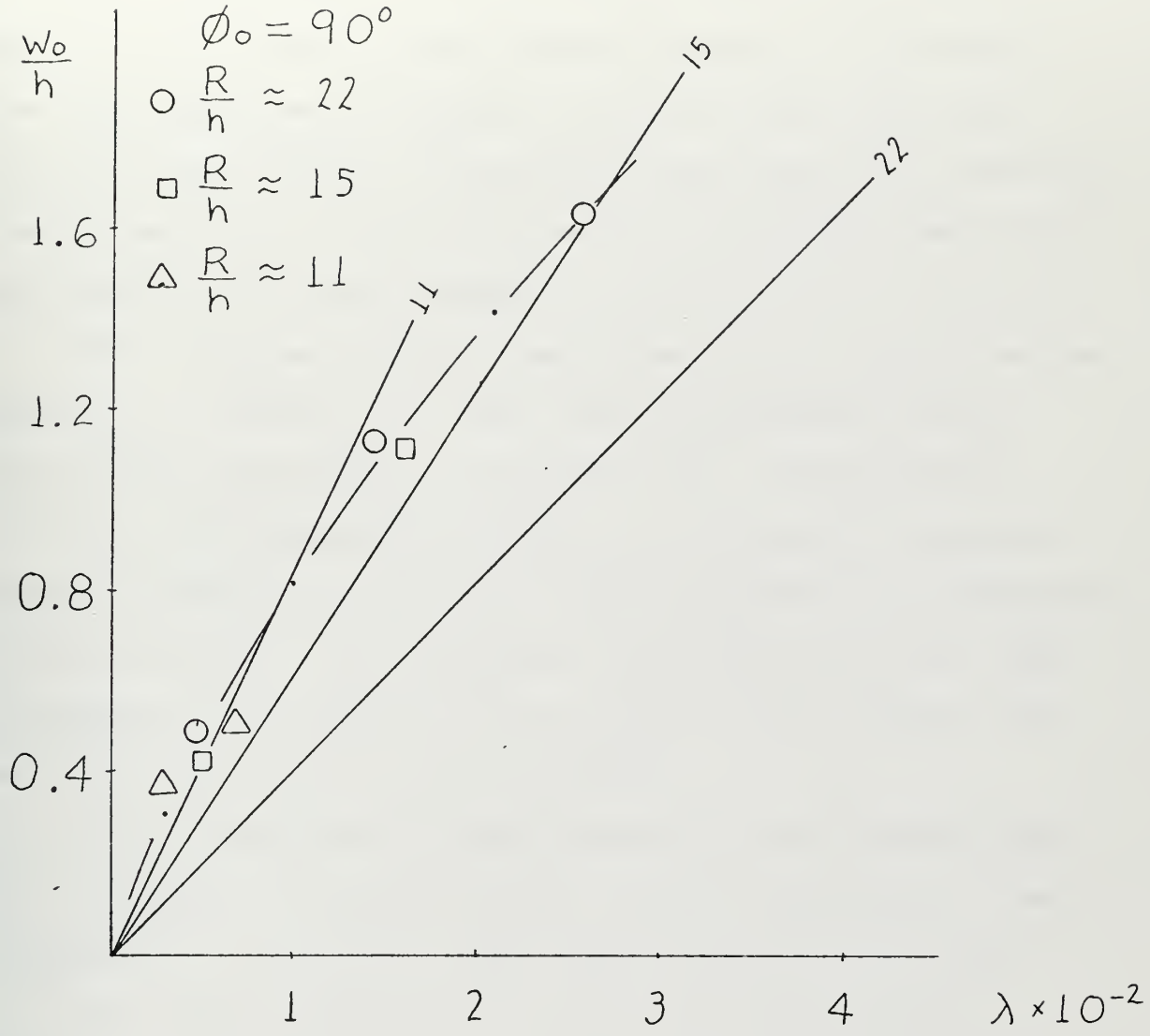

——————— Equation (8.73)

——— · ——— Experimental results

Fig. 8.13

It is also obvious that agreement with experimental results is only fair. Particularly noteworthy is the fact that some experimental results for the 60 degree caps are below the infinitesimal deflection lower bound for a perfectly plastic material and all experimental results for the 45 degree cap are below the lower bound.

The 90 degree cap approximate theoretical results can be plotted in a manner which show final displacement to be essentially independent of thickness for a given initial velocity. This behavior is indicative of membrane behavior. Indeed bending does have very little influence in the analysis of this problem. The experimental results do not show this independence of thickness, which indicates that bending may be of greater importance than assumed.

In the interests of simple analysis it was assumed that $\dot{u}=0$. In order to include greater bending dependence, it may be necessary to utilize a more complicated velocity field.

The simple infinitesimal results obtained for this problem may, however, serve as useful engineering estimates of shell response.

CHAPTER 9

SUMMARY AND CONCLUSIONS

Exact solutions of the response of shells dynamically loaded above the static plastic collapse load are quite complicated. General approximate theoretical procedures are developed herein for arbitrarily shaped shells with arbitrary boundary conditions and with arbitrary loading made of rigid-perfectly plastic material. The influence of finite transverse deflections is considered.

Approximate results were compared with exact analytic solutions for complete spheres and circular cylinders and also with experimental results for cylindrical panels and spherical caps.

The approximate results agreed exactly with the exact analysis for a complete sphere and agreed quite well with the exact analysis of a complete cylinder loaded axisymmetrically. The approximate results for partially loaded cylindrical panels also agreed favorably with experimental results.

The approximate results for explosive loading of spherical caps underpredicted some experimental results and overpredicted others. The variation was as great as 60% of the predicted results.

More scatter was observed in the experimental results for spherical caps than has been observed in related dynamic experiments (e.g. the cylindrical panel results). Some of

the spherical cap experimental results are below a lower bound on displacement for infinitesimal deflection of a perfectly plastic material.

It appears from the approximate results obtained that the influence of finite deflections is quite small if the shell geometry requires the development of sizeable membrane stresses with infinitesimal deflections. Therefore, it seems reasonable to use infinitesimal theory to predict permanent displacements for such shells.

It would be desirable to develop the six-dimensional generalized stress space Tresca yield surface at least to determine the size ratio between inscribed and circumscribed approximate yield surfaces.

In future experiments concerning the dynamic behavior of explosively loaded shells, it would be instructive to determine photographically whether or not the assumed impulsive initial velocity profile is correct.

Finally, it would be worthwhile to apply the techniques of this thesis to other shell geometries and conditions as more experimental results become available.

APPENDIX A

RELATION BETWEEN THE TWO-DIRECTION LIMITED INTERACTION YIELD SURFACE AND THE TRESCA YIELD SURFACE

In Chapter 4 it was stated that the two-moment limited interaction yield surface and the two-direction limited interaction yield surface (Figures 4.1 and 4.2) circumscribe the exact Tresca yield surface and that if each were reduced in size to 0.618 times original size they would inscribe the Tresca yield surface.

This appendix contains as a sample calculation the limiting condition for the two-direction limited interaction yield surface.

The procedure used to inscribe an approximate yield surface within the Tresca yield surface is outlined in reference [A-1]. It consists of assuming a state of stress corresponding to a vertex of the approximate yield surface and then finding the common positive factor by which the stresses must be multiplied in order for the vertex to lie on the Tresca yield surface. The smallest value of the scale factor must be used to inscribe the approximate yield surface within the Tresca yield surface.

Since yield surfaces exhibit symmetry, not every combination of vertices has to be examined. Symmetry of the two-direction limited interaction yield surface is such (see Figure 4.2) that only the first quadrant of each curve need be examined.

A limiting vertex of the approximate surface is the state of stress

$$n_1 = \frac{N_1}{N_0} = 0$$

$$n_2 = \frac{N_2}{N_0} = 1$$

$$m_1 = \frac{M_1}{M_0} = 1$$

$$m_2 = \frac{M_2}{M_0} = 0$$

If these values are multiplied by the common scale factor ξ and the values $n_1 = m_2 = 0$ and $n_2 = m_1 = \xi$ are substituted into the defining equations of the Tresca yield surface [A-1], the limiting equation is found to be

$$m_1 - m_2 = 1 - (n_1 - n_2)^2 \qquad \text{(A.1)}$$

which becomes

$$\xi = 1 - \xi^2 \qquad \text{(A.2)}$$

Solving for the positive value of the scale factor yields

$$\xi = \frac{-1 + \sqrt{5}}{2} = 0.618 \qquad \text{(A.3)}$$

ACKNOWLEDGEMENT

The author wishes to express his appreciation for the continual interest, guidance, and encouragement of Professor Norman Jones. The interest and ideas of Professors William Murray and Thomas Lardner were also greatly appreciated.

BIOGRAPHICAL NOTE

The author was born and raised in New Jersey where he attended public schools. After graduation from high school in 1955 he attended Stevens Institute of Technology for one year. In 1956 he entered the United States Naval Academy and was awarded the degree of Bachelor of Science in 1960. He attended the Catholic University of America as a part-time graduate student from 1962 to 1964. In 1966 he entered the Massachusetts Institute of Technology and in 1969 was awarded the degree of Master of Science in Mechanical Engineering and the degree of Naval Engineer. In 1971 he was awarded the degree of Master of Civil Engineering by the Catholic University of America. From 1969 to 1971 he was a candidate for the degree of Doctor of Philosophy at the Massachusetts Institute of Technology. He has served in several positions aboard ship and within the nuclear power program of the United States Navy.

REFERENCES

2-1 Drucker, D.C., "A More Fundamental Approach to Plastic Stress-Strain Relations", Proc. 1st. U.S. Natl. Cong. Appl. Mech., ASME, 1952 pp. 487-491.

2-2 Mendelson, A., Plasticity, MacMillan, New York, 1966.

2-3 Hill, R., "On the State of Stress in a Plastic-Rigid Body at the Yield Point", Phil. Mag., Vol. 42, 1951, pp. 868-875.

2-4 Hill, R., "A Note on Estimating the Yield Point Loads in a Plastic-Rigid Body", Phil. Mag., Vol. 43, 1952, pp. 353-355.

2-5 Drucker, D.C., Greenberg, H.J., and Prager, W., "The Safety Factor for an Elastic-Plastic Body in Plain Strain", J. Appl. Mech., Vol. 18, 1951, pp. 371-378.

2-6 Drucker, D.C., Greenberg, H.J., and Prager, W., "Extended Limit Design Theorems for Continuous Media", Quart. Appl. Math., Vol. 9, 1952, pp. 381-389.

2-7 Drucker, D.C., Greenberg, H.J., Lee, E.H., and Prager, W., "On Plastic-Rigid Solutions and Limit Design Theorems for Elastic-Plastic Bodies", Proc. 1st U.S. Natl. Cong. Appl. Mech., ASME, 1951, pp. 533-538.

2-8 Neal, B.G. and Symonds, P.S., "The Rapid Calculation of the Plastic Collapse Load of a Framed Structure", Proc. Inst. Civil Engineers (London), Vol. 1, 1952, pp. 58-71.

2-9 Hopkins, H.G. and Prager, W., "The Load Carrying Capacity of Circular Plates", J. Mech. Phys. Solids, Vol. 2, 1953, pp. 1-13.

2-10 Hodge, P.G. Jr., "Yield Point Load of an Annular Plate", J. Appl. Mech., Vol. 76, 1959, pp. 454-455.

2-11 Wood, R.H., Plastic and Elastic Design of Slabs and Plates, Ronald Press, New York, 1961.

2-12 Onat, E.T. and Prager, W., "Limit Analysis of Shells of Revolution", Proc. Roy. Netherlands Acad. Sci., Vol. B57, 1954, pp. 534-548.

2-13 Drucker, D.C., "Limit Analysis of Cylindrical Shells Under Axially-Symmetric Loading", Proc. 1st. Midw. Conf. Solid Mech. (Urbana), 1953, pp. 158-163.

2-14 Hodge, P.G. Jr., Limit Analysis of Rotationally Symmetric Plates and Shells, Prentice-Hall, Englewood Cliffs, 1963.

2-15 Olszak, W. and Sawczuk, A., Inelastic Behavior in Shells, Noordhoff Ltd., Groningen, 1967.

2-16 Hopkins, H.G. and Prager, W., "On the Dynamics of Plastic Circular Plates", J. Appl. Math. Phys., Vol. 5, No. 4, 1954, pp. 317-330.

2-17 Hodge, P.G., "Ultimate Dynamic Load of Circular Cylindrical Shells", Proc. 2nd Midw. Conf. Solid Mech. (La Fayette), 1956, pp. 150-177.

2-18 Hodge, P.G., "The Influence of Blast Characteristics on the Final Deformation of Circular Cylindrical Shells", J. Appl. Mech., Vol. 23, 1956, pp. 617-624.

2-19 Sankaranarayanan, R., "On the Dynamics of Plastic Spherical Shells", J. Appl. Mech., Vol. 30, 1963, pp. 87-90.

2-20 Symonds, P.S., and Mentel, T.J., "Impulsive Loading of Plastic Beams with Axial Constraints", J. Mech. Phys. Solids, Vol. 6, 1958, pp. 186-202.

2-21 Symonds, P.S. and Jones, N., "Impulsive Loading of Fully Clamped Beams with Finite Plastic Deflections", Brown University Report N00014-0003/11

2-22 Jones, N., "Finite Deflections of a Rigid-Viscoplastic Strain-Hardening Annular Plate Loaded Impulsively", J. Appl. Mech., Vol. 35, 1968, pp. 349-356.

2-23 Jones, N. and Walters, R.M., "Large Deflections of Rectangular Plates", to appear in Journal of Ship Research.

2-24 Duszek, M., "Plastic Analysis of Cylindrical Shells Subjected to Large Deflections", Arch. Mech. Stos., Vol. 18, 1966, pp. 599-614.

2-25 Jones, N., "The Influence of Large Deflections on the Behavior of Rigid-Plastic Cylindrical Shells Loaded Impulsively", J. Appl. Mech., Vol. 37, 1970, pp. 416-425.

2-26 Martin, J.B., "A Displacement Bound Principle for Inelastic Continua Subjected to Certain Classes of Dynamic Loading", J. Appl. Mech., Vol. 32, 1965, pp. 1-6.

2-27 Morales, W.J. and Nevill, G.E. Jr., "Lower Bounds on Deformations of Dynamically Loaded Rigid-Plastic Continua", AIAA Jnl., Vol. 8, 1970, pp. 2043-2048.

2-28 Jones, N., "A Theoretical Study of the Dynamic Plastic Behavior of Beams and Plates with Finite Deflections", M.I.T. Nav. Arch. and Mar. Eng. Report 70-14, 1970 (to appear in International Journal of Solids and Structures)

3-1 Sokolnikoff, I.S., Tensor Analysis, Theory and Applications to Geometry and Mechanics of Continua, 2nd. ed., Wiley, New York, 1965, Chapter 3.

3-2 Ibid., Chapter 6.

3-3 Novozhilov, V.V., Thin Shell Theory, 2nd. ed., P. Noordhoff Ltd., Groningen, 1964.

3-4 Wang, C., Applied Elasticity, McGraw-Hill, New York, 1953.

3-5 Love, A.E.H., A Treatise on the Mathematical Theory of Elasticity, 4th. ed., Cambridge Union Press, Cambridge, 1927.

3-6 Koiter, W.T., "A Consistent First Approximation in the General Theory of Thin Elastic Shells", Proc. Symp. Theory of Thin Elastic Shells (1959), North Holland Publishing Co., Amsterdam, 1960, pp. 12-33.

3-7 Donnell, L.H., "General Thin Shell Displacement-Strain Relations", Proc. 4th. U.S. Natl. Cong. Appl. Mech., 1962, pp. 529-536.

3-8 Budiansky, B. and Sanders, J.L., "On the Best First-Order Linear Shell Theory", Progress in Applied Mechanics, 1963, pp. 129-141.

3-9 Krauss, H., Thin Elastic Shells, Wiley, New York, 1967.

3-10 Jones, N., "Consistent Equations for the Large Deflections of Structures", M.I.T., June 1969.

4-1 Onat, E.T., and Prager, W., "Limit Analysis of Shells of Revolution", Proc. Royal Netherlands Acad. Sci., Vol. B57, 1954. pp. 534-548.

4-2 Hodge, P.G. Jr., "The Mises Yield Condition for Rotationally Symmetric Shells", Q. Appl. Math., Vol. 18, 1961, pp. 305-311.

4-3 Hodge, P.G. Jr., Limit Analysis of Rotationally Symmetric Plates and Shells, Prentice-Hall, Englewood Cliffs, 1963.

4-4 Hodge, P.G. Jr., "Yield Conditions for Rotationally Symmetric Shells Under Axisymmetric Loading", J. Appl. Mech., Vol. 27, 1960, pp. 323-331.

4-5 Onat, E.T. and Prager, W., "Limit Analysis of Arches", J. Mech. Phys. Solids, Vol. 1, 1953, pp. 77-89.

4-6 Hildebrand, F.B., Advanced Calculus for Engineers, Prentice-Hall, New York, p. 334.

4-7 Hopkins, H.G., "On the Plastic Theory of Plates", Proc. Roy. Soc. A., Vol. 241, 1957, pp. 153-179.

5-1 Hildebrand, F.B., Op.cit., p. 306.

6-1 Onat, E.T. and Prager, W., Op.cit.

6-2 Sawczuk, A., "On Initiation of the Membrane Action in Rigid-Plastic Plates", J. de Mec., Vol. 3, No. 1, 1964, pp. 15-23.

6-3 Jones, N., Op.cit. [2-28]

6-4 Cox, A.D. and Morland, L.W., "Dynamic Plastic Deformations of Simply-Supported Square Plates", J. Mech. Phys. Solids, Vol. 7, 1959, pp. 229-241.

6-5 Hopkins, H.G. and Prager, W., Op.cit.

6-6 Hodge, P.G. Jr., "Impact Pressure Loading of Rigid-Plastic Cylindrical Shells", J. Mech. Phys. Solids, Vol. 3, 1955, pp. 176-188.

6-7 Martin, J.B. and Symonds, P.S., "Mode Approximations for Impulsively-Loaded Rigid-Plastic Structures", J. Eng. Mech. Div., ASCE, Vol. 92, No. EM5, October 1966, pp. 43-66.

7-1 Janas, M., "Limit Analysis of Non-Symmetric Plastic Shells by a Generalized Yield Line Method", Non-Classical Shell Problems, North Holland Publishing, Amsterdam, 1964, pp. 997-1010.

8-1 Sankaranarayanan, R., Op.cit.

8-2 Hodge, P.G., Op.cit. [2-18]

8-3 Jones, N., Op.cit. [2-25]

8-4 Martin, J.B., and Symonds, P.S., Op.cit.

8-5 Handbook of Chemistry and Physics, 46th ed., Chemical Rubber Co., Cleveland, 1965, pg. A-189

8-6 Jones, N., Dumas, J.W., Giannotti, J.G., and Grasset, K.E., "The Dynamic Plastic Behavior of Shells", Symposium on Dynamic Response of Structures, Stanford University, 1971. To be published by Pergamon Press.

8-7 Janas, M., Op.cit.

8-8 Giannotti, J.G., "An Experimental Study into the Behavior of Shell Intersections", M.I.T. Thesis, June 1971.

8-9 Onat, E.T. and Prager, W., Op.cit. [4-1]

8-10 Bateman, H., Partial Differential Equations of Mathematical Physics, Dover, 1944, pp. 497-498.

8-11 Morales, W.J., and Nevill, G.E., Jr., Op.cit.

A-1 Hodge, P.G., Op.cit.[2-14]

Thesis
W2246 Walters 127254
Dynamic response of
thin, rigid-plastic
shells subjected to
transverse loads.